

AFWAL-TR-80-2032



HIGH BYPASS TURBOFAN COMPONENT DEVELOPMENT
MODIFICATION II

GW Armstrong
JA Palladino
LI Zirin

Aircraft Engine Group
General Electric Co.
Lynn, Massachusetts 01910

March 1980

Technical Report AFWAL-TR-80-2032
Report for Period August 1979 - November 1979

Approved for public release; distribution unlimited.

AERO PROPULSION LABORATORY
AIR FORCE WRIGHT AERONAUTICAL LABORATORIES
AIR FORCE SYSTEMS COMMAND
WRIGHT-PATTERSON AIR FORCE BASE, OHIO 45433

DTIC

ELECTE

DEC 22 1980

FILE COPY

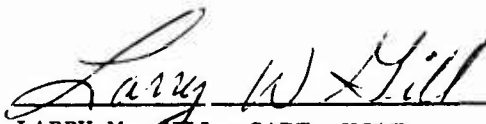
80 12 22 014

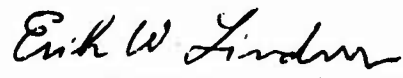
NOTICE

When Government drawings, specifications, or other data are used for any purpose other than in connection with a definitely related Government procurement operation, the United States Government thereby incurs no responsibility nor any obligation whatsoever; and the fact that the government may have formulated, furnished, or in any way supplied the said drawings, specifications, or other data, is not to be regarded by implication or otherwise as in any manner licensing the holder or any other person or corporation, or conveying any rights or permission to manufacture use, or sell any patented invention that may in any way be related thereto.

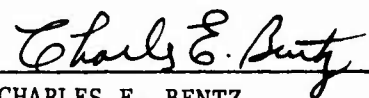
This report has been reviewed by the Office of Public Affairs (ASD/PA) and is releasable to the National Technical Information Service (NTIS). At NTIS, it will be available to the general public, including foreign nations.

This technical report has been reviewed and is approved for publication.


LARRY M. GILL, CAPT, USAF
Project Engineer
Performance Branch


ERIK W. LINDNER, Technical Area Manager
Special Engine Technology
Performance Branch

FOR THE COMMANDER


CHARLES E. BENTZ
Acting Deputy Director
Turbine Engine Division

"If your address has changed, if you wish to be removed from our mailing list, or if the addressee is no longer employed by your organization please notify AFWAL/POTA, W-PAFB, OH 45433 to help us maintain a current mailing list".

Copies of this report should not be returned unless return is required by security considerations, contractual obligations, or notice on a specific document.

19 REPORT DOCUMENTATION PAGE		READ INSTRUCTIONS BEFORE COMPLETING FORM
1. REPORT NUMBER AFWAL-TR-80-2032	2. GOVT ACCESSION NO. AD-A093	3. RECIPIENT'S CATALOG NUMBER 256
4. TITLE (and Subtitle) HIGH BYPASS TURBOFAN COMPONENT DEVELOPMENT. MODIFICATION II		5. TYPE OF REPORT & PERIOD COVERED Final Report Aug. '79 - Nov. '79
7. AUTHOR(s) GW/Armstrong JA/Palladino LJ/zirin		5. PERFORMING ORG. REPORT NUMBER
9. PERFORMING ORGANIZATION NAME AND ADDRESS Aircraft Engine Group General Electric Co. Lynn, MA 01910		8. CONTRACT OR GRANT NUMBER(s) F33615-78-C-2060
11. CONTROLLING OFFICE NAME AND ADDRESS Aero Propulsion Laboratory (AFWAL/POTP) Wright Patterson AFB, OH 45433 Air Force Wright Aeronautical Laboratories		10. PROGRAM ELEMENT, PROJECT, TASK AREA & WORK UNIT NUMBERS 3066/15 26
14. MONITORING AGENCY NAME & ADDRESS (if different from Controlling Office)		12. REPORT DATE March 1980
		13. NUMBER OF PAGES 88
		15. SECURITY CLASS. (of this report) Unclassified
		15a. DECLASSIFICATION/DOWNGRADING SCHEDULE
16. DISTRIBUTION STATEMENT (of this Report) Approved for public release; distribution unlimited.		
17. DISTRIBUTION STATEMENT (of the abstract entered in Block 20, if different from Report)		
18. SUPPLEMENTARY NOTES		
19. KEY WORDS (Continue on reverse side if necessary and identify by block number) Small Turbofan High Speed Balancing Fan Shaft Dynamics Simulator Vibratory Response to Unbalance Fan Shaft Dynamics Rig Testing Fan Shaft Dynamic Balancing		
20. ABSTRACT (Continue on reverse side if necessary and identify by block number) The assembly, instrumentation, and test of a fan shaft dynamics simulation vehicle was completed under this contract. Testing included low speed mechanical checkout, followed by operation up to 45,000 RPM using high speed modal balancing, as required. The procedure was repeated for two sets of bearing support stiffness values. Balance sensitivity of the rotor system was investigated by creating various amounts of unbalance in the fan disk, the (Continued)		

20. Abstract - Continued

turbine disk, and the shaft, and recording the vibratory response up to 45,000 RPM. Finally, a ten-hour endurance test was conducted, completing the requirements of the contract.

TABLE OF CONTENTS

SECTION	PAGE
I. SUMMARY	1
II. INTRODUCTION	2
III. DESCRIPTION OF TECHNICAL WORK	
3.1 Description of Test Vehicle	3
3.2 Description of Instrumentation & Data Acquisition System	4
3.3 Design Analysis	6
3.3.1 Model Description	6
3.3.2 Input Description	8
3.3.3 Critical Speeds and Mode Shapes	8
3.3.4 Balance Criteria	9
3.4 Test Results	
3.4.1 Short Shaft	10
3.4.2 Long Shaft, Spring Ring Set No. 1	11
3.4.3 Long Shaft, Spring Ring Set No. 2	12
3.4.4 Sensitivity to Unbalance	13
3.4.5 10-hour Endurance Test	13
3.5 Comparison of Design Analysis & Test Results	
3.5.1 Critical Speeds	15
3.5.2 Forced Response	15
3.5.3 Bearing Loads	16
IV. CONCLUSIONS	17
APPENDIX	18
Tables	
1 Effective Bearing Spring Rates for Spring Ring Sets No. 1 and No. 2	21
2 Comparison between Measured and Calculated Critical Speeds	22
3 Measured and Calculated Bearing Radial Loads	23

LIST OF ILLUSTRATIONS

FIGURE	DESCRIPTION	PAGE
1	Test Vehicle Layout	24
2	Fan Shaft Dynamics Simulation Vehicle	25
3	LP Shaft Dynamics Rig - Bently Probe Locations	26
4	Typical File of Digitized Data	27
5	Typical Bently Probe & Keyphasor Output vs. Time	28
6	LP Shaft Dynamics Rig-Typical Bently Probe Deflections vs. Speed	29
7	LP Shaft Dynamics Rig - Phase Angle vs. Speed Run No. 21	30
8	Partial View of Data Acquisition and Data Analysis System	31
9	Mathematical Model of Fan Shaft Dynamics Rig	32
10	Fan Shaft Bending Rigidity Distribution	33
11	Fan Shaft Weight Distribution	34
12	LPT Critical Mode Shape Spring Ring Set No. 1	35
13	Fan and Shaft Critical Mode Shape - Spring Ring Set No. 1	36
14	1st Shaft Bending Critical Mode Shape - Spring Ring Set No. 1	37
15	2nd Shaft Bending Critical Mode Shape - Spring Ring Set No. 1	38
16	LPT Critical Mode Shape - Spring Ring Set No. 2	39
17	Fan and Shaft Critical Mode Shape - Spring Ring Set No. 2	40
18	1st Shaft Bending Critical Mode Shape - Spring Ring Set No. 2	41
19	2nd Shaft Bending Critical Mode Shape - Spring Ring Set No. 2	42
20	LP Shaft Dynamics Rig - Bently Probe & Accelerometer Output vs. Speed	43
21	LP Shaft Dynamics Rig - Typical Mid-Shaft and Fan Disk Deflections - Run No. 9	44
22	LP Shaft Dynamics Rig - Turbine disk and Aft Shaft Deflections - Run No. 9	45
23	LP Shaft Dynamics Rig - Typical Amplitude and Phase Angle Output	46
24	LP Shaft Dynamics Rig - Typical Bently Probe Output vs. Time - Run No. 9	47
25	LP Shaft Dynamics Rig - Typical Bently Probe Output vs. Time - Run No. 9	48
26	LP Shaft Dynamics Rig - Typical Bently Probe and Keyphasor Output vs. Time - Run No. 9	49
27	LP Shaft Dynamics Rig - Unbalance Sensitivities on Mid-Shaft and Fan Disk Deflections	50
28	Shaft Dynamics Rig - Run 36	51

LIST OF ILLUSTRATIONS - Continued

FIGURE	DESCRIPTION	PAGE
29	Shaft Dynamics Rig - Run 36	52
30	Shaft Dynamics Rig - Runs 43 & 48	53
31	Shaft Dynamics Rig - Runs 43 & 48	54
32	Shaft Dynamics Rig - Runs 43 & 48	55
33	Shaft Dynamics Rig - Run 56	56
34	Shaft Dynamics Rig - Run 56	57
35	Shaft Dynamics Rig - Run 56	58
36	Shaft Dynamics Rig - Run 69	59
37	Shaft Dynamics Rig - Run 69	60
38	Shaft Dynamics Rig - Run 69	61
39	LPT Non Synchronous Response - Run 91	62
40	LPT Non Synchronous Response - Run 91	63
41	Shaft Dynamics Rig - Run 80	64
42	Shaft Dynamics Rig - Run 80	65
43	Shaft Dynamics Rig - Run 80	66
44	Shaft Dynamics Rig - Run 01	67
45	Shaft Dynamics Rig - Run 01	68
46	Shaft Dynamics Rig - Run 01	69
47	Vibration Amplitude vs. Speed - Run 14	70
48	Vibration Amplitude vs. Speed - Run 14	71
49	Vibration Amplitude vs. Speed - Run 14	72
50	Vibration Amplitude vs. Speed - Run 29	73
51	Vibration Amplitude vs. Speed - Run 29	74
52	Vibration Amplitude vs. Speed - Run 29	75
53	Response to Unbalance - Base Rotor - Run 22	76
54	Response to Unbalance - 1.0 GM-IN at LPT - Run 24	77
55	Response to Unbalance - 1.0 GM-IN at FAN - Run 25	78
56	Response to Unbalance - 0.75 GM-IN at FWD SHAFT - Run 26	79
57	Response to Unbalance - 0.75 GM-IN at MID-SHAFT - Run 27	80
58	Response to Unbalance - 0.75 GM-IN at AFT SHAFT - Run 28	81
59	Mission Profile for Endurance Test	82
60	Endurance Test Vibration Amp. - Start-A through E1	83
61	Endurance Test Vibration Amp. - End-F1 through A2	84
62	Predicted vs. Measured Response	85

SECTION I

SUMMARY

The effort described in this final report was conducted under Modification II of the High Bypass Turbofan Component Development Contract, USAF Contract F-33615-78-C-2060. The work-scope of this Contract Modification consists of the assembly, instrumentation, and test of a fan shaft dynamics simulation vehicle for testing a low pressure shaft of a small turbofan engine. Effort was initiated on 1 August 1979 and will terminate with the approval and distribution of this final report.

The Contractor designed and procured the hardware for a vehicle to simulate the dynamics of the rotor/bearing system of a small turbofan engine at speeds up to 45000 RPM. The purpose of this program was to conduct the assembly, instrumentation, and test of this vehicle. Testing included a low speed mechanical checkout, followed by operation up to 45,000 RPM. Modal high speed balancing was performed, as required. Instrumentation sufficient to determine shaft deflections and bearing loads was included. The procedure was repeated for the two sets of bearing stiffness values. Balance sensitivity of the rotor system was investigated by creating various amounts of unbalance in the fan disk, the turbine disk, and the shaft, and operating the simulator up to 45,000 RPM. After completion of the above testing, a ten-hour endurance test was conducted.

Test results agreed well with design analyses in terms of critical speeds and dynamic response, and spring ring supports where shown to be a satisfactory means of supporting and damping a small-scale, high speed fan shaft rotor. However, measurements of bearing loads using strain gages on the spring rings were unsatisfactory, and improved techniques to measure bearing loads are required. Efficient high speed balancing procedures were demonstrated in this test series.

SECTION II

INTRODUCTION

Advanced technology small turbine engines are expected to be constrained to achieve the required performance in the smallest possible engine volume and diameter. To this end, the diameter and length can be reduced by the employment of high tip speeds in the compressors and turbines to reduce the number of stages. The results of this approach to small turbofan engine design is that the fan shaft becomes a significant design challenge, since the shaft will necessarily be small in diameter (to fit through the core shaft) and will tend to have critical speeds within the engine operating range.

The purpose of this program was to determine the fan shaft critical speeds, deflections, and bearing loads by test of a fan rotor system simulator, and to match the measured results with analytical predictions made prior to test.

The effects on the critical speeds, shaft deflections, and bearing loads of two different sets of bearing support stiffnesses (or spring rates) were also to be determined for the purposes of optimization.

Another purpose of the test was to verify the need for multiplane/multispeed (high speed) balancing and to develop the technique for such high speed balancing. As planned, the testing was to consist of the following:

1. Conduct a low speed mechanical checkout of the simulator, instrumentation, and lubrication system.
2. Operate the rig up to 45,000 RPM, performing modal high speed balancing, if required.
3. Determine balance sensitivities by varying amounts of unbalance on the fan disk, turbine disk, and shaft.
4. Change bearing support stiffnesses to investigate the resulting shaft deflections and bearing loads.
5. Conduct a 10-hour endurance test.

SECTION III

DESCRIPTION OF TECHNICAL WORK

3.1 DESCRIPTION OF TEST VEHICLE

The test vehicle layout is shown in Figure 1. The rotor assembly contains smooth fan and turbine disks sized to provide the correct shaft dynamic characteristics. The shaft is supported by ball and roller bearings at the fan disk and a roller bearing at the turbine disk. The bearings are mounted in spring rings which are squeezed film oil-damped. A rigid aluminum housing supports the spring rings. The complete assembly can be seen in the photograph of Figure 2.

The fan disk end of the shaft is supported by a ball bearing and a roller bearing spaced about 2.31 inches apart. The drive end of the shaft is bored to accommodate a female spline bushing. The 3/8 inch pitch-diameter male spline driving the test shaft was made short (.28") so that any slight angular misalignment would not apply leverage loading to the driven shaft and affect its operating characteristics. The third bearing is another roller bearing located 16.57 inches aft of the second (roller) bearing and is near the turbine disk.

Each of the engine design bearings is mounted in a flexible spring ring. Each ring has six shallow lands on the outside and six internal lands staggered in spacing with the external ones. Two strain gages are mounted 180° apart on the external diameter, between lands, in order to measure bending stress and, thus, deflection.

To ensure adequate damping of the bearing, lube oil under pressure is provided to each bearing support area. Lube oil pressures are set to provide 0.3 GPM to the ball bearing and 0.2 GPM to each roller bearing.

A bumper bearing with .050 inch shaft radial clearance and made of plastic material is installed mid-way along the length of the shaft.

This support is intended to limit extreme excursions of the shaft when accelerating through critical speeds.

The simulated fan rotor is driven by a hydraulic motor through a Cotta speed-increasing gearbox at speeds up to 45,000 RPM.

3.2 DESCRIPTION OF INSTRUMENTATION AND DATA ACQUISITION SYSTEM

The prime instrumentation used to perform high speed dynamic balancing of the simulated fan rotor were non-contacting distance sensors and their associated signal conditioning and data acquisition equipment. In addition, secondary instrumentation was used to measure bearing loads, and accelerometers were used to monitor any movement of the non-contacting distance sensor base supports. Additional instrumentation was employed to measure bearing temperatures, oil flow and pressure, and facility drive operating parameters. The following is a description of the prime instrumentation, recognizing that rotor movement is the key measurement in high speed dynamic balancing. The non-contacting distance sensors were Bently Nevada proximity probes based upon the eddy current principle. Six were located in a plane along the rotor vertically below the axis at the 6 o'clock position and five additional probes were located in a plane along the axis at the 3 o'clock position. Hence there were two probes 90° apart located at the fan disk, three more 90° pairs spaced along the shaft, a pair at the turbine disc and one probe sensing the drive spline shaft. See Figure 3 for the location of the probes. A fiber optic sensor was located at 12 o'clock measuring the one-per-rev count of the gearbox output shaft. This is the key phase reference for determining the RPM and phase angle between all the other Bently probes and the keyphasor. The fiber optics probe signal, after proper conversion and amplification, was connected to the input of the Bently Nevada Digital Vector Filter 2 balance diagnostic unit. This unit displays RPM and amplitude and phase angle of any of the eleven proximity probes inputted to it. The eleven proximity probes after proper signal conditioning and nominalization are recorded on five different systems.

System 1

The probes are fed one at a time through a switching box to the Digital Vector Filter 2 unit. The Digital Vector Filter 2 displays amplitude and phase at constant rotor speed as well as producing a DC voltage proportional to amplitude and phase. These voltages are then fed to a Doric Digitrend 220 Data Logger scanner and analog to digital voltmeter. The digital voltages are then fed to a Honeywell 6000 computer via a GE Terminet 1200 Teletype for a file generation, storage, and analysis. See Figure 4 for an example of this file.

System 2

The probes and keyphasor are captured on a Gould memo scope and then fed to an analog xyy plotter. The x axis is time and one y axis is for the keyphasor showing 1/rev pulse vs. time and the other y axis is for the probe amplitude vs. time. Data is taken for constant rotor speed and gives a plot of probe phase angle and displacement amplitude. This is used as an independent check of the results of system 1. See Figure 5 for an example of this plot.

System 3

Four probes on two xyy plotters are displayed. The x axis is RPM and the y, y axis are probe distance amplitudes. These plots clearly display the rotor resonances vs. RPM. Also xy plots are made of a probe phase vs. RPM. See Figure 6 and Figure 7 for examples of these plots.

System 4

An x, y, z oscilloscope is used to display a pair of probes 90° apart at the same axial location. One probe is on the x axis and one probe is on the y axis. The lissajous display from the oscilloscope, shows the circular motion of the rotor at that selected axial location. The z axis is connected to the keyphasor and produces a gap in the lissajous figure to mark the clock location of the keyphasor.

System 5

A fourteen channel tape recorder is used to record 8 probes, RPM, 3 strain gages, voice and time at 30 inches per second tape speed. The tape can be played back for recording on systems 1 through 4 above.

The photograph of Figure 8 shows a partial view of the test instrumentation readout and recording equipment used for this test program. Also shown are tracking filters and a spectrum analyzer for detailed frequency analysis and equipment to measure and display strain gages and accelerometer readings.

3.3 DESIGN ANALYSIS

The General Electric Company "VAST" system of computer programs was used in the design analysis. The VAST program with pre and post processors is used for critical speed, resonance and maneuver calculations. The VAST program is capable of finding the flexural natural frequencies of an axisymmetric system, tabulating and graphically representing each mode, as well as strains of the system resulting from any type of misalignment. It gives the vibratory energy of exciting forces, thus permitting the optimization of the balancing procedures and establishing the limits of misalignment and bearing clearances. The program calculates force and moment diagrams of the total system or any part thereof due to maneuver effects, angular acceleration, loading due to gravity, angular velocity and engine thrust. Rotary, inertia, gyroscopic effects, and shear deflections are also included in the analysis. The VASTD program uses complex arithmetic to calculate the damped response of the vehicle throughout the operating range.

3.3.1 Model Description

The mathematical model for the dynamics test rig is shown in Figure 9. The gearbox and its supporting structure are represented by a lumped mass system with a linear translational and rotational spring. The spline which connects the power shaft and the LP shaft is modeled as a spring; this transferring spring can only transmit

3.3.1 - Continued

shear force. All interference fits between the shaft and disks are also represented by springs with a linear stiffness - equal to 5×10^6 lbs/in. The weights, polar and transverse moments of inertia are lumped at the disk locations to account for weight and gyroscopic effects in calculating critical speeds and their corresponding mode shapes. Bearing spring rings which link bearings and the supporting structure are modeled as springs. The composite bearing stiffness which includes the effect of bearing races and bearing spring rings is assumed to be 60% of the stiffness of bearing ring alone. This assumption results in very good agreement between calculated critical speeds and test results. The spring ring supporting structures are also included in the analysis. The following table summarizes the span numbers and the components they represent.

<u>SPAN NUMBER</u>	<u>COMPONENTS</u>
1,2,3,4	Gearbox and Power Shaft
5,7,8,9,10,11,12,14	Low Pressure Turbine Shaft
6	Fan Disc
13	LPT Disc
15,16,17,18,19,20	Bearings No. 1 & 2 Supporting Structure
21,22,23,24	Bearing No. 3 Structure

<u>SPRING NUMBER</u>	<u>COMPONENTS</u>
1	No. 1 Bearing
2	No. 2 Bearing
3	No. 3 Bearing
4,6	Spline Coupling
5	Gearbox Supporting Structure
7,8	Fan Disc Fits
9,10	LPT Disc Fits
11	Gearbox and Power Shaft
12	No. 1 Bearing Ring Collar Structure
13	No. 2 Bearing Ring Collar Structure

SPRING NUMBERCOMPONENTS - Continued

14	No. 3 Bearing Ring Collar Structure
15	Bearings No. 1 & 2 Supporting Structure Connected to Grounded Table
16	Bearing No. 3 Supporting Structure Connected to Grounded Table

3.3.2 Input Description

The low pressure shaft is not uniform in diameter. The bending rigidity (EI) and weight distribution along the shaft axis are shown in Figures 10 and 11. The shaft detail dimensions are also incorporated into the VAST model.

3.3.3 Critical Speeds and Mode Shapes

In the dynamics test rig, two different sets of bearing spring rings (with their stiffnesses given in Table 1) were used. Basically, they have similar dynamic characteristics and critical speeds. The corresponding mode shapes for No. 1 and No. 2 sets are given in Figures 12 to 15 and 16 to 19, respectively. A brief description for No. 2 set bearing spring ring is as follows:

1. The first critical speed is 11060 RPM, with motion of the turbine disk on the No. 3 bearing, and very small vibration in fan disk and shaft. This is evidenced by the result that 85% of the potential energy is contained in No. 3 bearing. The mode shape for this critical speed is shown in Figure 16.
2. The second critical speed is 11978 RPM. This is a combined mode of the fan disk translating on the No. 1 bearing with some bending of the shaft between the No. 2 and No. 3 bearings. Small vibration of the turbine disk is reduced. The mode shape for this mode is given in Figure 17.
3. The third critical speed is 19906 RPM. This corresponds to the first bending mode of shaft supported by bearings No. 2 and No. 3. See Figure 18 for mode shape.

4. The fourth critical speed is 50708 RPM which is beyond the shaft top speed (45000 RPM). This mode is the second bending mode of the shaft. During testing the shaft began to respond to this mode at top speed, and was balanced to reduce that response. The mode shape is shown in Figure 19.

This fourth critical speed of 50,708 rpm represents a 12.7% margin over the rotor maximum operating speed. While this margin is less than required by Military Specification Mil-E-5007D, no trade-off in system reliability is expected. The high speed balancing technique used on this program should provide smooth operation through the critical mode in an overspeed condition. The high speed balancing technique requires that the rotor system must be on the ramp of the critical speed mode, i.e., starting to respond. Figures 50-52 show that the rotor was beginning to respond to this mode at maximum speed. The speed capability of the facility used for this program did not allow operation up to the fourth critical. However, during the normal course of engine full scale development, it would be the intent to show that the system reliability implicit in the 20% speed margin requirement was met by utilizing the high speed balancing technique and designing for much less critical speed margin than 20%. This would be done by operating at the critical speed after high speed balancing of the rotor system. The technology of this program therefore allows greater design freedom to reduce engine complexity, cost and weight while still maintaining system reliability.

3.3.4 Balance Criteria

The balance criteria established prior to the rig testing was to limit bearing loads to 500 lbs. consistent with achieving a 50 hour engine design life with adequate margin. Two methods of measuring bearing loads were evaluated. The first was a direct approach involving placing strain gages on the spring ring supports. This technique has worked very well on other GE engines. This test was

the first time it has been tried by GE on spring rings and it was not successful for two reasons. The first was a high failure rate of the strain gage leads early in the test rendering the gages inoperative. The second was the complex output of the operating gages which did not permit on-line monitoring. The second method of measuring bearing loads was to relate rotor deflections to bearing load and to monitor the deflections as measured by the Bentley proximity probes. The relationship between the bearing load at each bearing and the rotor deflection at the five balance planes was determined analytically using the VAST computer program. The allowable deflections at the balance planes at each critical speed was determined. Since the bearing loads and deflections peak at these speeds, the speed range was divided into regions using the limit established at the peak conditions (critical speed) for the entire region. The balance criteria in terms of rotor deflection is shown in the following table.

ALLOWABLE DEFLECTION (MILS DA ABOVE RUNOUT)

<u>Speed (RPM)</u>	<u>Fan</u>	<u>Fwd Shaft</u>	<u>Mid Shaft</u>	<u>Aft Shaft</u>	<u>LPT</u>
0-11,500	6.0	7.8	1.4	4.2	10.0*
11,500-18,000	10.0*	7.7	13.0	8.5	3.5
18,000-40,000	3.5	6.9	12.0*	9.0	3.5
40,000-Max	1.4	6.5*	1.0	6.3*	3.5

*indicates most critical parameter

As can be seen from the final balance (Figures 50-52), the rotor deflections and bearing loads are well within limits.

3.4 TEST RESULTS

3.4.1 Short Shaft

Testing of the short shaft configuration was initiated in early September, 1979. The short shaft was run up to a speed of 46,000 RPM to check out the drive system, data collection system and the spring-ring bearing supports. A typical plot of fan disk

displacement vs. speed is shown in Figure 20. Displacement of the rotor was measured by a Bently proximity probe. Motion of the base of the Bently probe (which measures only relative displacement) was determined by an accelerometer. The associated accelerometer motion is also shown in Figure 20.

3.4.2 Long Shaft, Spring - Ring Set No. 1

A typical rotor response with the initial low speed balance is shown in Figures 21 through 26. The rotor displacement is measured by Bently proximity probes at the fan and turbine discs and at the three shaft balance planes (only two are shown). Plots of Bently displacement vs. speed are shown in Figures 21 and 22. Figure 23 shows the digitized response data. Figures 24 to 26 show a balance-plane Bently output (displacement) vs. time on the top and the keyphasor (timing reference) vs. time on the bottom. Amplitude and phase can be obtained from Figures 24 to 26, corresponding to the data in Figure 23 at three planes. Response data was taken at speeds where vibration levels are too high and which must be balanced. Trial weights were successively added at each balance-plane and response data obtained. Figure 27 shows the change in response at the mid shaft and fan disk balance-planes for three trial weights at the mid shaft.

The first critical mode (LPT) located at 11,000 RPM was successfully traversed, but the rotor responded in the second mode (fan and shaft bending) at 13,000 RPM. The first mode at 11,000 RPM is a typical translation mode and was easily controlled by low speed balancing. The second mode at 13,000 RPM had a significant amount of shaft bending which required correction by high speed balancing to correct for the resulting distributed unbalance. Figures 28 and 29 show the results of a three-plane balance at the fan, mid-shaft, and LPT. The rotor passed through two peaks of the second mode at 13,000 RPM and 18,000 RPM, and started to respond to the third mode at 23,000 RPM which is the shaft bending and fan mode. Multiple peaks were observed at all of the modes caused by the non-axisymmetric supports and an unintentional looseness in the

fit of the aft bearing spring ring support. Figures 30, 31, and 32 show the results of an additional balance correction at the fan to reduce the rotor response at 13,000 RPM. Figures 33, 34, and 35 show the reduction of the peak at 18,000 RPM. The next balance iteration was a five-plane correction which reduced the peak at 23,000 RPM and permitted operation up to full speed (see Figures 36, 37, and 38). Two additional peaks of the LPT can be seen in Figure 38 at 21,000 RPM and 28,500 RPM. A pronounced non-linear characteristic is evident in the LPT peaks at 10,000 RPM and 28,500 RPM. Spectral analysis of the LPT response identified the peaks above 11,000 RPM to be non-synchronous vibration at the first mode (see Figures 39 and 40). This non-synchronous response may have been amplified by a looseness which was observed in the aft bearing spring ring support. Figures 41, 42, and 43 show the results of an additional two-plane balance which reduced rotor response at all speeds below 35,000 RPM with the exception of the LPT peaks between 11,000 RPM and 22,000 RPM. The previously mentioned looseness at the aft bearing support prevented better control of these vibrations. It can be seen that the rotor was beginning to respond to the second shaft bending mode when operating above 40,000 RPM. This second shaft bending mode is characterized by nodes at the fan, mid-shaft and LPT, and by antinodes at the forward and aft shaft balance planes. The rotor response at maximum speed was within acceptable levels. It was then decided to install the second set of spring rings for evaluation, thus permitting an analytical teardown and resolution of the aft bearing support looseness, and also allowing refurbishment of the aft bearing strain gages.

3.4.3 Long Shaft, Spring Ring Set No. 2

The vehicle was reassembled with the second set of spring rings at No. 1 and No. 3 bearing locations. Whereas the old No. 3 spring ring was loose at disassembly (could easily be rotated in its housing) the new No. 3 ring was a tight, press-fit. The housing had been worn slightly, a few tenths of a thousandth of an inch, but was in the middle of the drawing tolerances (2.5020" diameter;

drawing 2.5022 to 2.5017 diameter). The second set of spring rings were assembled in the normal manner, lightly tapping them into their housings, then tapping the bearing outer races into the assembled spring rings. After the retainers had been secured, the strain gage leads were connected and the assembly was completed. For this build, the rotor balance weights (high speed) were left in place from the previous build. Figures 44, 45, and 46 show that despite the teardown and rebuild, the rotor was able to be operated up to full speed on the first run of build 2. In Figure 46, it is also evident that eliminating the aft bearing support looseness was effective in controlling the non-synchronous LPT response. Two additional high speed balance iterations were made involving a total of five corrections, one at each balance plane (see Figures 47 to 52). The ten-hour endurance run was made after the first iteration which was a two-plane correction at the Fwd and Aft shaft balance planes to suppress the 2nd shaft bending mode at top speed. The final correction was made even though the response after the previous correction was acceptable as demonstrated by the successful endurance run. The reason for this final correction was to determine if the high speed balance techniques were effective in reducing the response. Figures 50 to 52 show that the response was essentially reduced to the runout level over the entire speed range.

3.4.4 Sensitivity to Unbalance

The sensitivity to unbalance applied in each of the five balance planes is shown in Figures 53 through 58. These data were generated using spring ring set No. 2.

3.4.5 10-Hour Endurance Test

A ten-hour endurance test was run using the mission shown in Figure 59. This test used rotor balance shown in Figures 57 to 59. Figure 60 shows the vibration amplitudes for the first part of the test, including the starting accel and the cycles through E1 (Ref. Figure 59). Figure 61 shows the vibrations for the remainder of the test. An increased response at the end of the test during

shutdown was due to a failure of the high speed gearbox output shaft spline. This failure occurred during the endurance running and resulted in a run-out in excess of 30 mils at the end of the quill shaft away from the LP rotor. Since the LP rotor was running supercritically during the test (until shutdown), the response did not increase significantly in spite of the added unbalance.

3.5 COMPARISON OF DESIGN ANALYSIS AND TEST RESULTS

3.5.1 Critical Speeds

Before the bearing spring rings were installed their stiffnesses were measured statically, using a rigid collar support. In the dynamics test rig, the bearing spring rate is a composite characteristic of the bearing races and the spring ring connected in series. This results in the effective bearing stiffness being softer than that of bearing spring ring alone. To account for the softening, an equivalent stiffness of 60% of the bearing spring ring stiffness was used to calculate critical speeds (see Table 1 for static and dynamics values). The calculated critical speeds and test results are shown in Table 2.

3.5.2 Forced Response

An investigation was made of the LP rotor response resulting from an unknown unbalance distribution in the fan and LPT disks and the LP shaft. This unbalance distribution was represented by equivalent residual unbalances at the fan disk, the forward, middle, and aft shaft balancing lands, and the LPT disk. Their values were determined by employing the calculated influence coefficients to minimize the difference between the calculated responses and test results. This minimization was done at these five planes at speeds of 10000, 12000, 21500 and 42500 RPM through the application of the least squares technique. The comparison of a typical test result with the predicted response using equivalent residual unbalances is shown in Figure 62. It is seen that the predicted response matches the test results reasonably well over the entire speed range.

3.5.3 Bearing Loads

Measurements of the radial bearing loads were made using strain gages located on the spring ring supports. The gages were calibrated for static loads in a fixture with both rigid and flexible supports. In some cases complicated non-linear load vs. strain relationships resulted. As a consequence, difficulty in obtaining a direct measurement of radial bearing load was anticipated. The measured and calculated values for the key speeds in the endurance run are shown in Table 3. The measured strains have been converted to loads using the overall signals. It is apparent that these measured loads are not a good indication of the actual radial bearing loads, since the measured bearing loads do not vary significantly over a wide speed range and the load is a function of speed squared. It is likely that the bearing load is being masked by other responses in strain gage signals, since the one-per-rev content is small relative to the overall signal. The predicted values are much more reasonable, and the analytical model used to predict these loads agreed well with measured rotor deflections, as was discussed in Section 3.5.2.

SECTION IV

CONCLUSIONS

The following conclusions are drawn from this analysis and test series:

- (a) An efficient procedure for high speed balancing has been demonstrated which significantly reduces rotor response over the entire operating range. Reductions of the order of 5-to 10-fold have been demonstrated compared to vibration amplitudes after low speed balance.
- (b) A dynamics test rig which effectively simulates fan shaft rotor dynamics has been demonstrated. Successful operation of the fan shaft configuration was demonstrated up to 45,000 RPM.
- (c) Test results agree well with design analyses for both sets of spring ring supports in terms of critical speeds and response. Thus, a sound analytical base has been established for predicting the dynamic response of similar small-scale, high speed fan shaft rotors.
- (d) Spring ring supports provide an acceptable means of supporting and damping a small-scale, high speed fan shaft rotor.
- (e) A ten-hour endurance test, based on a simulated cruise-missile mission, was successfully completed.
- (f) Improved techniques are required to satisfactorily measure radial bearing loads.

APPENDIX

APPLICATIONS OF THE LEAST SQUARES TECHNIQUE TO HIGH SPEED ROTOR BALANCING

The application of the least square method to high speed balancing of the fan shaft dynamics test rig was very successful. In this appendix, this method is briefly described. The rig is simply represented as shown in Figure 9.

The influence coefficients which represent the responses resulting from unit trial unbalances are first calculated. In this analysis, their values are expressed in the form of complex numbers calculated from the equation:

$$C(m, k, l) = [S(m, l) - R(m, l)] / p(k)$$

WHERE m = Speed indicator
 k = Trial unbalance applied plane
 l = Response plane

C = Influence Coefficient
 R = Response in Rotor Before Trial Unbalance is Added.
 S = Response in Rotor After Trial Unbalance is Added.
 p = Trial Weight

Throughout the analysis, the indices m, k, l have the following meanings:

m = Speed indicator, with values equal to 1, 2, 3 and 4 for 10000, 12000, 21500 and 42500 RPM, respectively.
 k, l = Location indicators with values equal to 1, 2, 3, 4, 5 for the fan, forward shaft, middle shaft, Aft shaft and LP turbine, respectively.

As an example, C (2, 3, 1) means response at fan disk (l = 1) resulting from unit unbalance at middle shaft (k = 3) at speed 12000 RPM (m = 2).

In actual rotor systems, the distribution of unbalance is not known. In the practice of balancing, correcting weights are placed at selected balancing planes and adjusted to reduce the vibration levels down to acceptable levels. Judged from this fact, we can assume that the unbalance of the rotor system is represented by an equivalent residual unbalance at five balance planes. They are denoted by: $W(k) = x(k) + i y(k)$

Where, k represents the plane location.

For example, W (3) = Equivalent residual unbalance at the middle shaft.

Application of the method of least squares determines equivalent residual unbalances at selected balancing planes. The rotor response is minimized using the previously determined influence coefficients and the basic initial rotor response. First a function G which is the difference between the predicted response and the actual response is constructed. The function G is defined by:

$$G = \sum_{m=1}^M \sum_{l=1}^L \sum_{k=1}^K \left\| C(m, k, l) * W(k) - R(m, l) \right\|$$

WHERE

M = Number of speeds used

l and k = Locations of balancing planes used.

AND $\left\| \right\|$ is the absolute value of the complex number.

The equivalent residual unbalances x_k and y_k ($k = 1, \dots, K$) are determined by the following stationary conditions of the function G. They are:

$$\frac{\partial G}{\partial x_k} = 0$$

$$(k = 1, \dots, K)$$

$$\frac{\partial G}{\partial y_k} = 0$$

These conditions constitute $2 \times K$ simultaneous equations for $2 \times K$ unknowns $(x_k, y_k \dots x_K, y_K)$. The required balancing weights are equal to the equivalent residual unbalances in magnitude but 180° out of phase, at each selected balancing plane.

TABLE 1

EFFECTIVE BEARING SPRING RATES FOR SPRING RING SETS NO. 1 & NO. 2

SPRING RING SET NO.	BEARING NO.	SPRING RATE - LB / IN	
		RIGID COLLAR TEST DATA	EFFECTIVE SPRING RATE
1	1	2.13×10^5	1.28×10^5
1	2	1.17×10^5	7.0×10^4
1	3	4.6×10^4	2.7×10^4
2	1	0.98×10^5	6.0×10^4
2	2	1.25×10^5	7.2×10^4
2	3	4.6×10^4	2.7×10^4

TABLE 2

COMPARISON BETWEEN MEASURED AND CALCULATED CRITICAL SPEEDS

<u>SPRING RING SET NO.</u>	<u>MODE</u>	<u>TEST RESULT (RPM)</u>	<u>CALCULATED (RPM)</u>
1	LPT MODE	11000	11060
1	FAN / SHAFT	13000	13670
1	1 st SHAFT BENDING	22500 (#28)	21890
2	LPT MODE	11000	11060
2	FAN / SHAFT	12000	11978
2	1 st SHAFT BENDING	20000 (#28)	19906

TABLE 3

MEASURED AND CALCULATED BEARING RADIAL LOADSMEASURED RADIAL LOADS

<u>SPEED (RPM)</u>	<u>BEARING LOAD (LBS)</u>		
	<u>NO. 1</u>	<u>NO. 2</u>	<u>NO. 3</u>
24,100	201	198	203
38,700	217	207	215
44,600	221	212	221

CALCULATED RADIAL LOADS

<u>SPEED (RPM)</u>	<u>BEARING LOAD (LBS)</u>		
	<u>NO. 1</u>	<u>NO. 2</u>	<u>NO. 3</u>
24,100	14	4	63
38,700	20	80	80
44,600	75	235	120

24

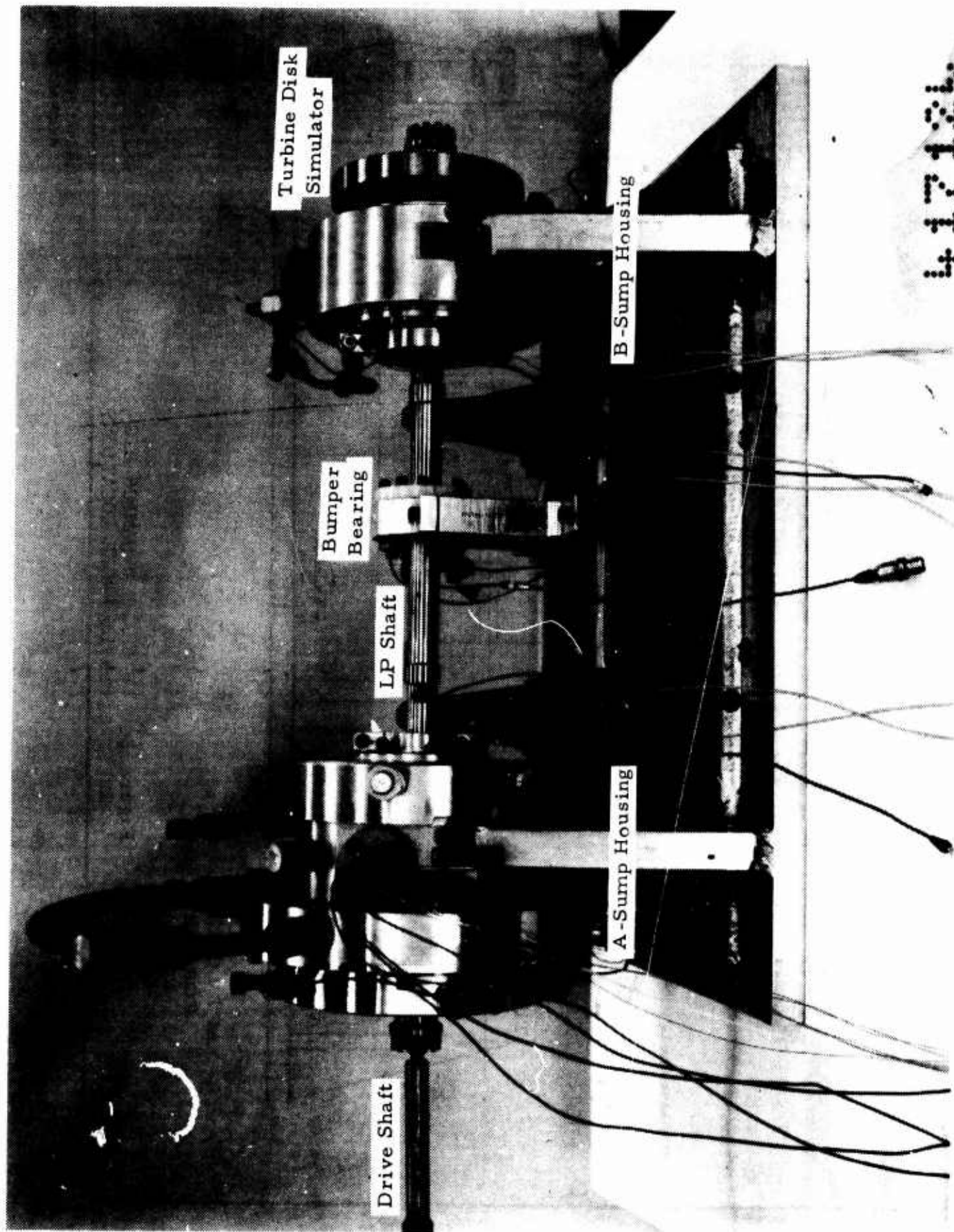
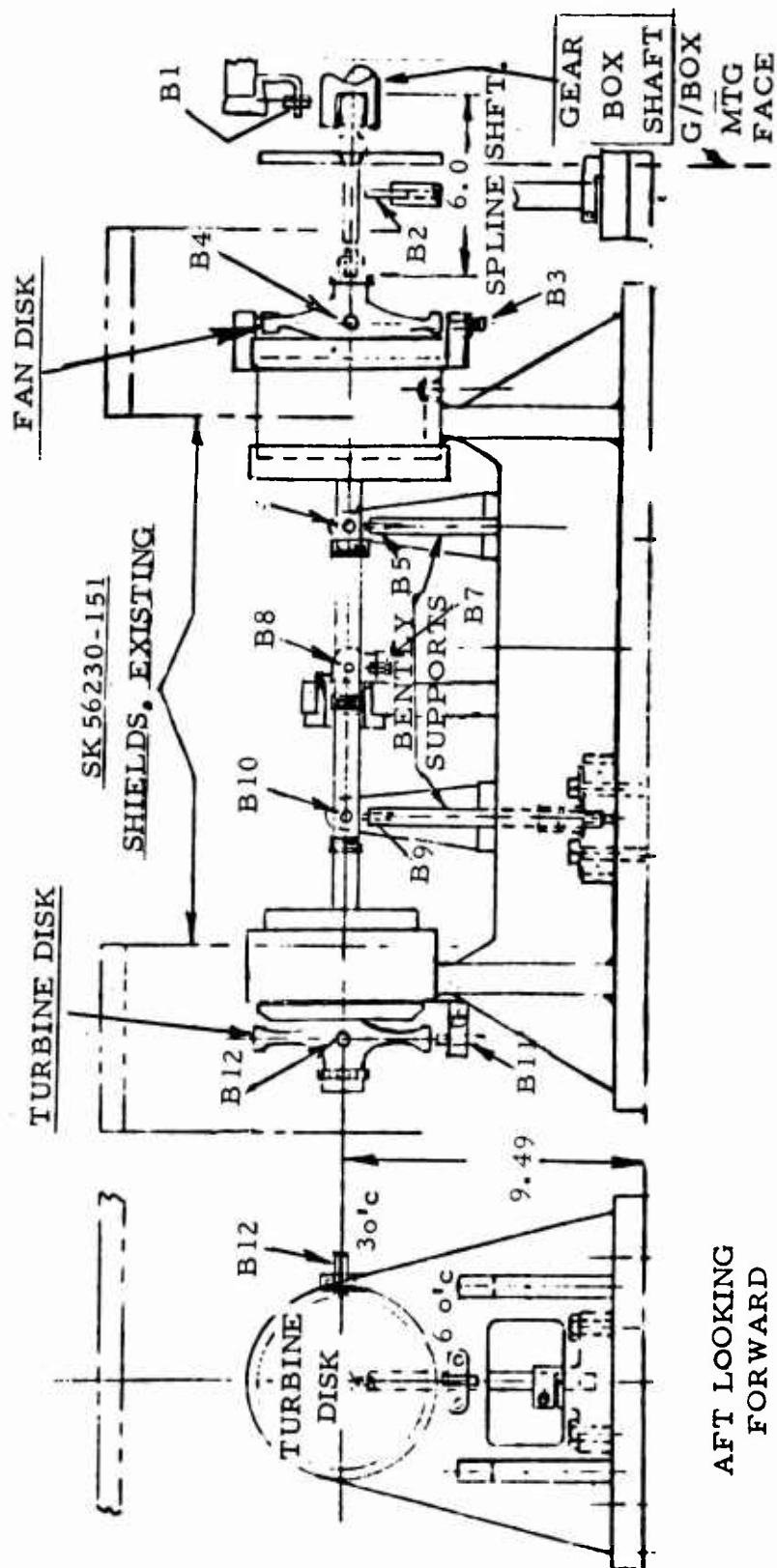


Figure 2. Fan Shaft Dynamics Simulation Vehicle.

ALL BENTLYS B3-B12 AT 30°c & 60°c



AFT LOOKING
FORWARD

Figure 3 LP SHAFT DYNAMICS RIG-
BENTLY PROBE LOCATIONS

Channel Identification

Channel Number	volts	proportional	to probe	Calibration Signal
000	"	"	"	3 amplitude
001,002,003,004	"	"	"	3 phase angle
005,006,007,008,009	"	"	"	rotor speed
010	"	"	"	probe 5 amplitude
011,012,013,014	"	"	"	probe 5 phase angle
015,016,017,018,019	"	"	"	rotor speed
020	"	"	"	probe 7 amplitude
021,022,023,024	"	"	"	probe 7 phase angle
025,026,027,028,029	"	"	"	rotor speed
030	"	"	"	probe 9 amplitude
031,032,033,034	"	"	"	probe 9 phase angle
035,036,037,038,039	"	"	"	rotor speed
040	"	"	"	probe 11 amplitude
041,042,043,044	"	"	"	probe 11 phase angle
045,046,047,048,049	"	"	"	strain gages
050,051,052	"	"	"	rotor speed
053,054	"	"	"	
055,056,057	spare channels			
000	0.5000V	001 0.4067V	002 0.4065V	003 0.4067V
005-1.8363V	006-1.8475V	007-1.8436V	008-1.8556V	009-1.8396V
010 0.9790V	011 0.4065V	012 0.327V	013 0.3254V	014 0.3251V
015-1.0734V	016-1.0735V	017-1.0735V	018-1.0736V	019-1.0735V
020 0.9802V	021 0.3275V	022 0.3893V	023 0.4964V	024 0.5075V
025-0.8922V	026-0.8944V	027-0.8915V	028-0.8915V	029-0.8904V
030 0.9817V	031 0.5083V	032 0.2755V	033 247.99M	034 244.44M
035-0.9141V	036-0.9080V	037-0.9109V	038-0.9123V	039-0.9138V
040 0.9795V	041 0.449V	042 0.4499V	043 0.4512V	044 0.4504V
045-032.75M	046-032.72M	047-035.09M	048-032.73M	049-032.73M
050 026.95M	051 0.9220V	052 07.084M	053 0.9800V	054 0.9801V
055 012.24M	056 007.34M	057-028.55M		

Figure 4 - TYPICAL FILE OF DIGITIZED DATA

RUN NO. 18 - 12,500 RPM

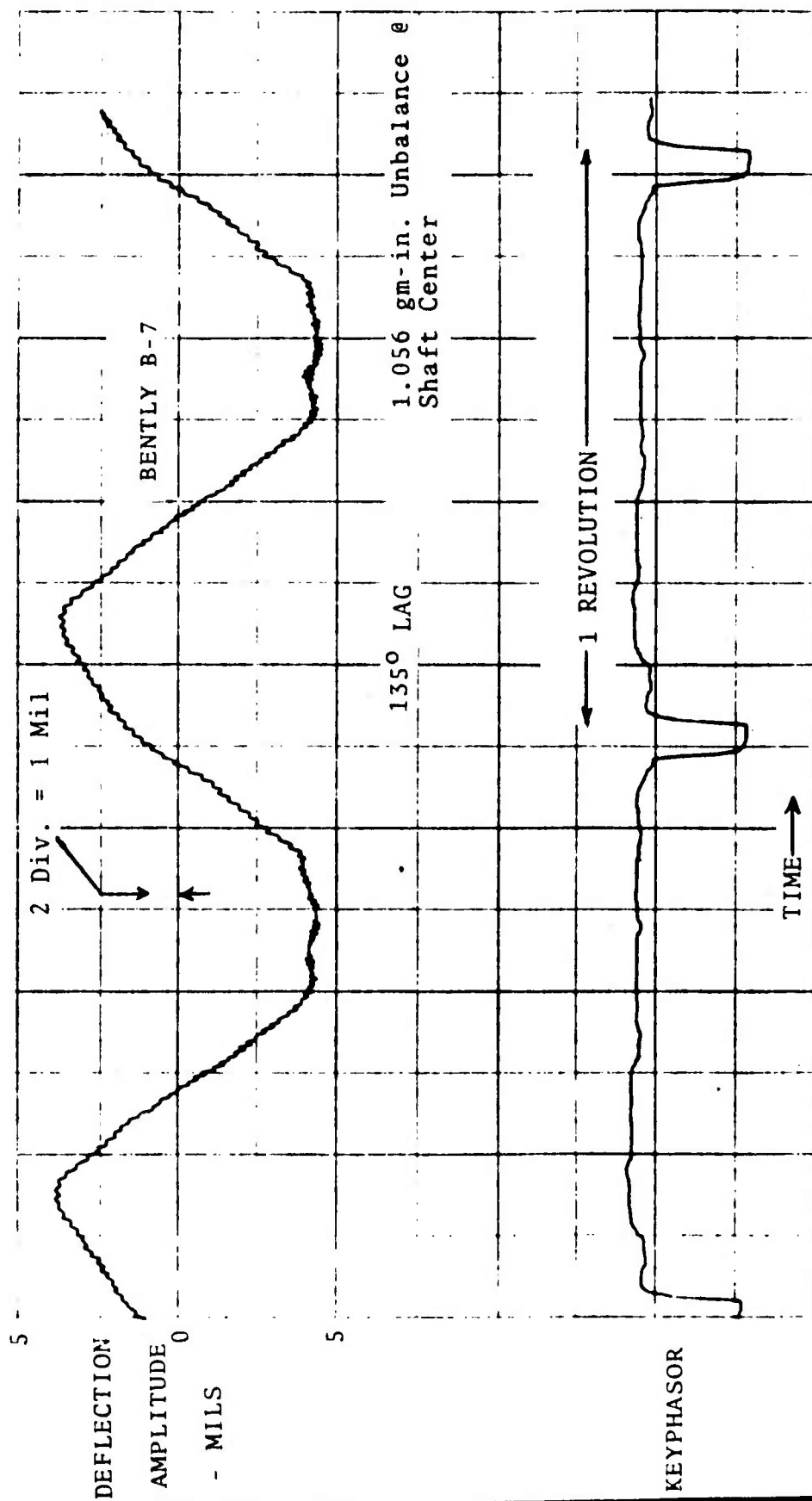


Figure 5 TYPICAL BENTLY PROBE
& KEYPHASOR OUTPUT
VS. TIME

RUNS 14 & 15

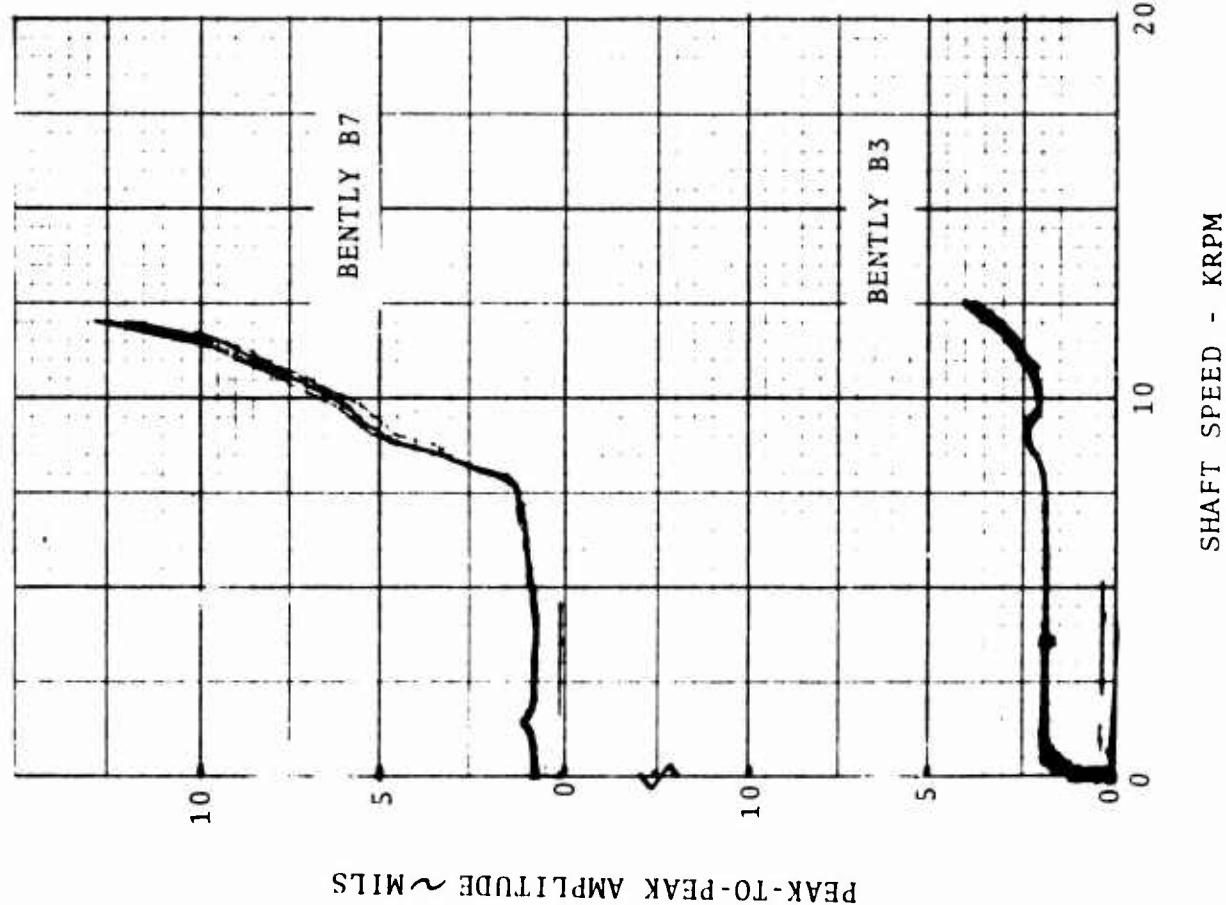


Figure 6 LP SHAFT DYNAMICS RIG-TYPICAL BENTLY PROBE DEFLECTIONS VS. SPEED

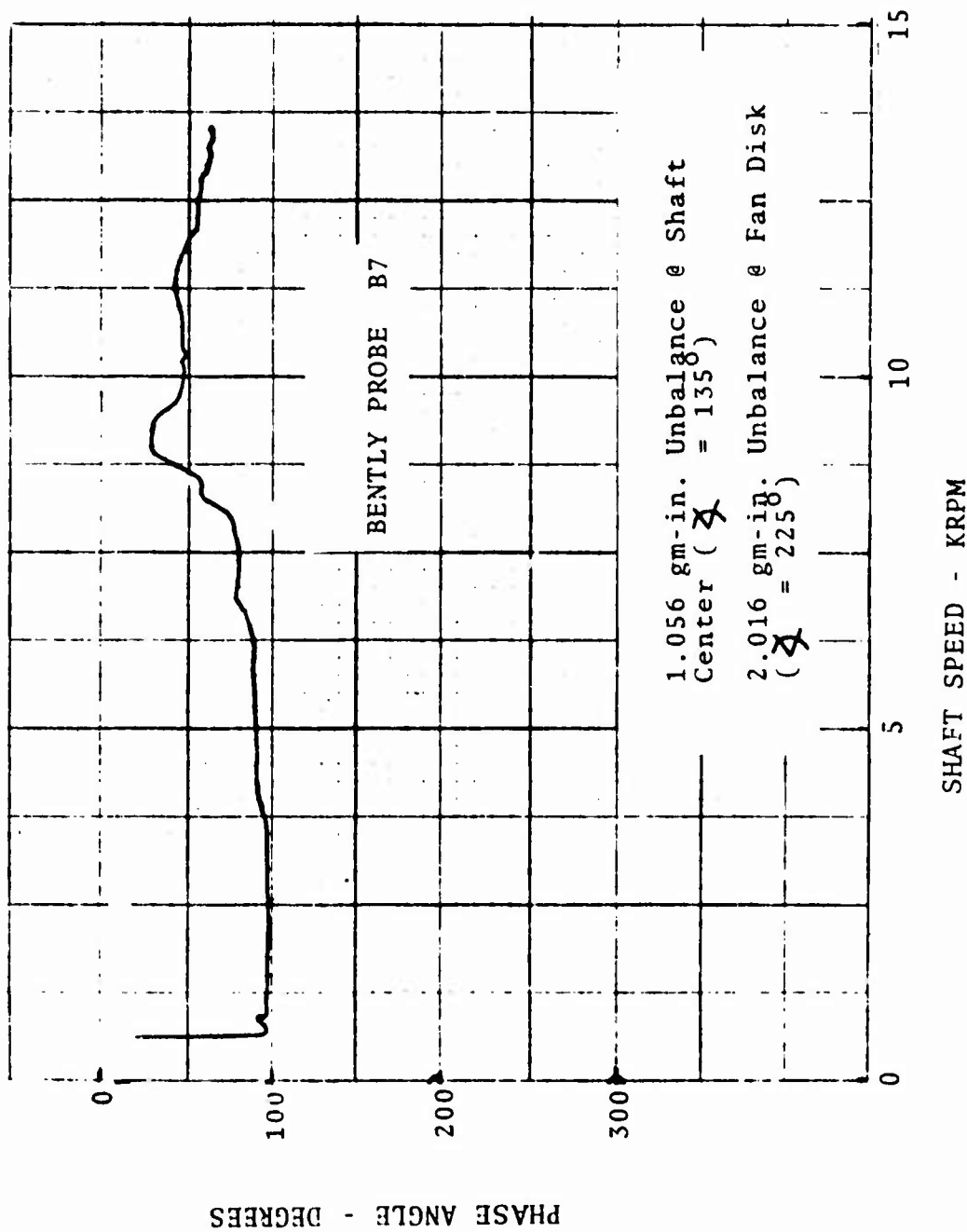


Figure 7 - LP SHAFT DYNAMICS RIG -
 PHASE ANGLE VS. SPEED -
 RUN NO. 21

GENERAL ELECTRIC COMPANY
 AIRCRAFT ENGINE GROUP

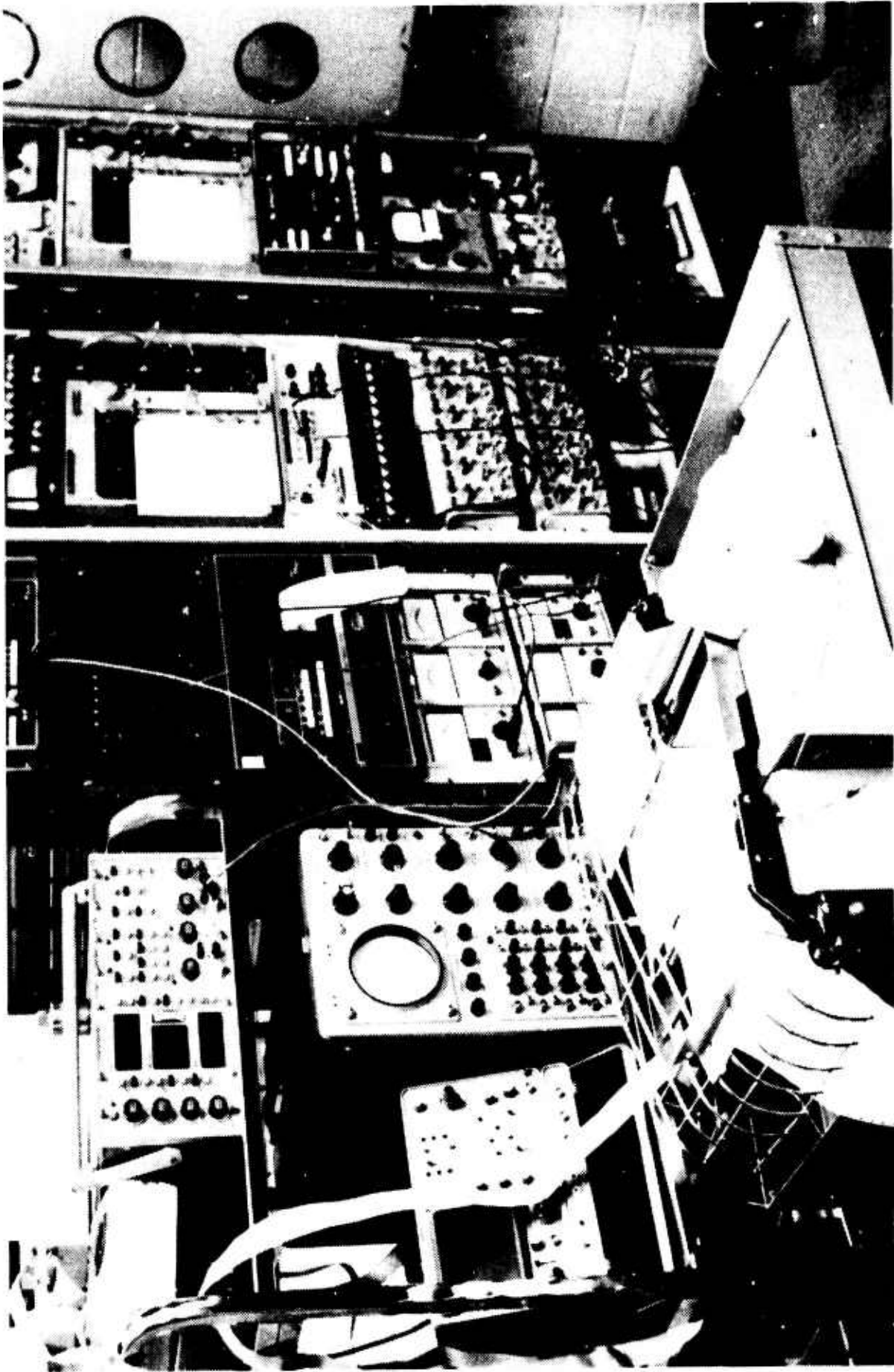
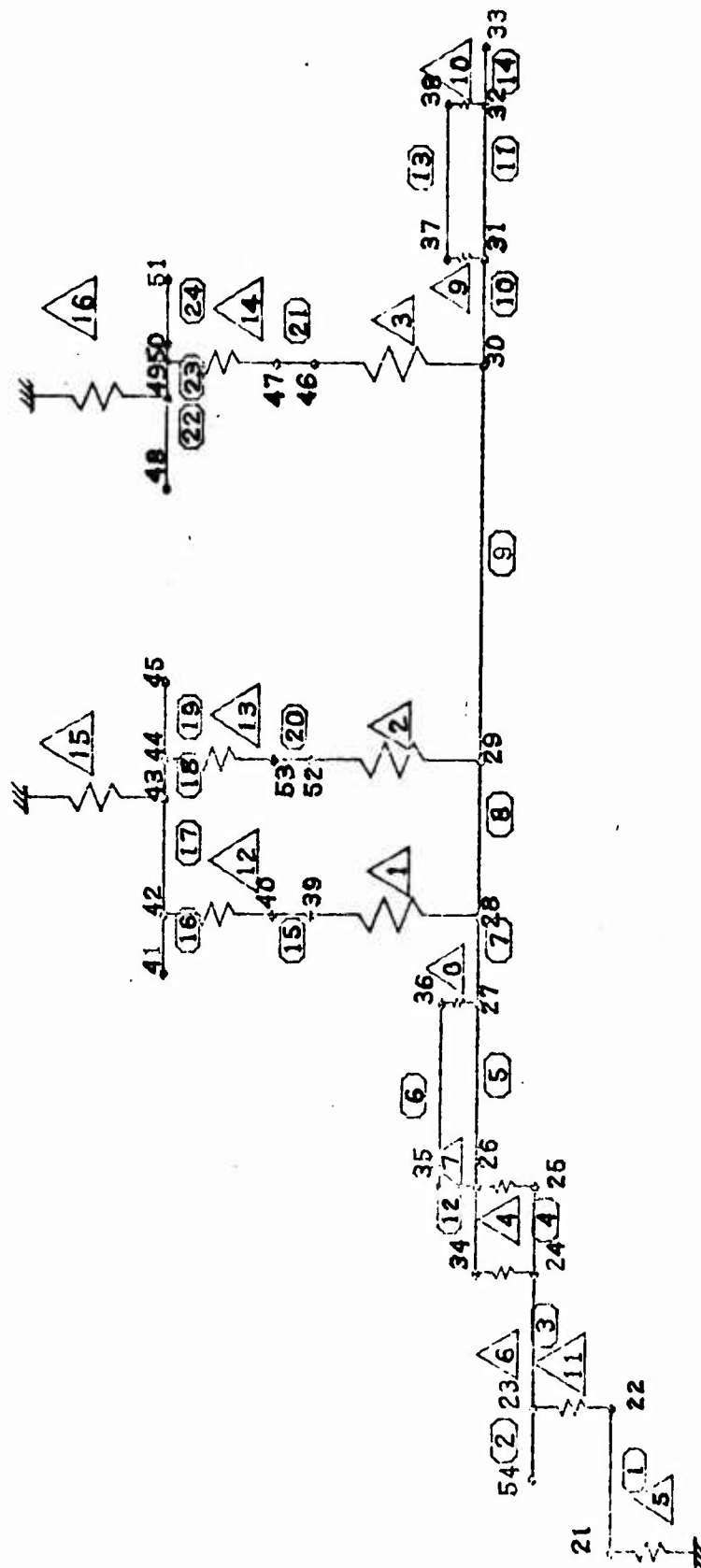


Figure 8. Partial View of Data Acquisition and Data Analysis System.



(NN) SPAN NUMBER

△ NN SPRING NUMBER

NN JOINT NUMBER

Figure 9. Mathematical Model of Fan Shaft Dynamics Rig.

Weight = 6.19 LBS.

C.G. @ 12.5 in.

Bending Rigidity - $EI \times 10^6$ LB-IN²

Ball Bearing Location
Roller Bearing Location

Roller Bearing Location

Shaft Location (in.)

Figure 10. Fan Shaft Bending Rigidity Distribution.

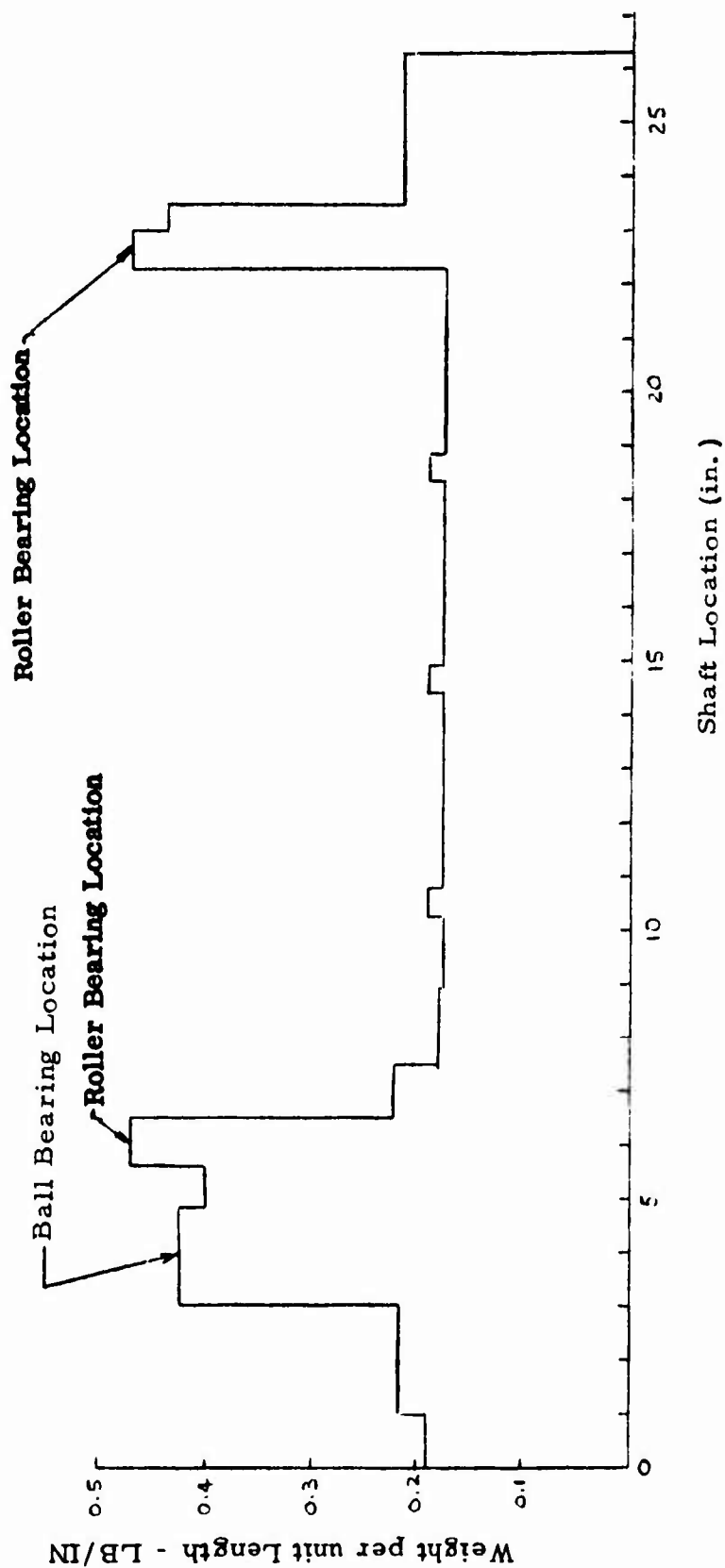


Figure 11. Fan Shaft Weight Distribution

% K = % of Total Kinetic Energy in System
 % P = % of Total Potential Energy in System

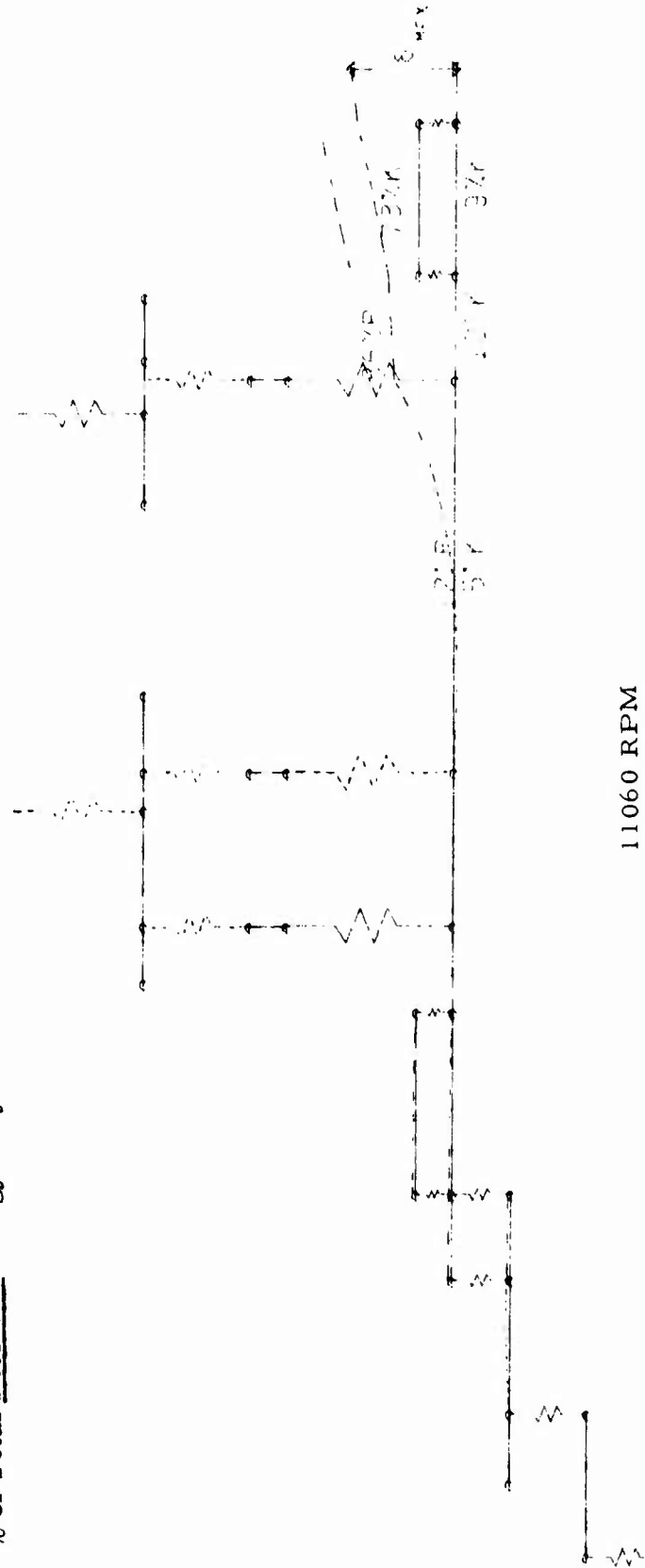


Figure 12. LPT Critical Mode Shape Spring Ring Set No. 1

% K = % of Total Kinetic Energy in System
 % P = % of Total Potential Energy in System

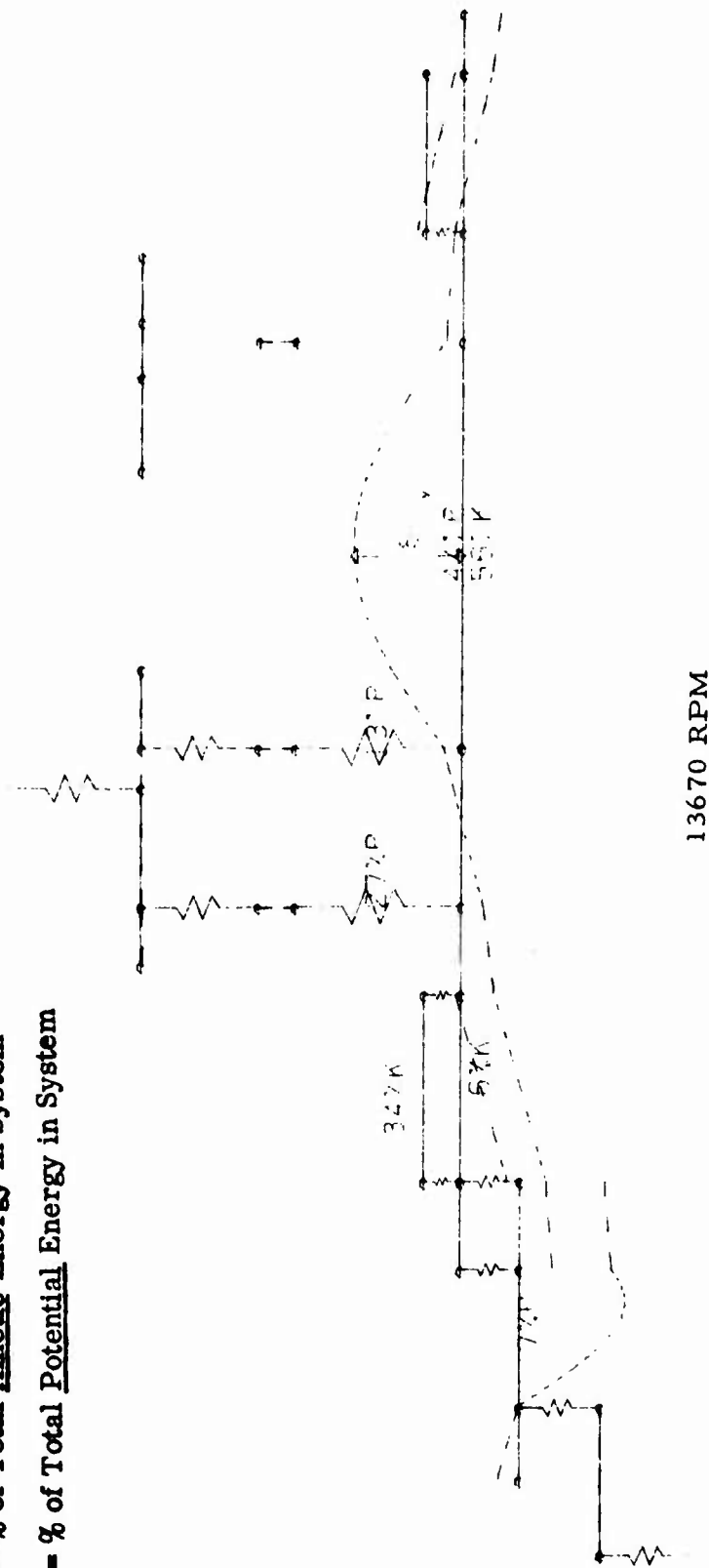


Figure 13. Fan & Shaft Critical Mode Shape - Spring Ring Set No. 1

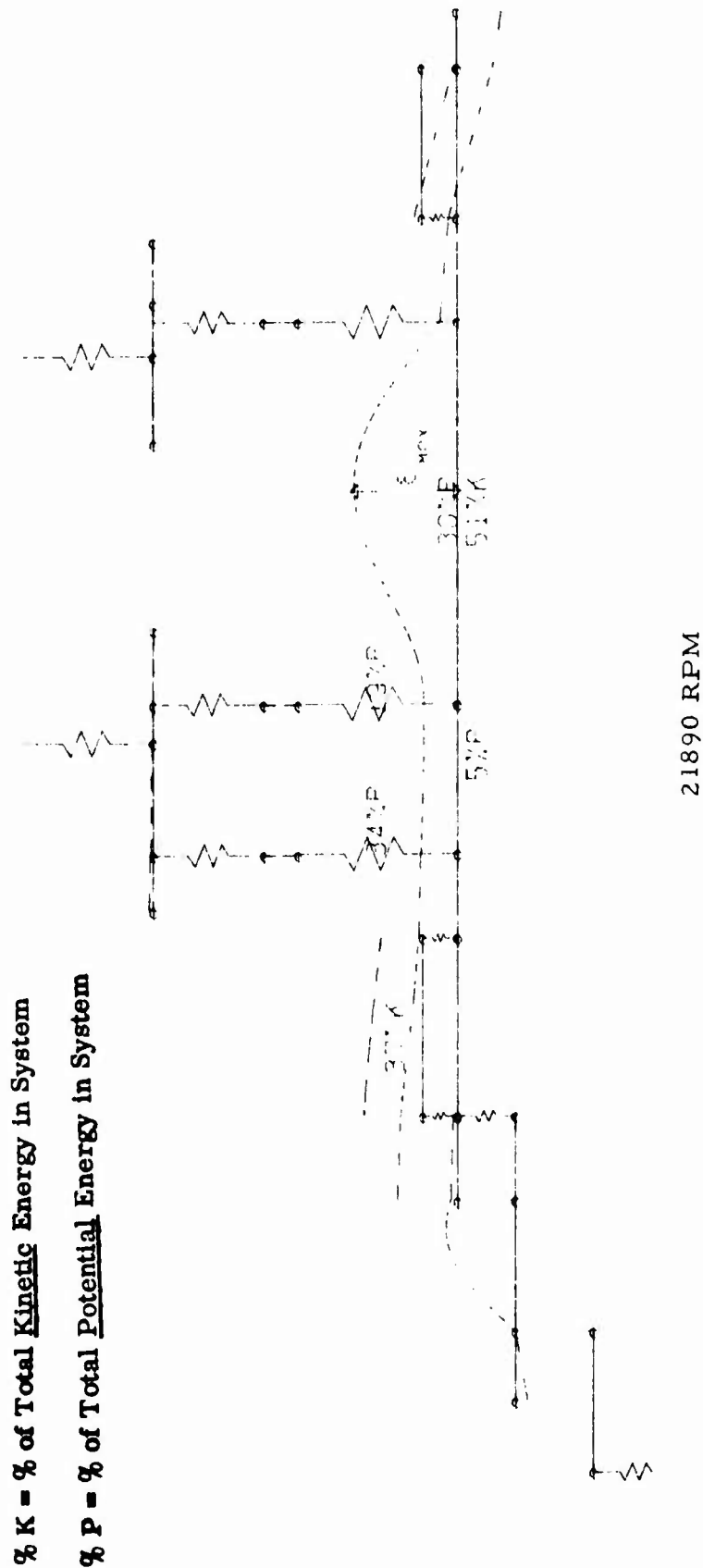


Figure 14. 1st Shaft Bending Critical Mode
Shape - Spring Ring Set No. 1

% K = % of Total Kinetic Energy in System
 % P = % of Total Potential Energy in System

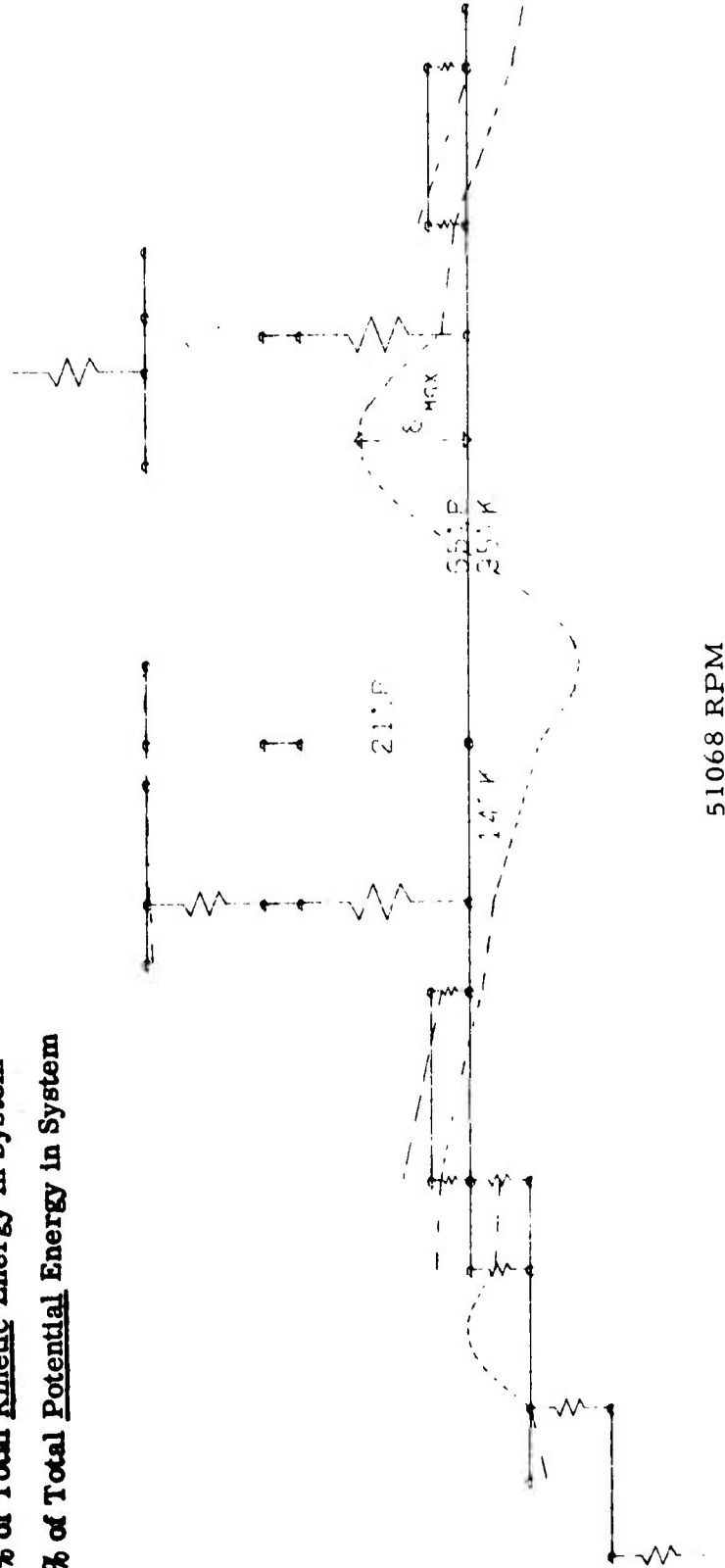


Figure 15. 2nd Shaft Bending Critical Mode Shape - Spring Ring Set No. 1

% K = % of Total Kinetic Energy in System
 % P = % of Total Potential Energy in System

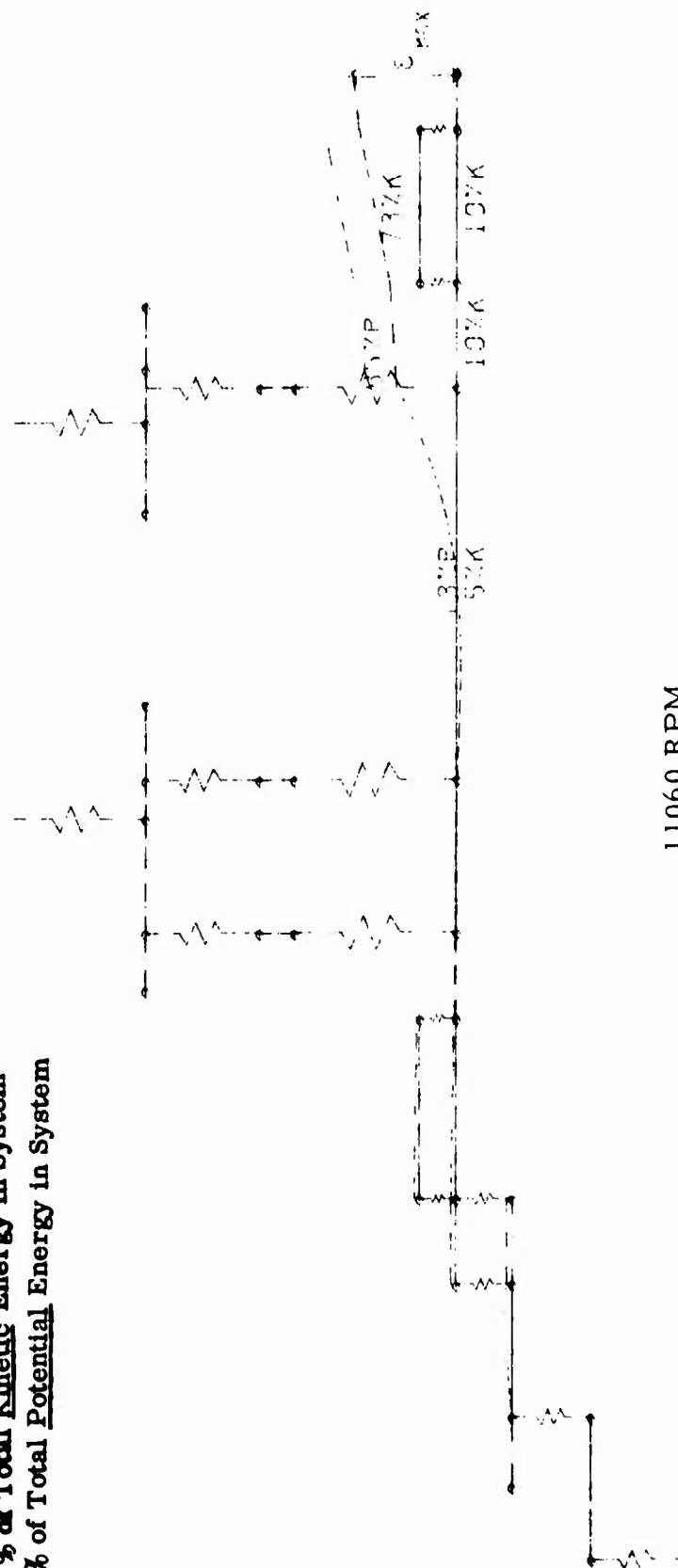
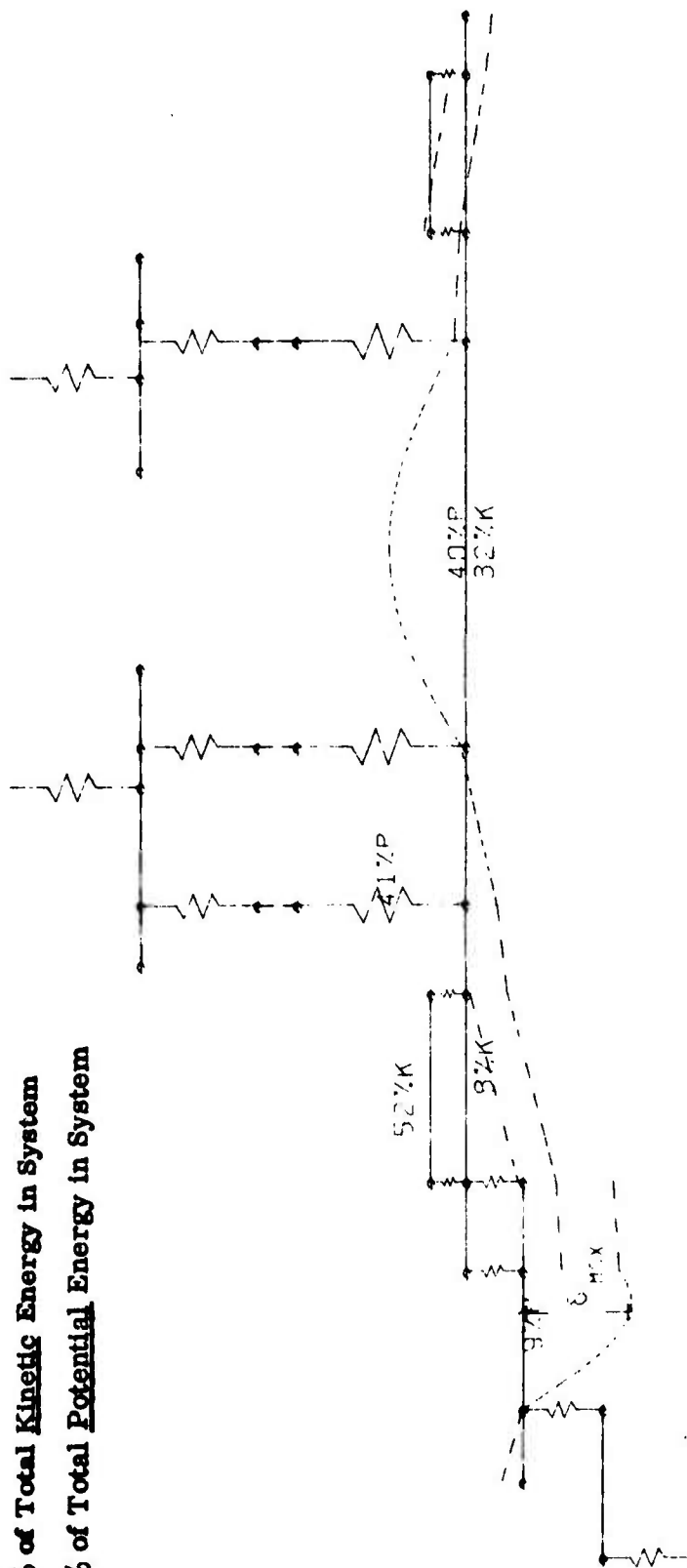


Figure 16. LPT Critical Mode Shape - Spring Ring Set No. 2

% K = % of Total Kinetic Energy in System
 % P = % of Total Potential Energy in System



11978 RPM

Figure 17. Fan & Shaft Critical Mode Shape - Spring Ring Set No. 2

% K = % of Total Kinetic Energy in System
 % P = % of Total Potential Energy in System

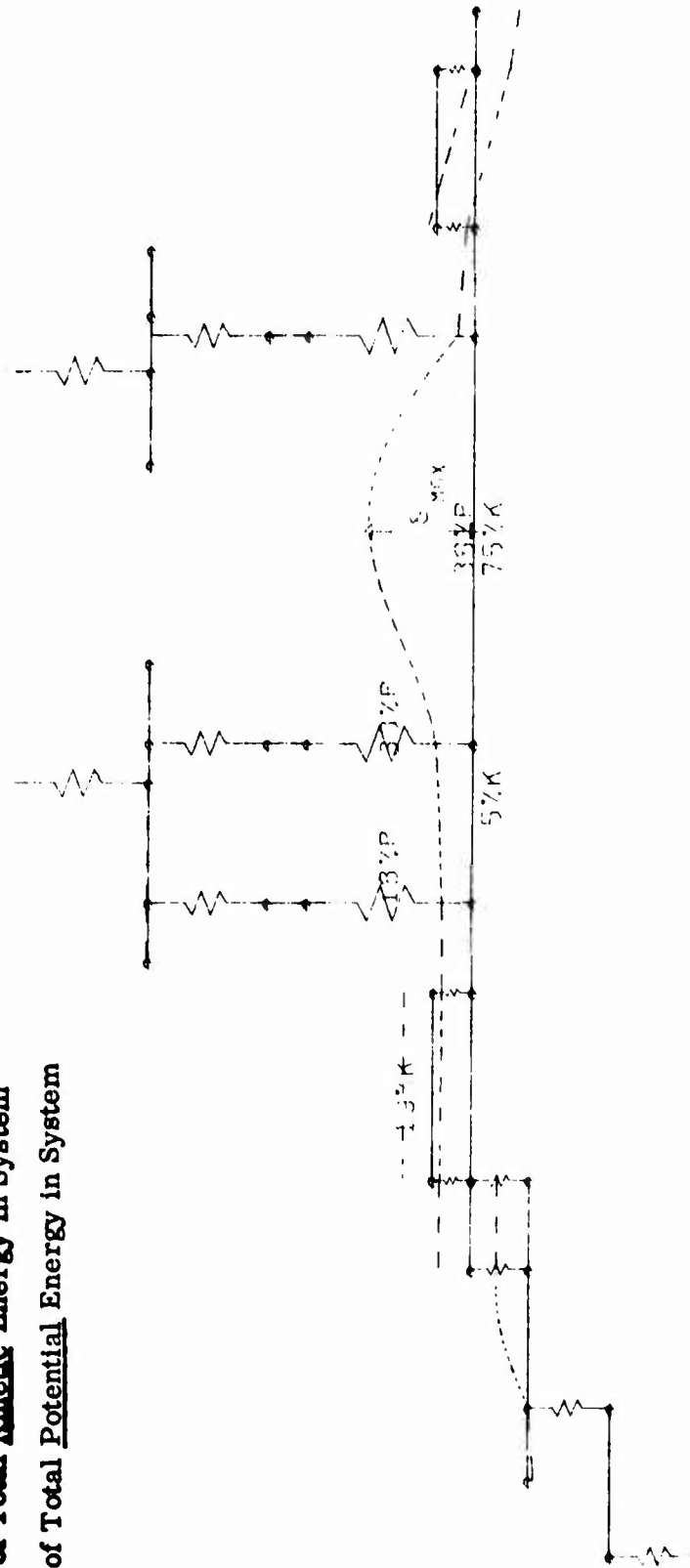


Figure 18. 1st Shaft Bending Critical Mode Shape — Spring Ring Set No. 2

% K = % of Total Kinetic Energy in System
 % P = % of Total Potential Energy in System

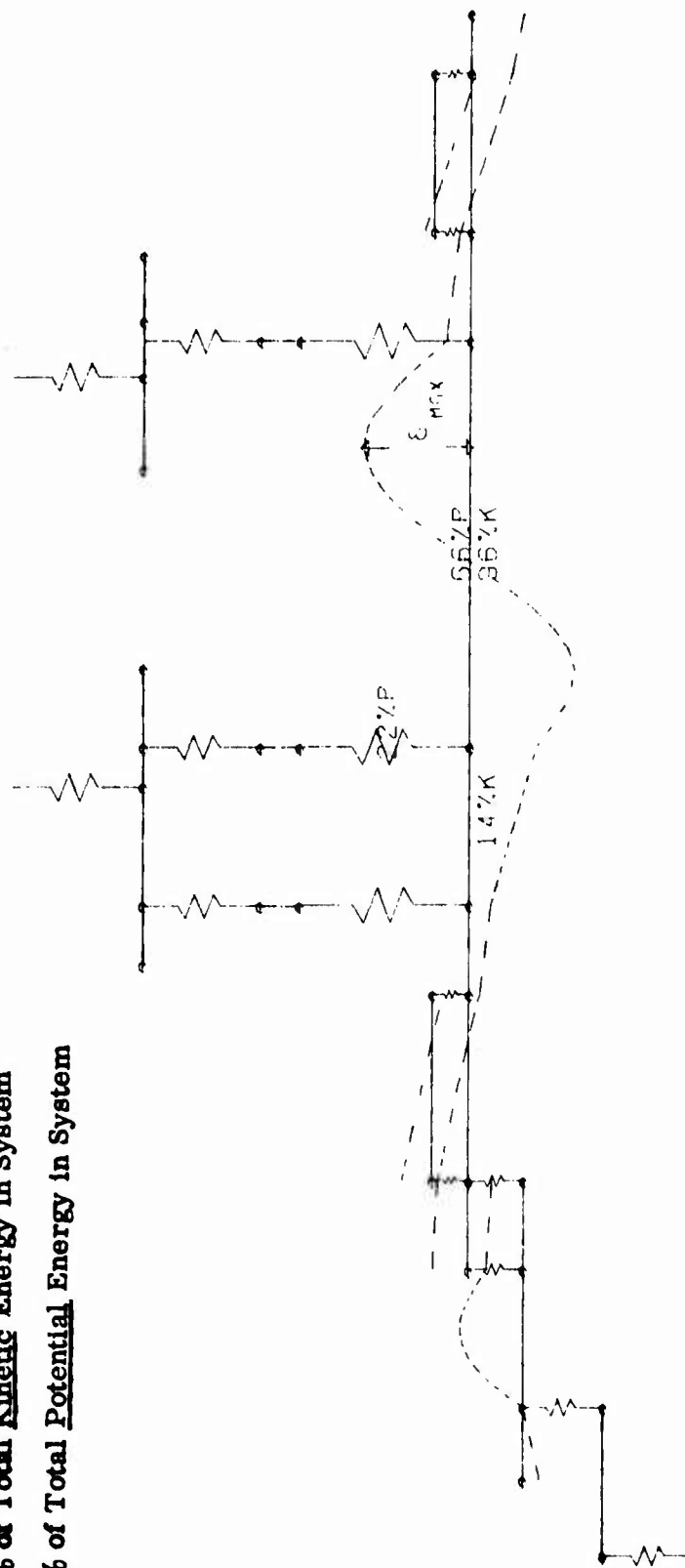


Figure 19. 2nd Shaft Bending Critical Mode Shape - Spring Ring Set No. 2

ACCELEROMETER A1

BENTLY B4

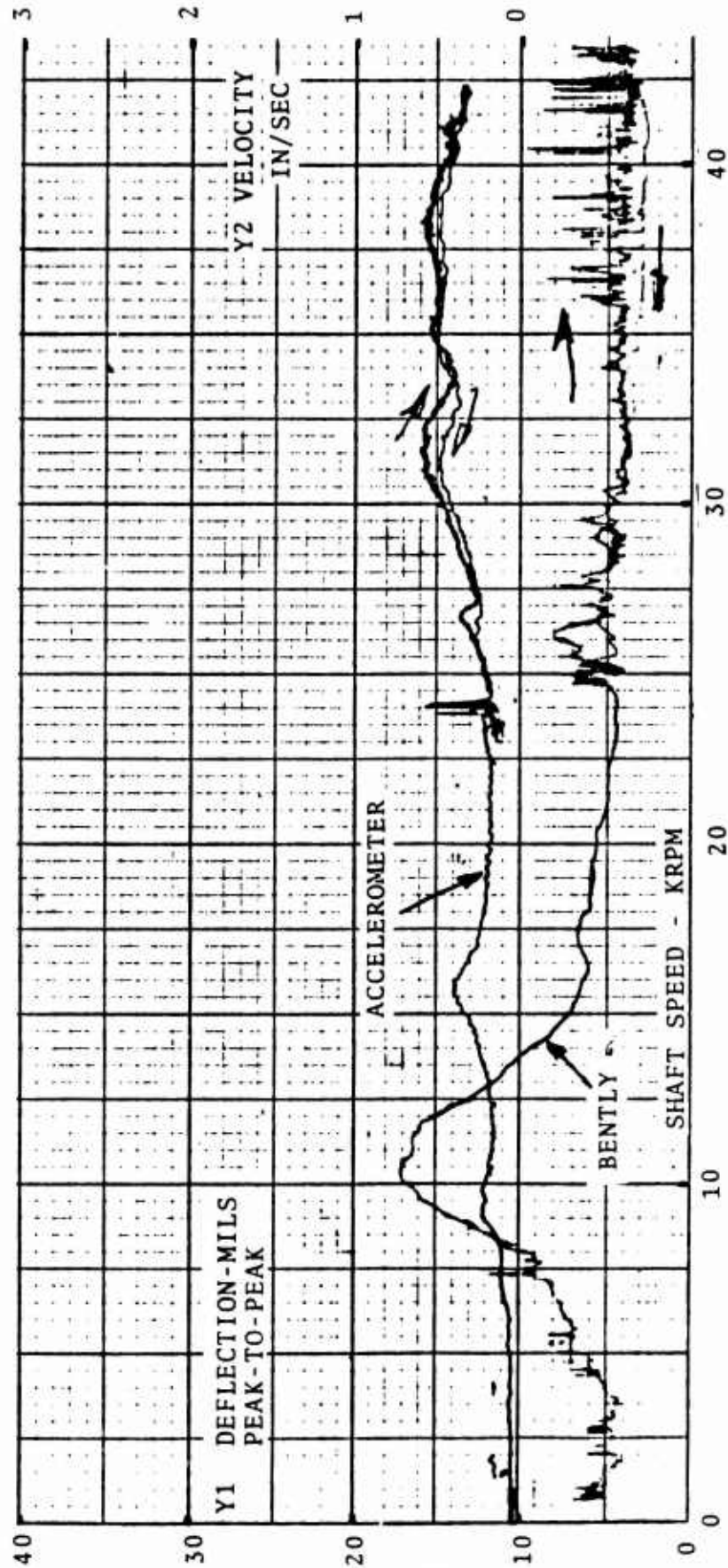
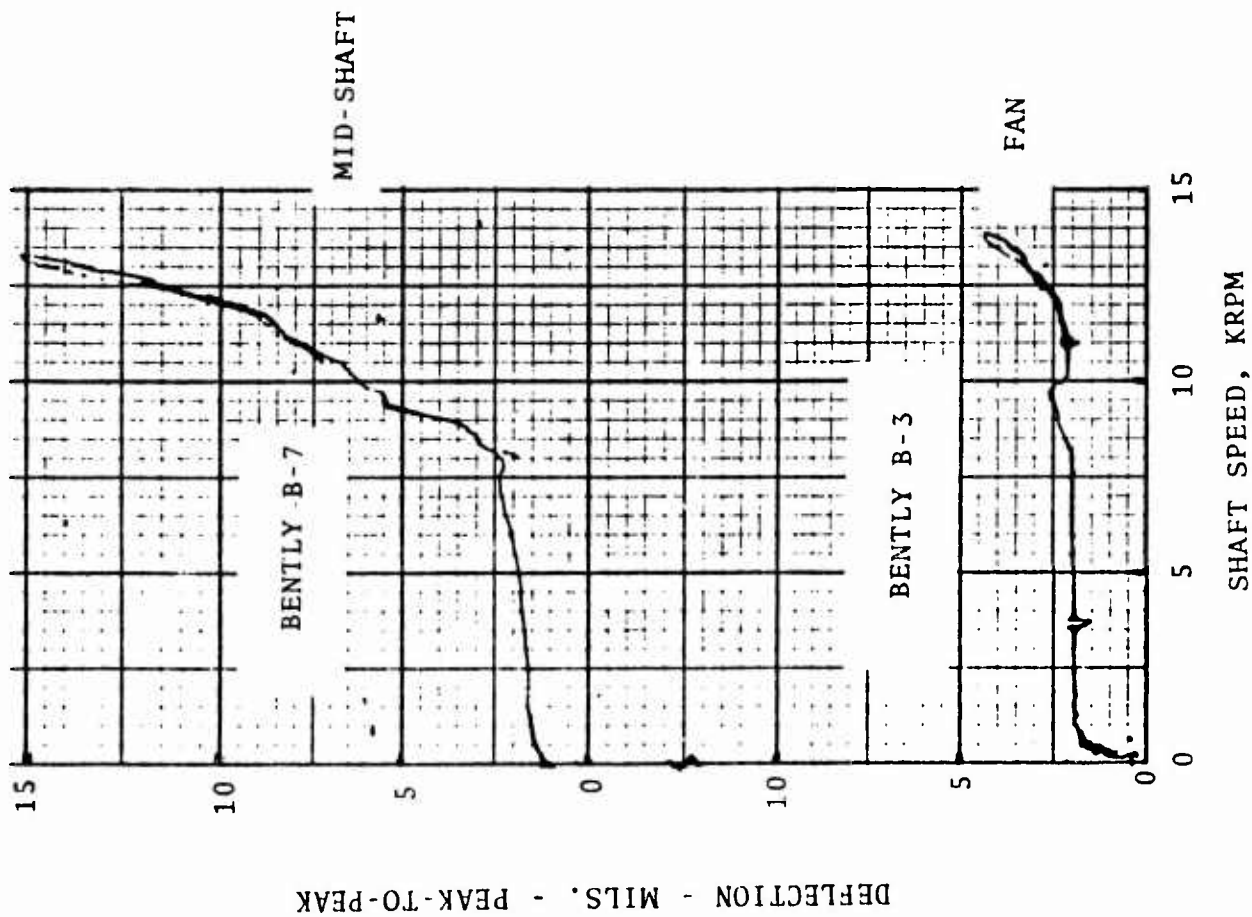


Figure 20. LP SHAFT DYNAMICS RIG- BENTLY PROBE AND ACCELEROMETER OUTPUT VS. SPEED



Spring Ring Set No. 1

NO UNBALANCE WEIGHTS ADDED

Figure 21. LP SHAFT DYNAMICS RIG-TYPICAL MID-SHAFT AND FAN DISK DEFLECTIONS-RUN NO. 9

Spring Ring Set No. 1

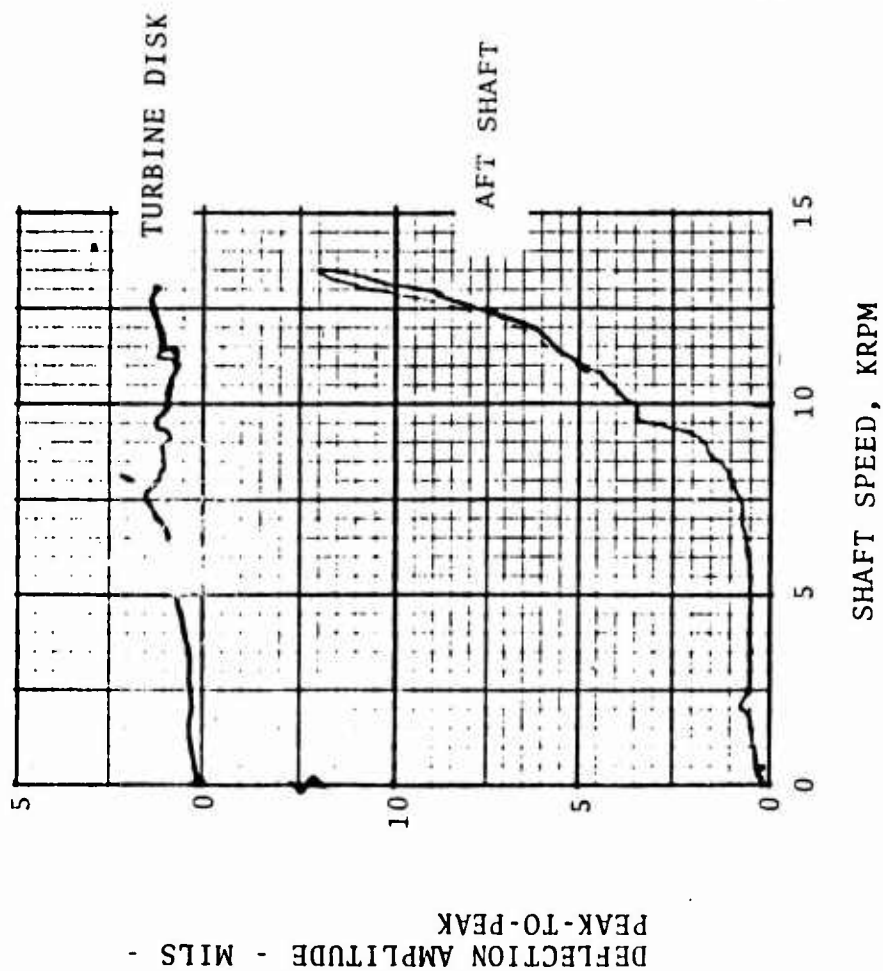


Figure 22 LP SHAFT DYNAMICS RIG-
TURBINE DISK & AFT
SHAFT DEFLECTIONS -
RUN NO. 9

CONSTANT SPEED (12,580 RPM)

NOTE: DATA IS IN VOLTS OR MILLIVOLTS. CONVERSION FACTORS MUST BE APPLIED TO GET MILS (AMPLITUDE) AND DEGREES (PHASE).

Figure 23. LP SHAFT DYNAMICS RIG-TYPICAL AMPLITUDE & PHASE ANGLE OUTPUT

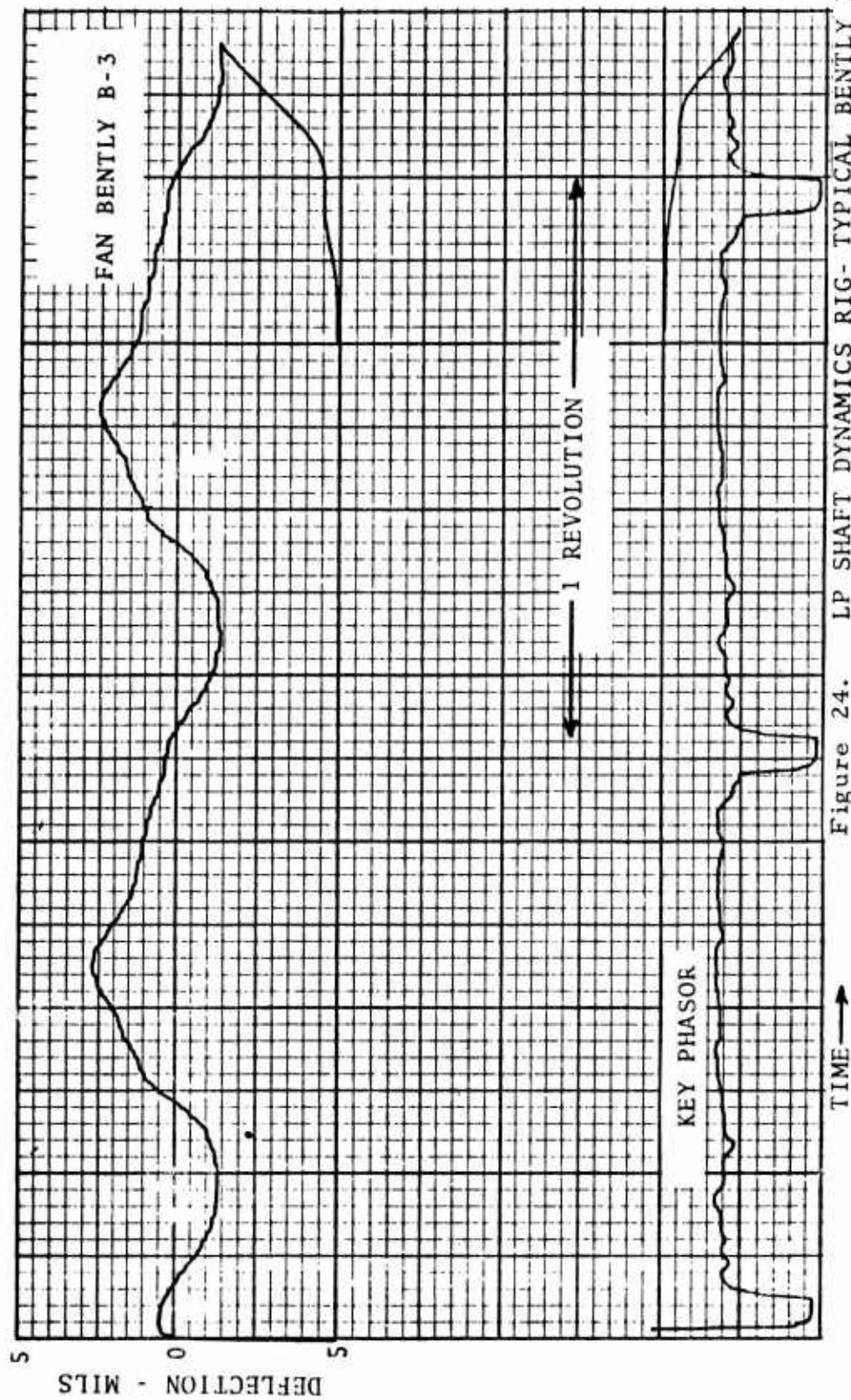


Figure 24. LP SHAFT DYNAMICS RIG- TYPICAL BENTLY PROBE
OUTPUT VS. TIME -
RUN NO. 9

BENTLY B-7 (MID-SHAFT)

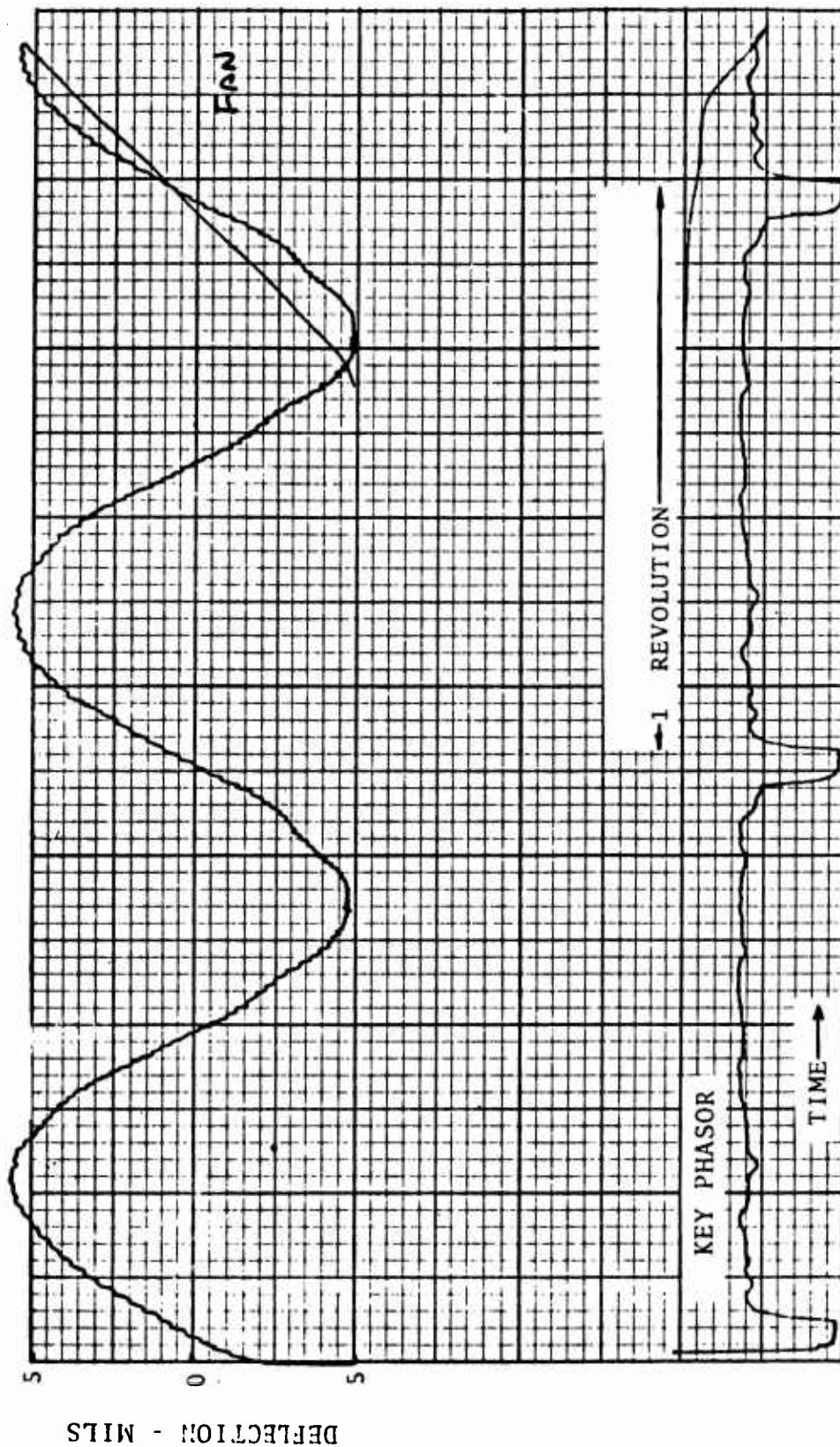
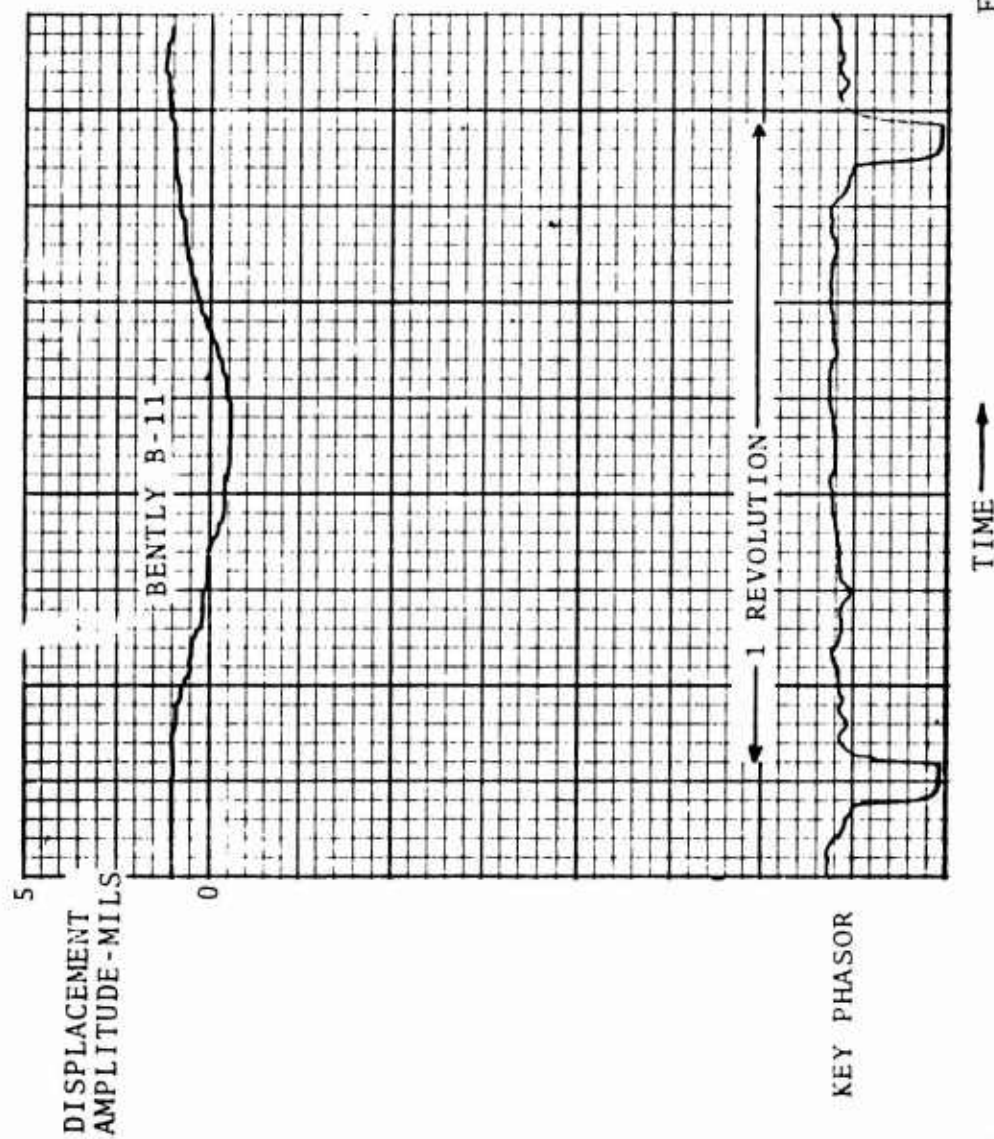


Figure 25. LP SHAFT DYNAMICS RIG- TYPICAL BENTLY PROBE
OUTPUT VS. TIME -
RUN NO. 9

GENERAL ELECTRIC COMPANY
AIRCRAFT ENGINE GROUP



CONSTANT SPEED (12,580 RPM)

Figure 26. LP SHAFT DYNAMICS RIG-TYPICAL BENTLY PROBE & KEY PHASOR OUTPUT V'S. TIME-RUN NO. 9

RUNS 16, 17, & 18

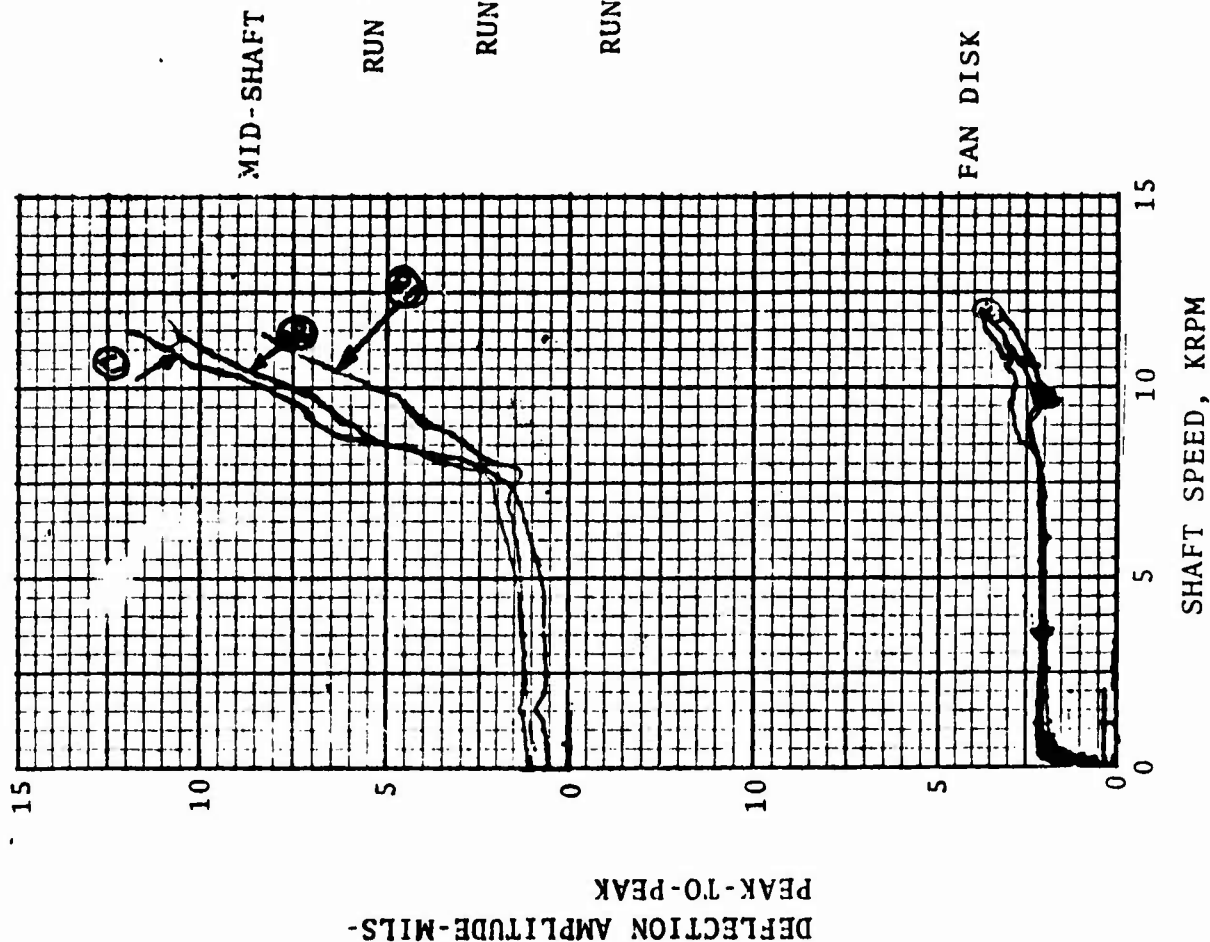


Figure 27. LP SHAFT DYNAMICS RIG-
UNBALANCE SENSITIVITIES
ON MID-SHAFT & FAN DISK
DEFLECTIONS

VIB AMPLITUDE
MILS (P-P)

BALANCE WEIGHTS AFFECTING
BENTLEY READING

MID-SHAFT BENTLY B-7

Initial 3-Plane Balance

Spring Ring Set No. 1

10

5

0

FAN BENTLY B-3

10

5

0

0

10

5

0

0

10

5

0

0

10

5

0

0

10

5

0

0

10

5

0

0

10

5

0

0

10

5

0

0

10

5

0

0

10

5

0

0

10

5

0

0

10

5

0

0

10

5

0

0

10

5

0

0

10

5

0

0

10

5

0

0

10

5

0

0

10

5

0

0

10

5

0

0

10

5

0

0

10

5

0

0

10

5

0

0

10

5

0

0

10

5

0

0

10

5

0

0

10

5

0

0

10

5

0

0

10

5

0

0

10

5

0

0

10

5

0

0

10

5

0

0

10

5

0

0

10

5

0

0

10

5

0

0

10

5

0

0

10

5

0

0

10

5

0

0

10

5

0

0

10

5

0

0

10

5

0

0

10

5

0

0

10

5

0

0

10

5

0

0

10

5

0

0

10

5

0

0

10

5

0

0

10

5

0

0

10

5

0

0

10

5

0

0

10

5

0

0

10

5

0

0

10

5

0

0

10

5

0

0

10

5

0

0

10

5

0

0

10

5

0

0

10

5

0

0

10

5

0

0

10

5

0

0

10

5

0

0

10

5

0

0

10

5

0

0

10

5

0

0

10

5

0

0

10

5

0

0

10

5

0

0

10

5

0

0

10

5

0

0

10

5

0

0

10

5

0

0

10

5

0

0

10

5

0

0

10

5

0

0

10

5

0

0

10

5

0

0

10

5

0

0

10

5

0

0

10

5

0

0

10

5

0

0

10

5

0

0

10

5

0

0

10

5

0

0

10

5

0

0

10

5

0

0

10

5

0

0

10

5

0

0

10

5

0

0

10

5

0

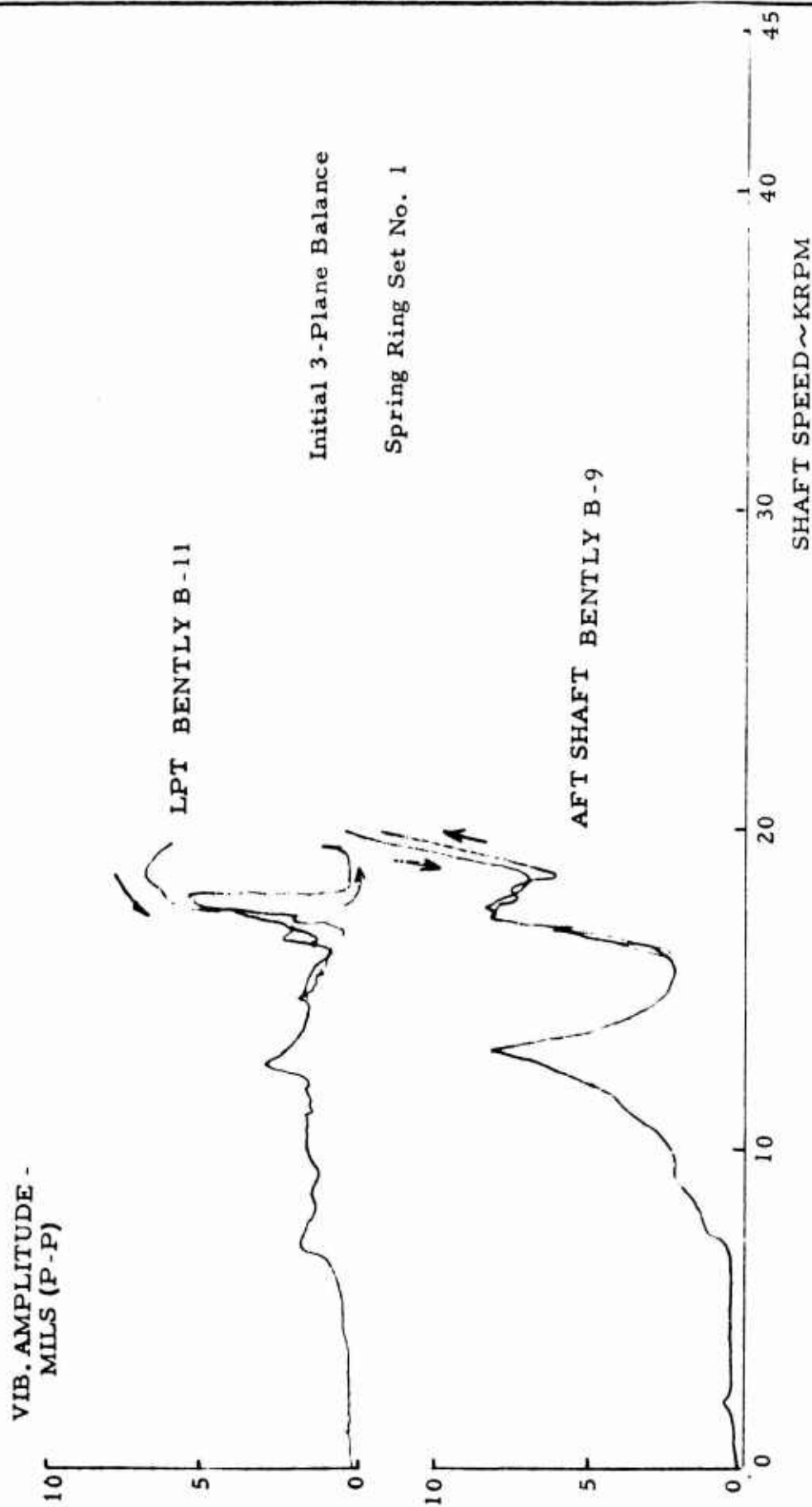


Figure 29-Shaft Dynamics Rig - Run 36

VIB. AMPLITUDE -
MILS (P-P)

Additional 1 Plane Balance
Spring Ring Set No. 1

FWD SHAFT BENTLY B-5

FAN BENTLY B-3

SHAFT SPEED ~KRPM

Figure 30 Shaft Dynamics Rig - Runs 43 & 48

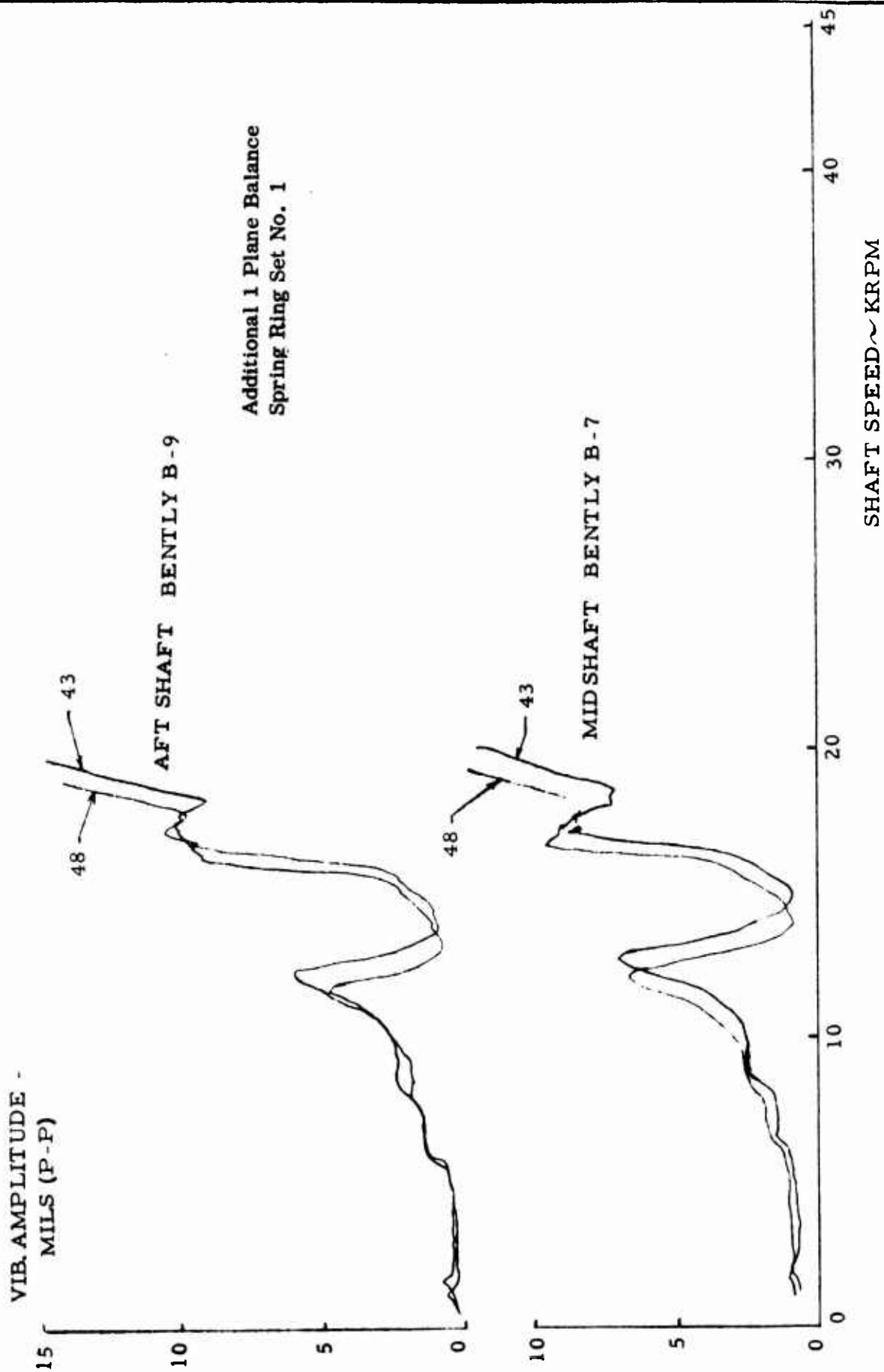


Figure 31 Shaft Dynamics Rig - Runs 43 & 48

Additional 1 Plane Balance
Spring Ring Set No. 1

VIB. AMPLITUDE -
MILS (P-P)

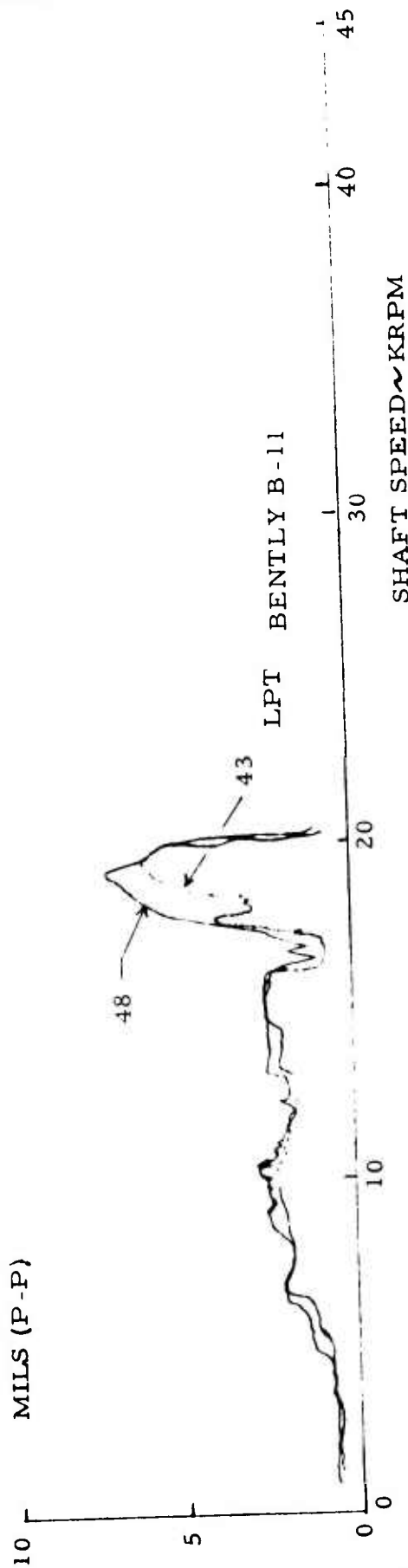


Figure 32 - Shaft Dynamics Rig - Runs 43 & 48

VIB. AMPLITUDE
MILS (P-P)

Spring Ring Set No. 1

FWD SHAFT BENTLY B-5

FAN BENTLY B-3

SHAFT SPEED ~ KRPM

Figure 33 - Shaft Dynamics Rig - Run 56

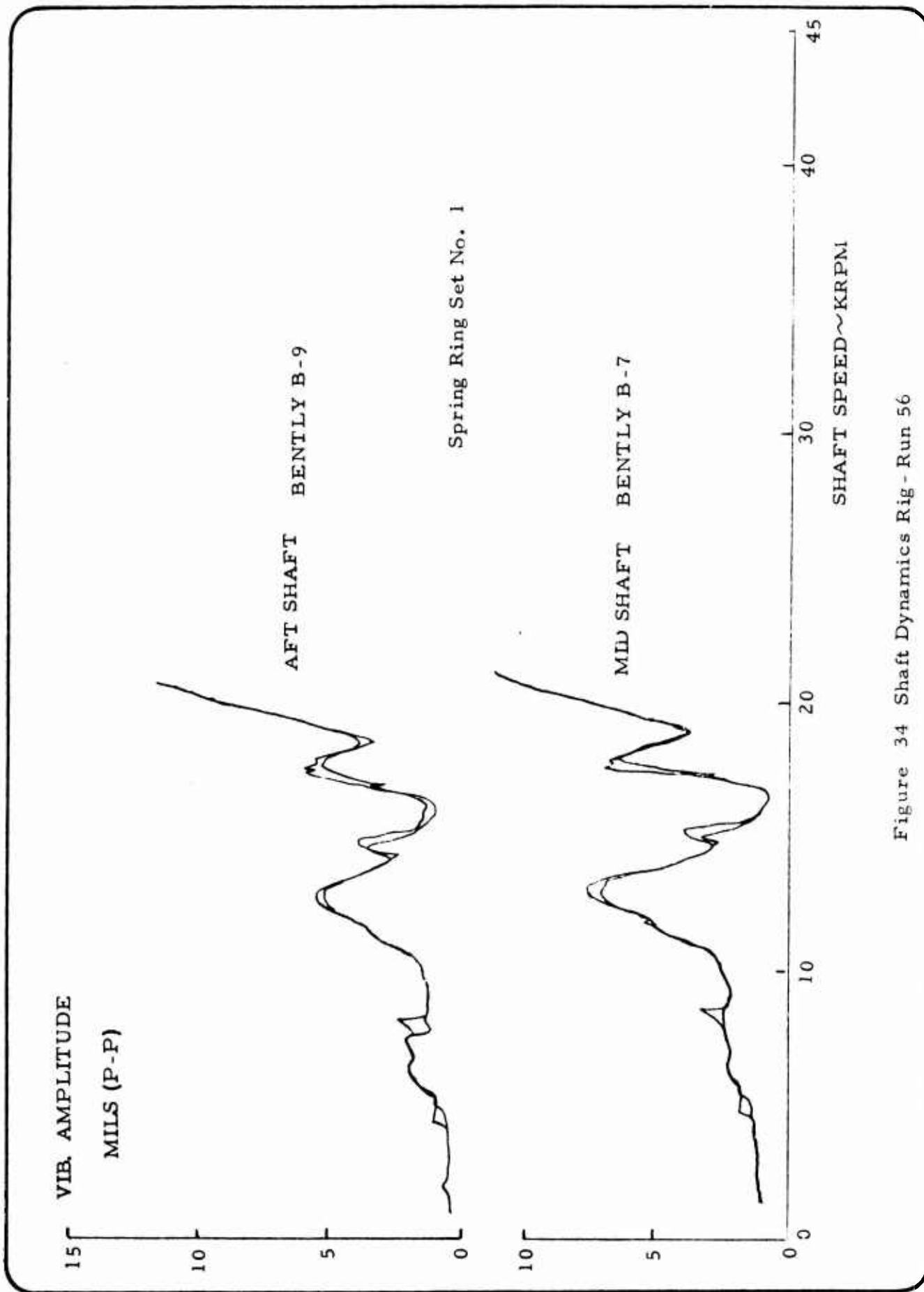


Figure 34 Shaft Dynamics Rig - Run 56

Spring Ring Set No. 1

VIB. AMPLITUDE -
MILS (P-P)

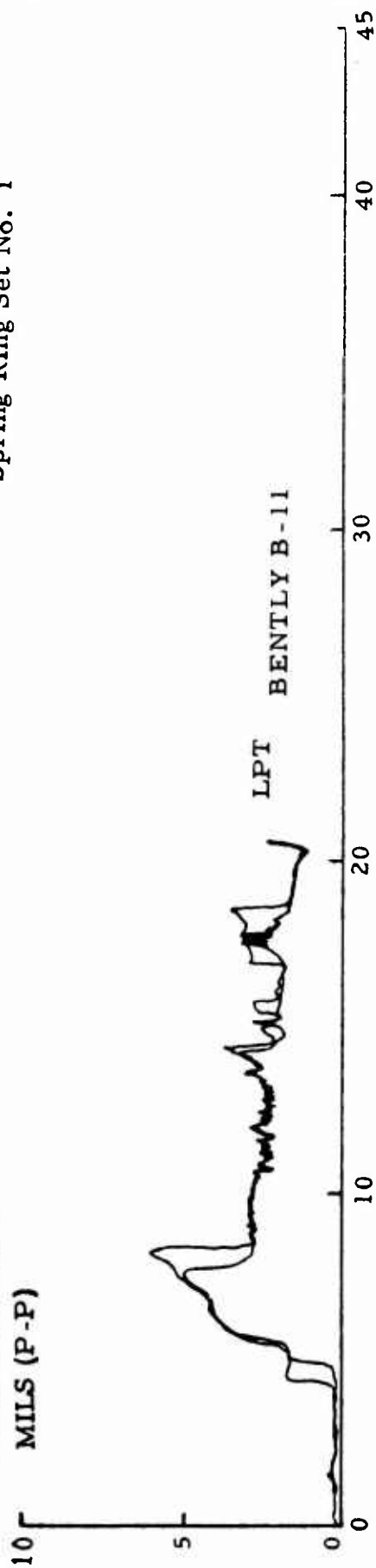


Figure 35 - Shaft Dynamics Rig - Run 56

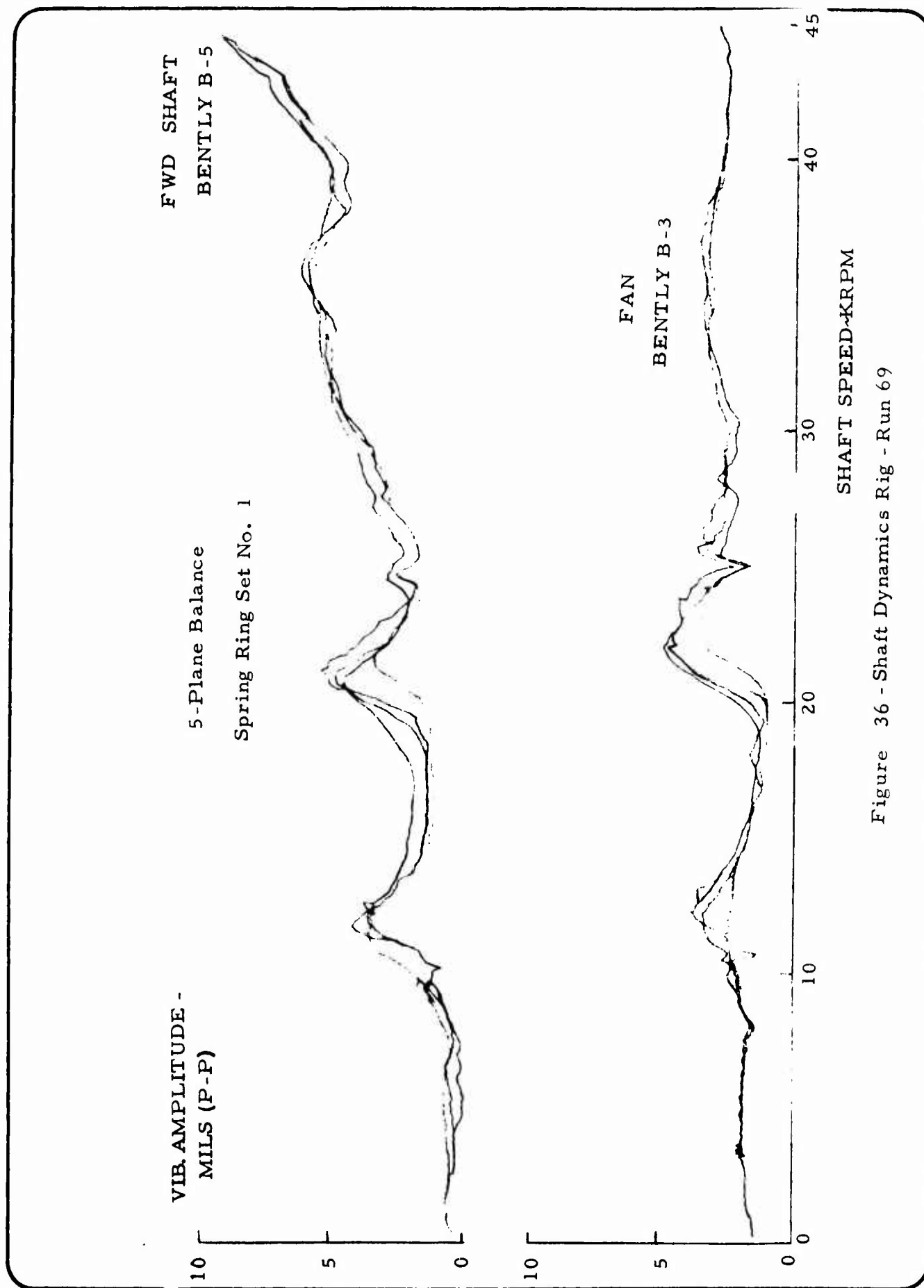


Figure 36 - Shaft Dynamics Rig - Run 69

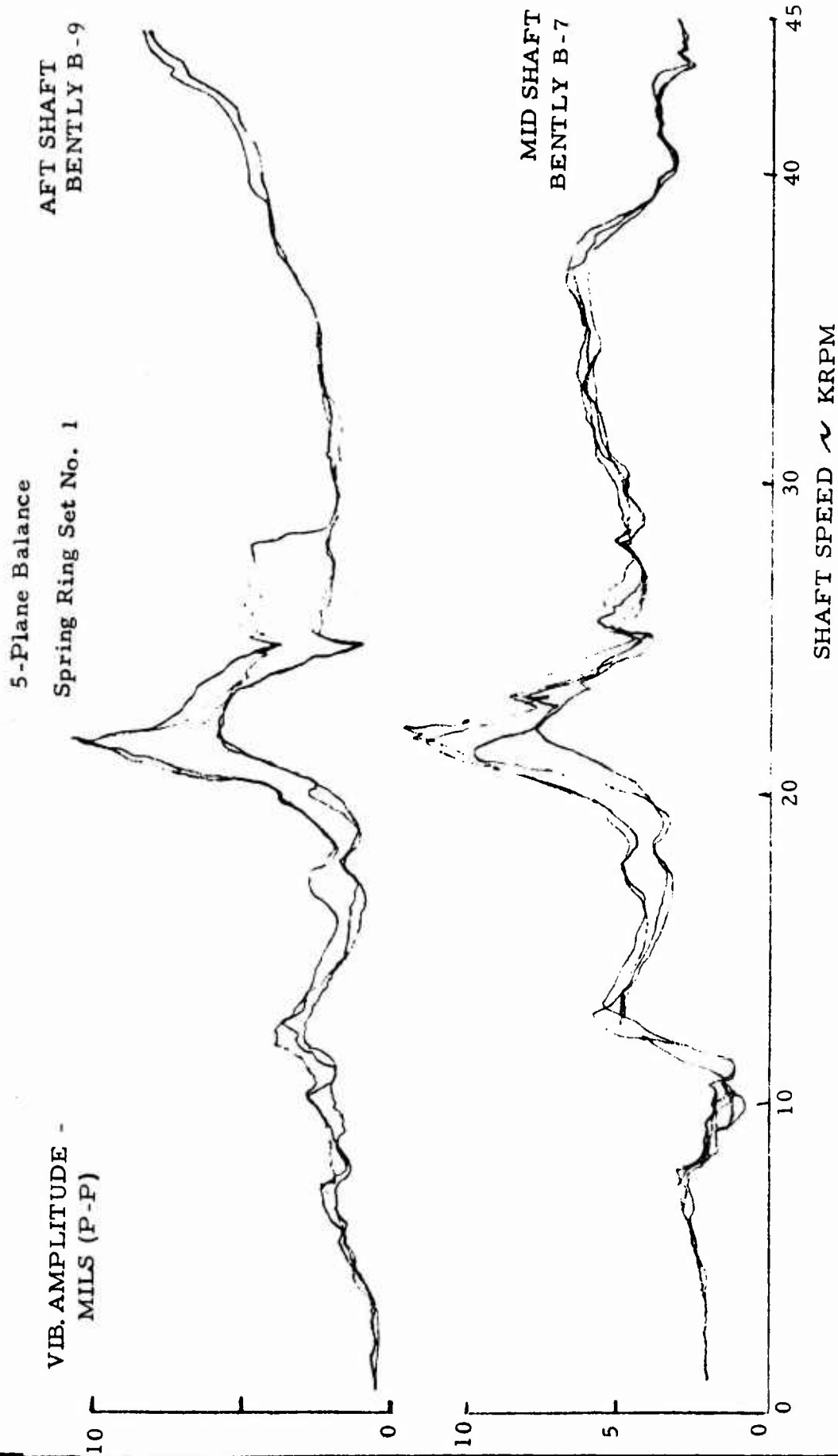


Figure 37 - Shaft Dynamics Rig - Run 69

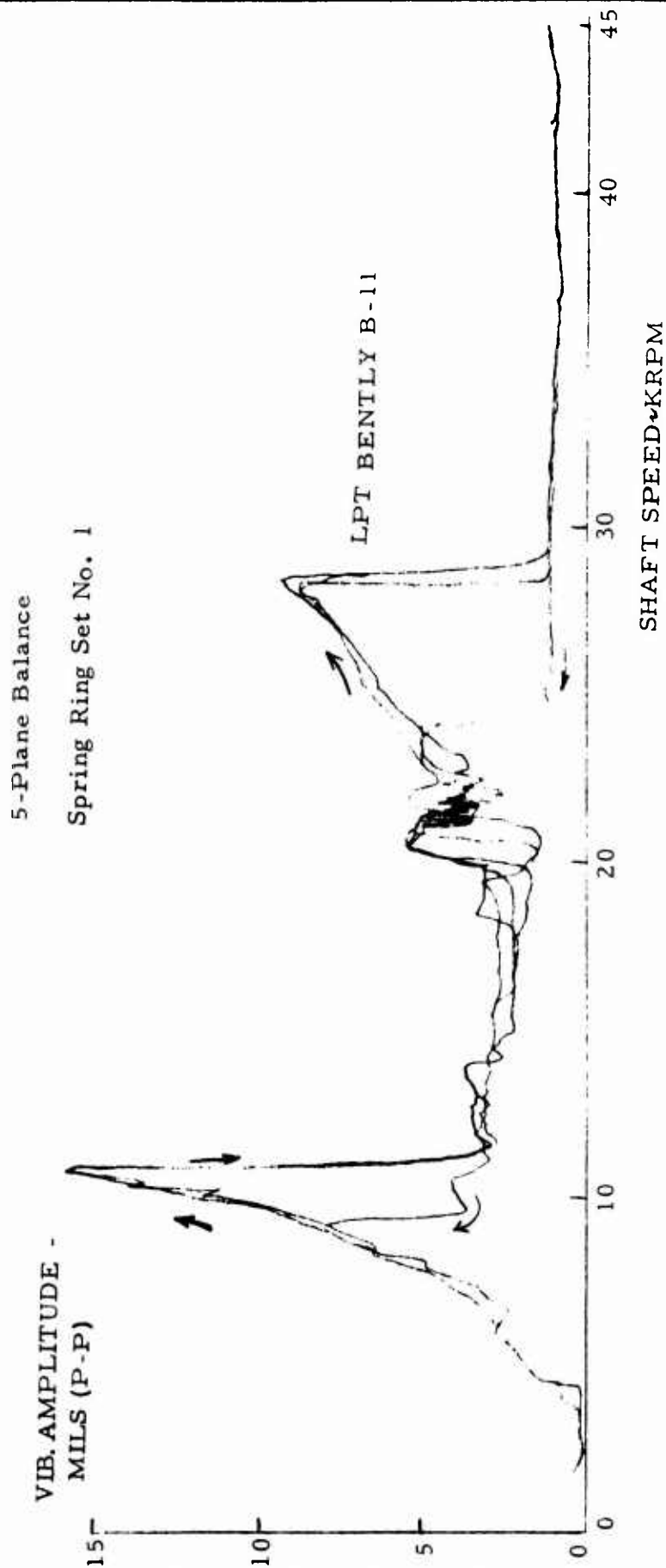
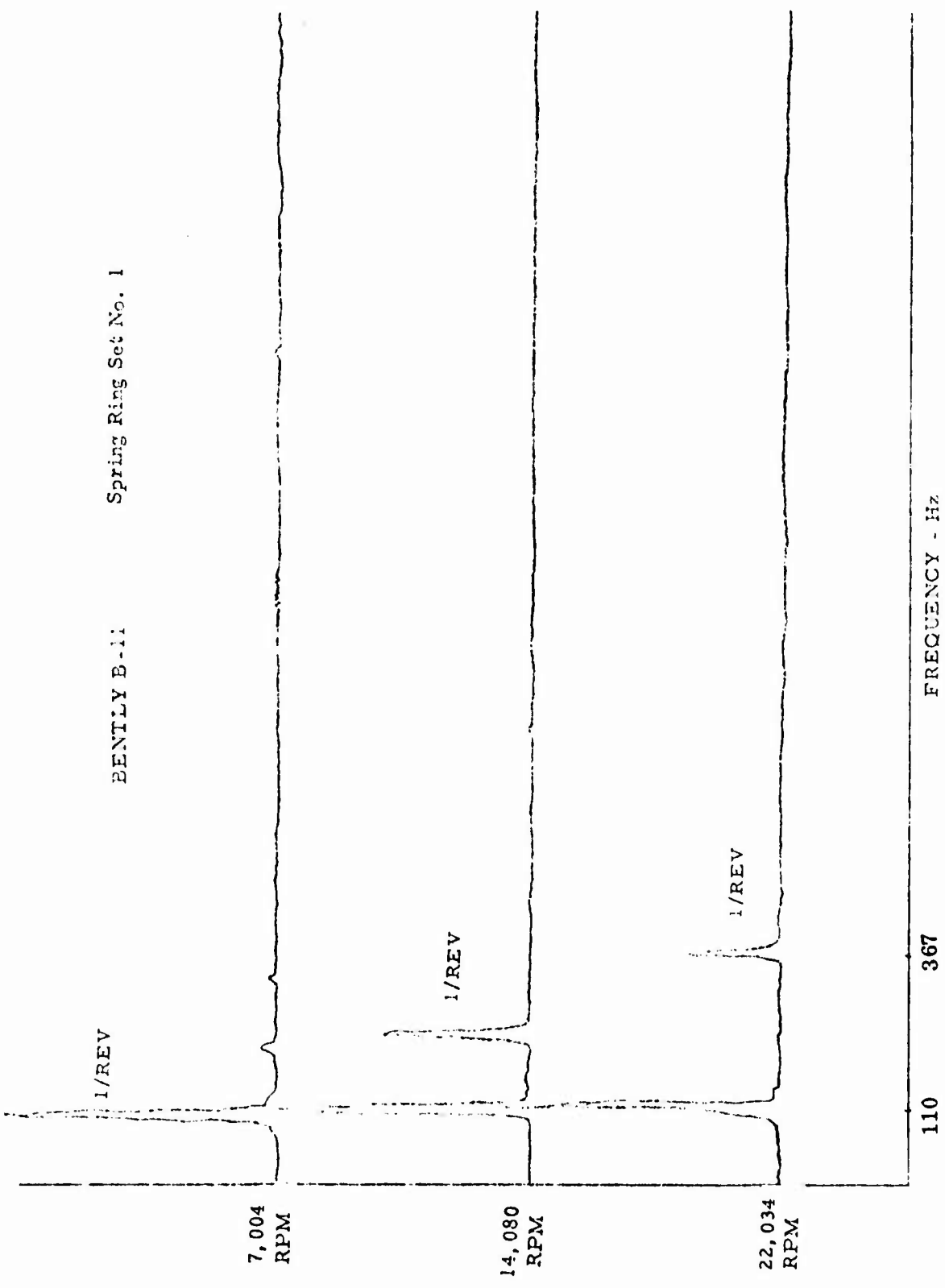


Figure 38 -Shaft Dynamics Rig-Run 69

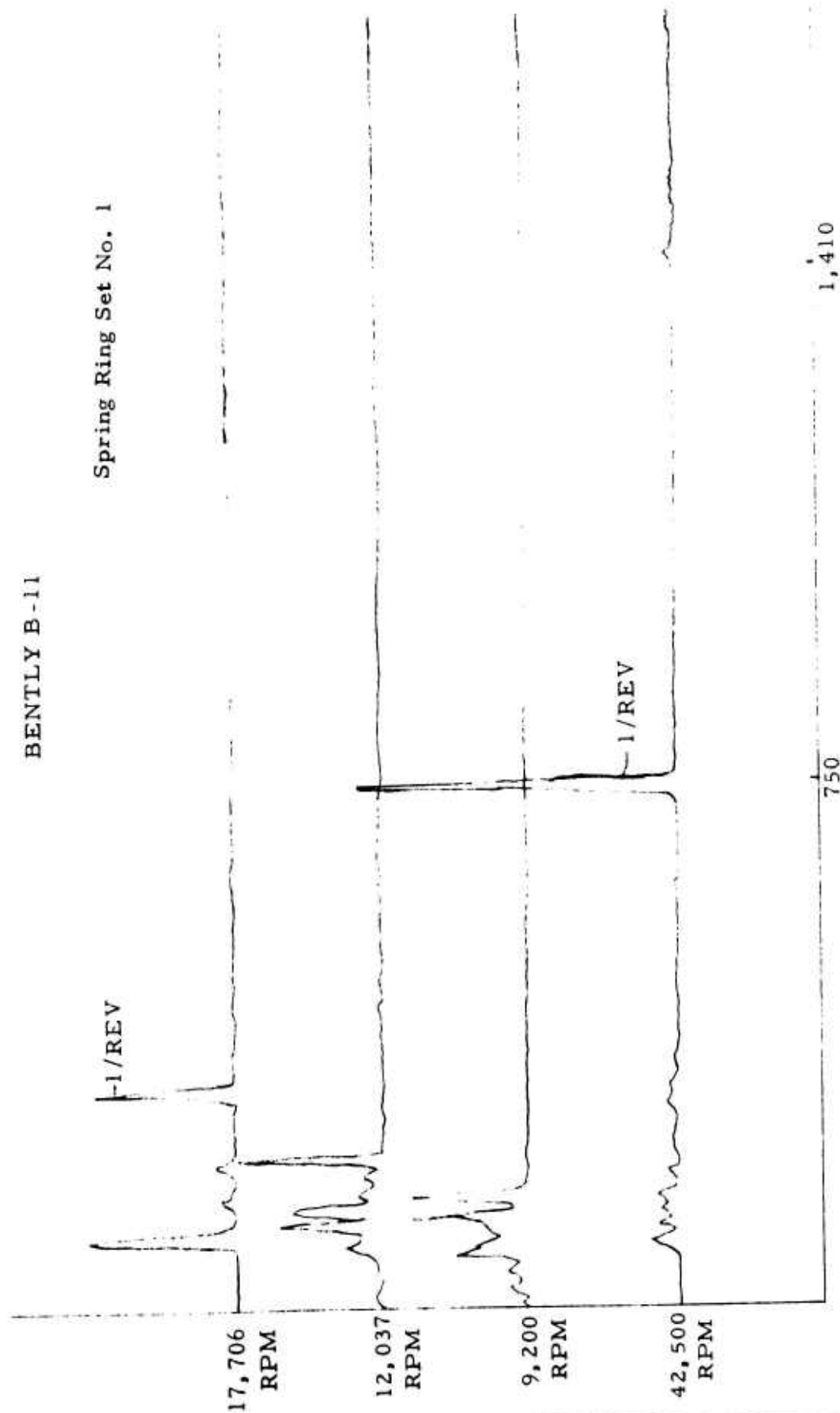


BENTLY B-II Spring Ring Set No. 1

Figure 39-LPT Non-Synchronous Response RUN #91

BENTLY B-11

Spring Ring Set No. 1



FREQUENCY - Hz

Figure 40 -LPT NonSynchronous Response - RUN #91

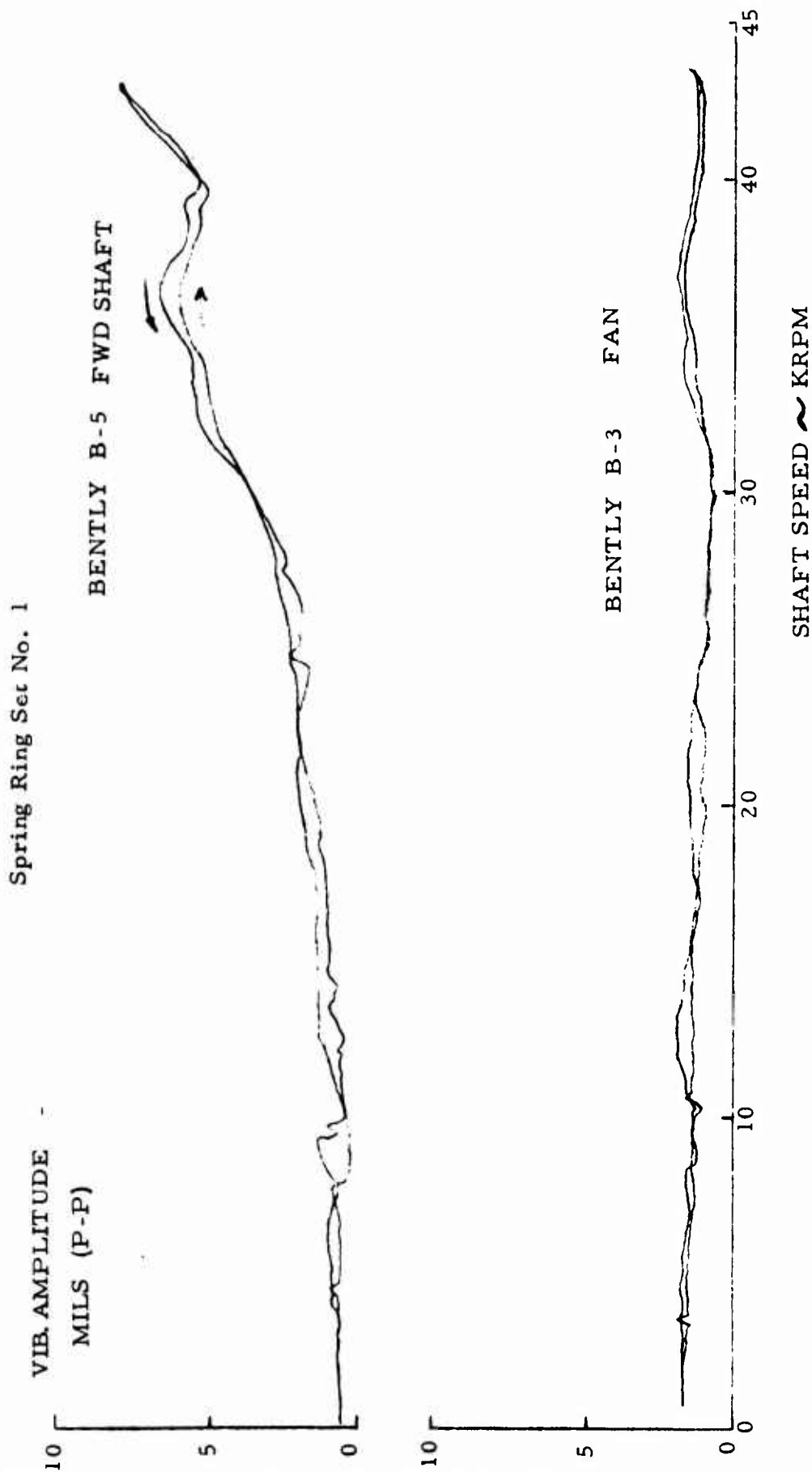


Figure 41 - Shaft Dynamics Rig - Run 80

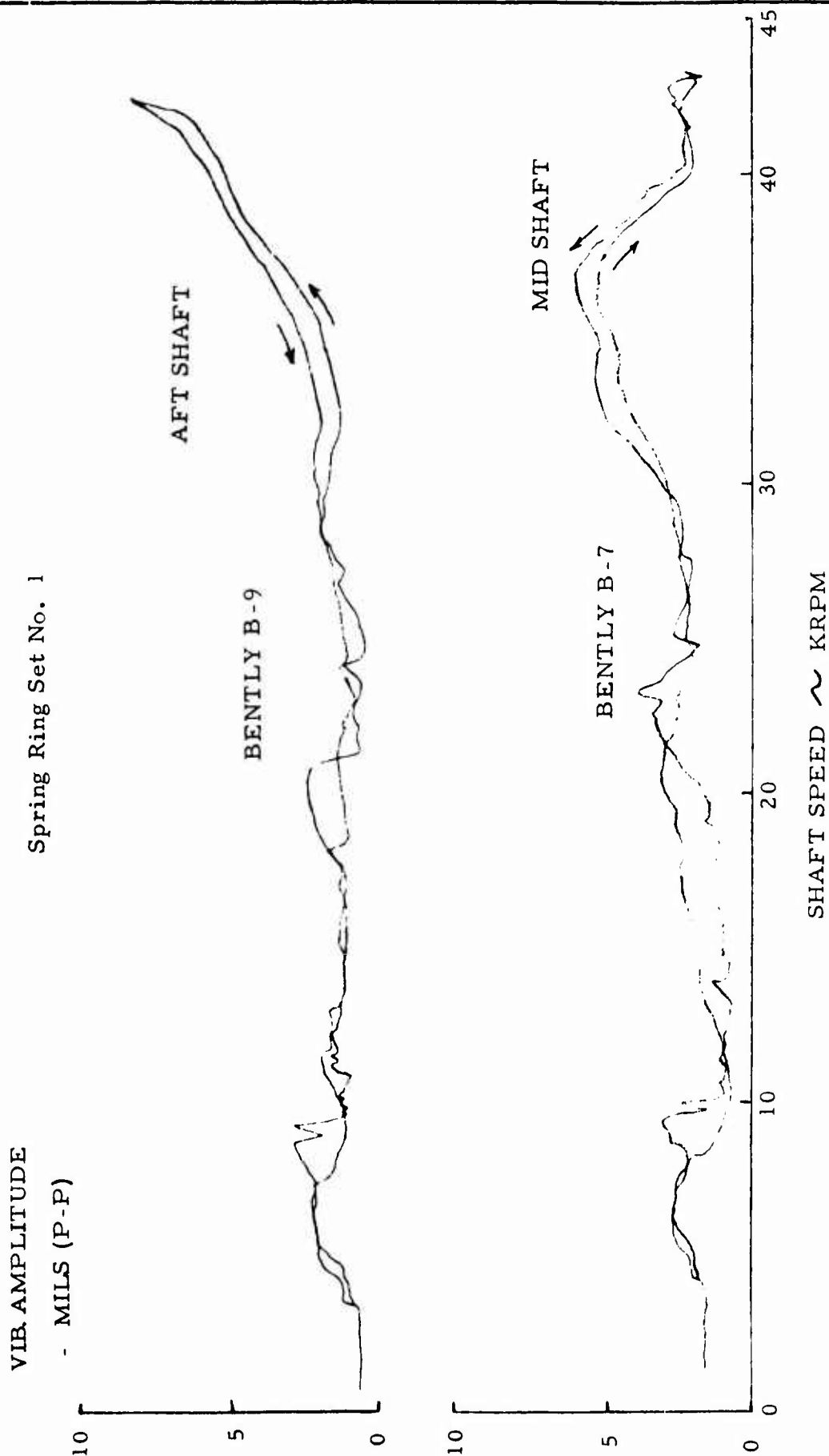


Figure 42 - Shaft Dynamics Rig - Run 80

VIB. AMPLITUDE
- MILS (P-P)

Spring Ring Set No. 1

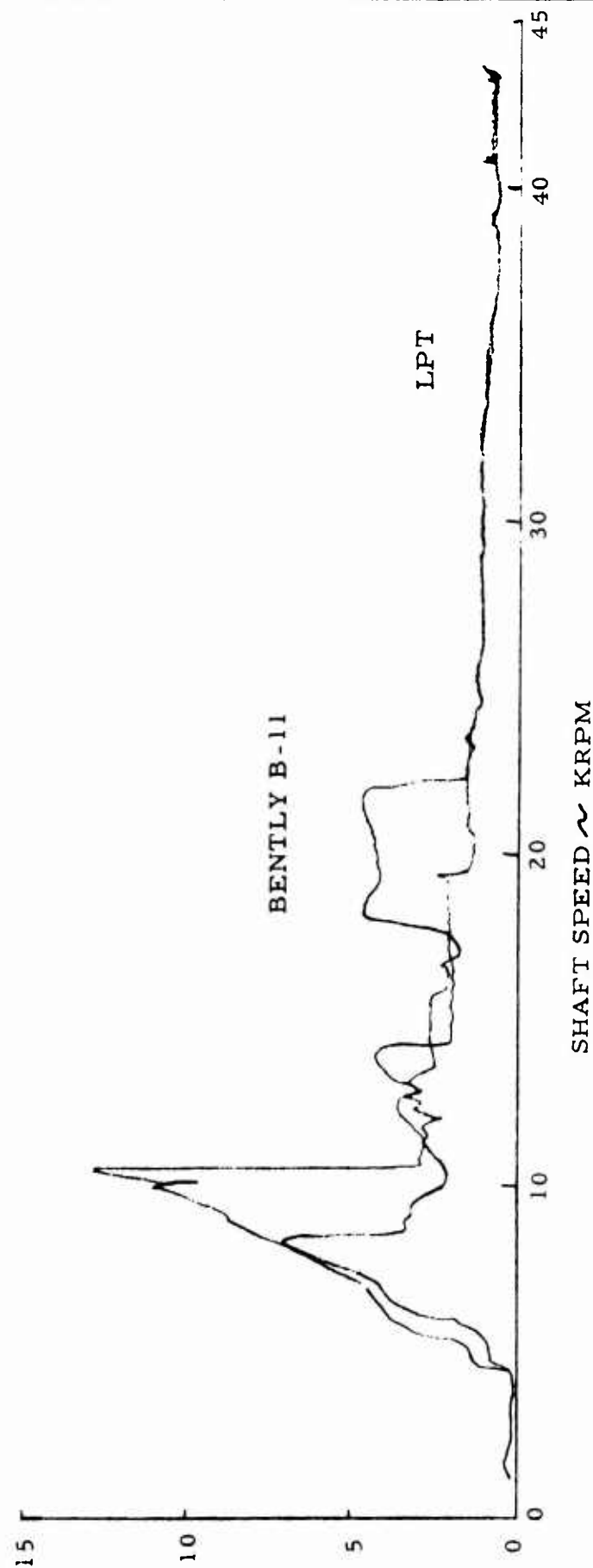


Figure 43 - Shaft Dynamics Rig - Run 80

VIB. AMPLITUDE
- MILS (P-P)

Spring Ring Set No. 2

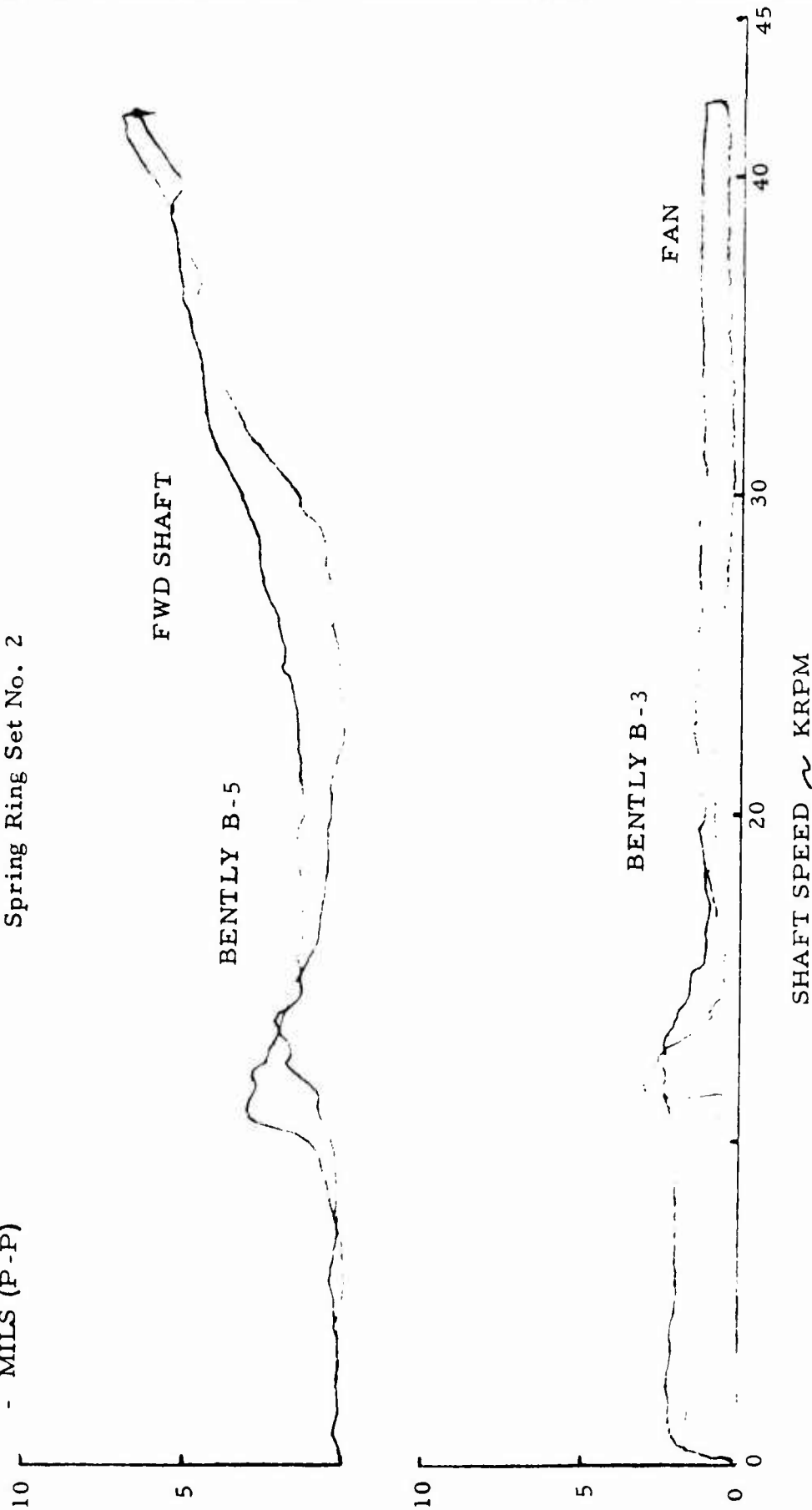


Figure 44 - Shaft Dynamics Rig - Run 01

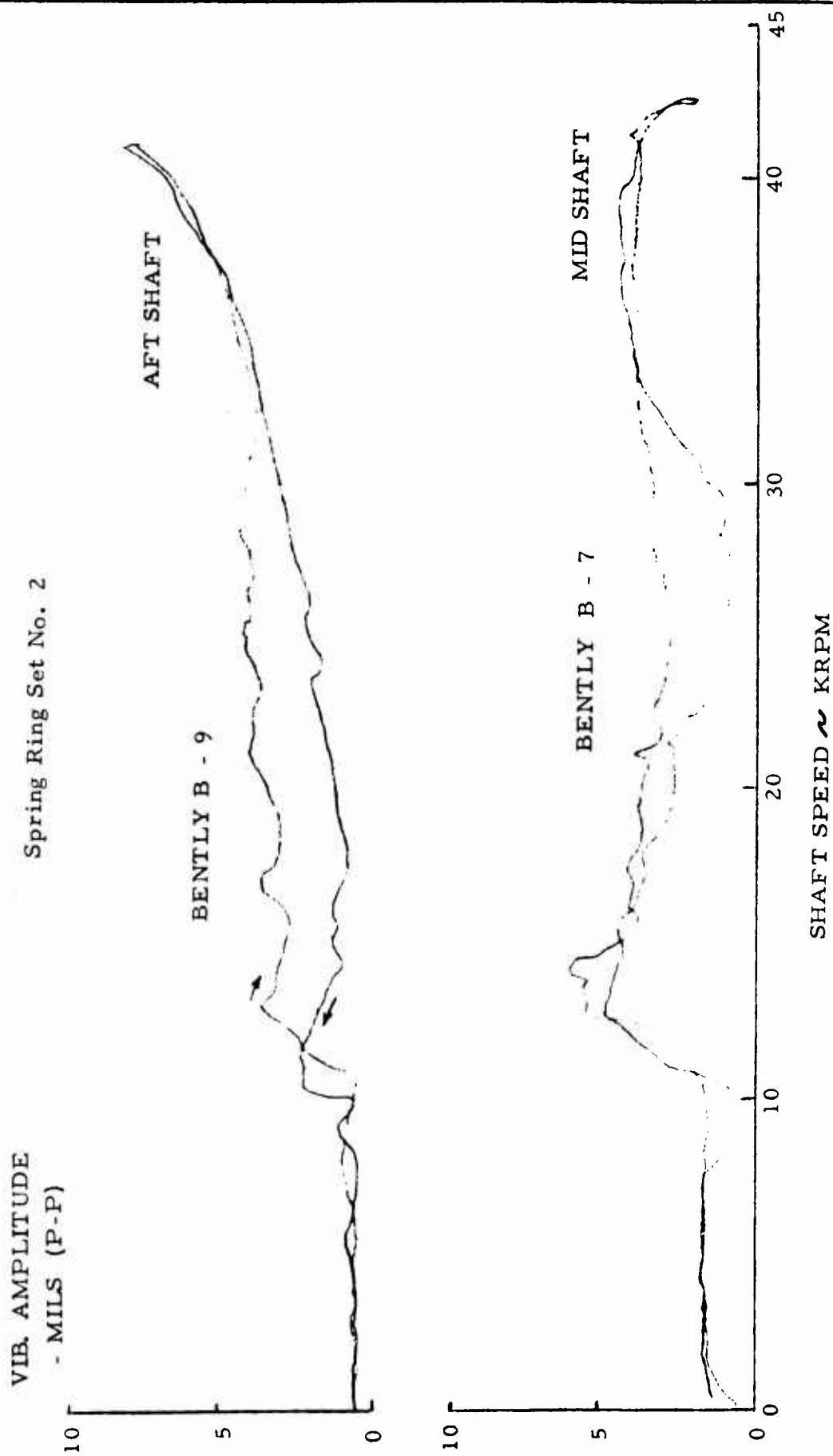


Figure 45 - Shaft Dynamics Rig-Run 01

Spring Ring Set No. 2

VIB. AMPLITUDE

- MILS (P-P)

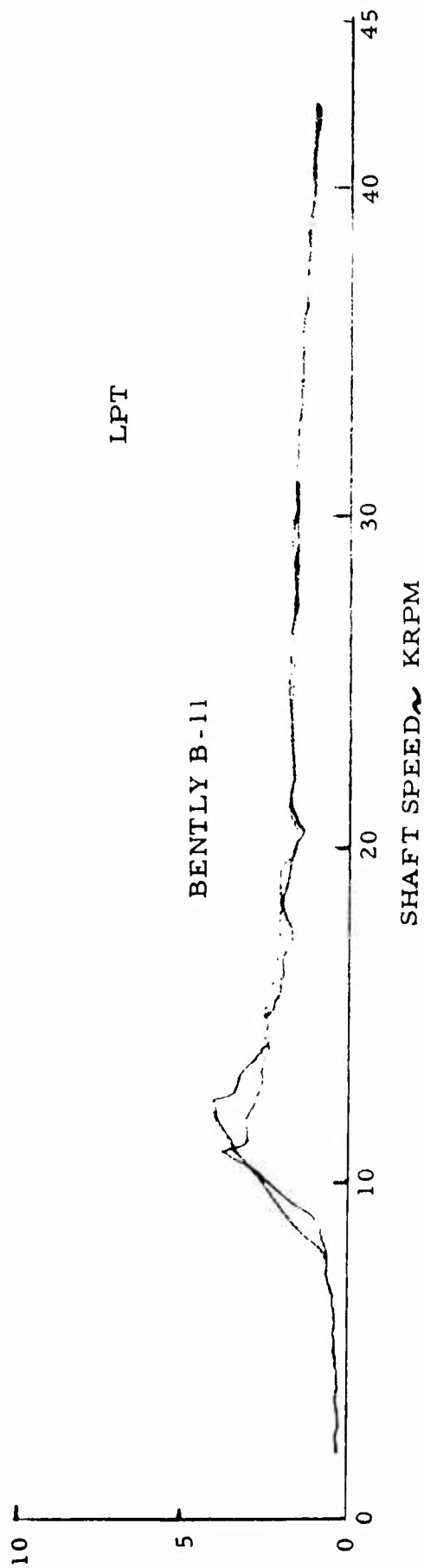


Figure 46 - Shaft Dynamics Rig - Run 01

VIBRATION AMPLITUDE
- MILS - (P - P)

Spring Ring Set No. 2

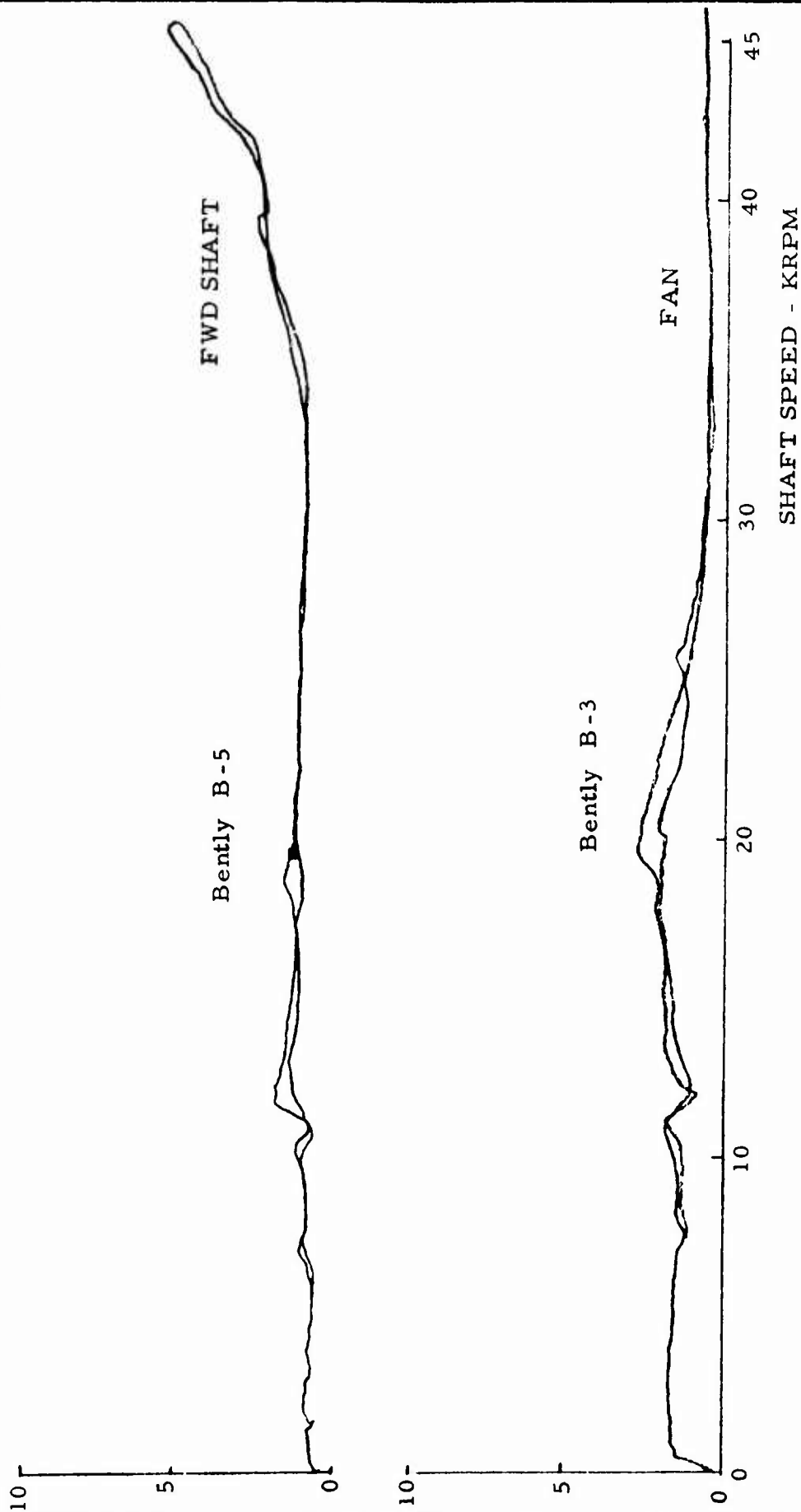


Figure 47 - Vibration Amplitude vs Speed -
Run No. 14

Spring Ring Set No. 2

VIBRATION AMPLITUDE
- MILS - (P - P)

10

AFT - SHAFT

Bently B-9

5

0

MID - SHAFT

Bently B-7

10

20

30

40

45

SHAFT SPEED - KRPM

Figure 48.- Vibration Amplitude vs Speed -
Run No. 14

Spring Ring Set No. 2

VIBRATION AMPLITUDE
-MILS- (P - P)

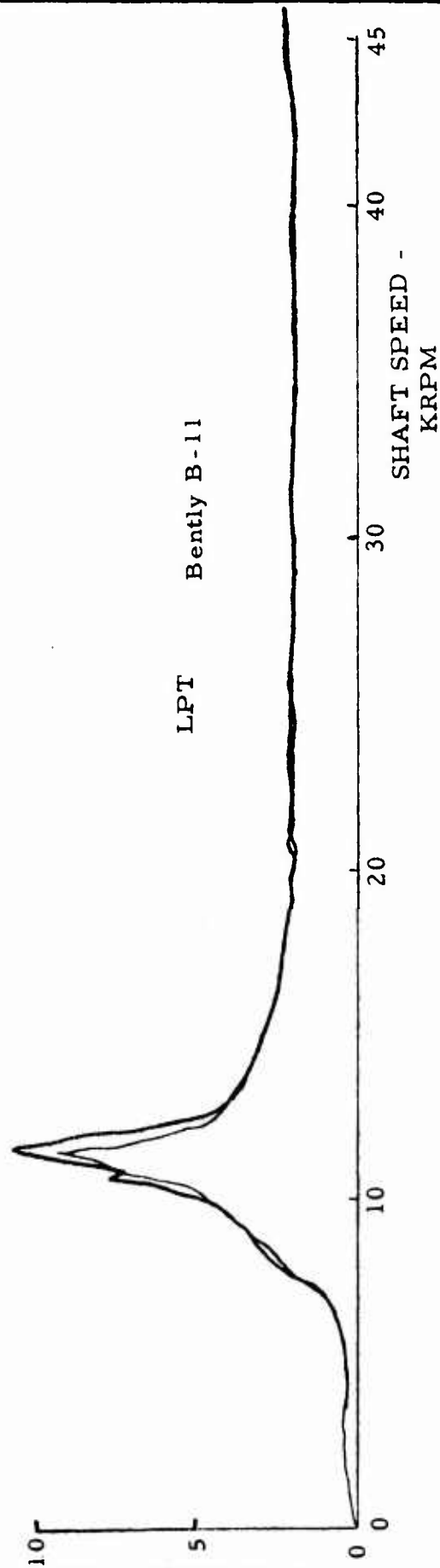


Figure 49. - Vibration Amplitude vs Speed -
Run No. 14

VIBRATION AMPLITUDE
-MILS- (P - P)

Spring Ring Set No. 2

Bently B-5

FWD SHAFT

Bently B-3

FAN

SHAFT SPEED -
KRPM

Figure 50. - Vibration Amplitude vs Speed -
Run No. 29

VIBRATION AMPLITUDE
- MILS - (P - P)

Spring Ring Set No. 2

10
5
0

AFT SHAFT

Bently B-9



10
5
0

MID-SHAFT

Bently B-7



SHAFT SPEED -
KRPM

Figure 51. - Vibration Amplitude vs Speed -
Run No. 29

Spring Ring Set No. 2

VIBRATION AMPLITUDE
- MILS - (P - P)

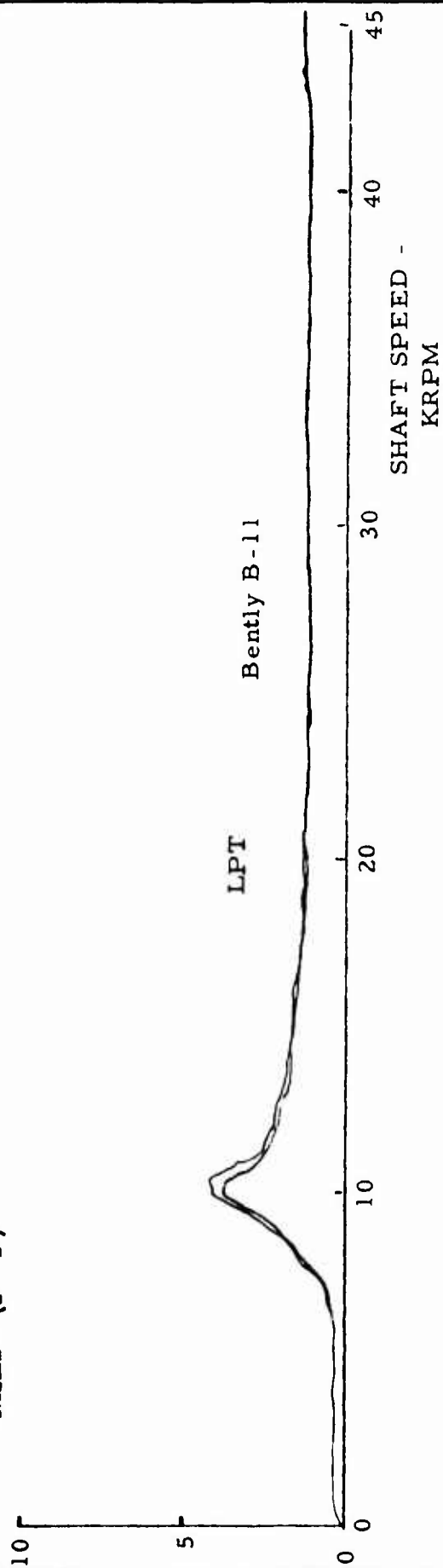


Figure 52. - Vibration Amplitude vs Speed -
Run No. 29

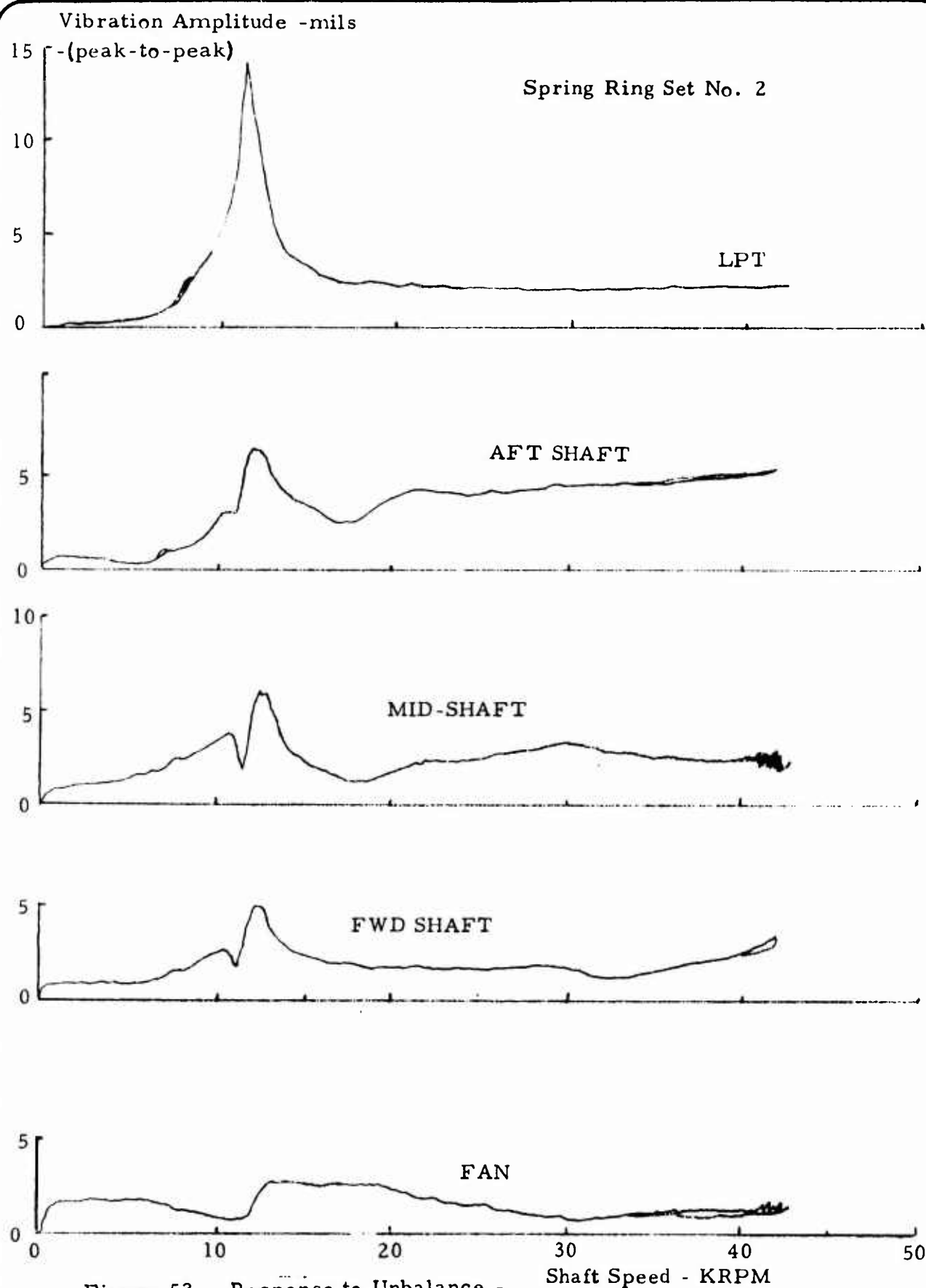


Figure 53. - Response to Unbalance -
Base Rotor - Run No. 22

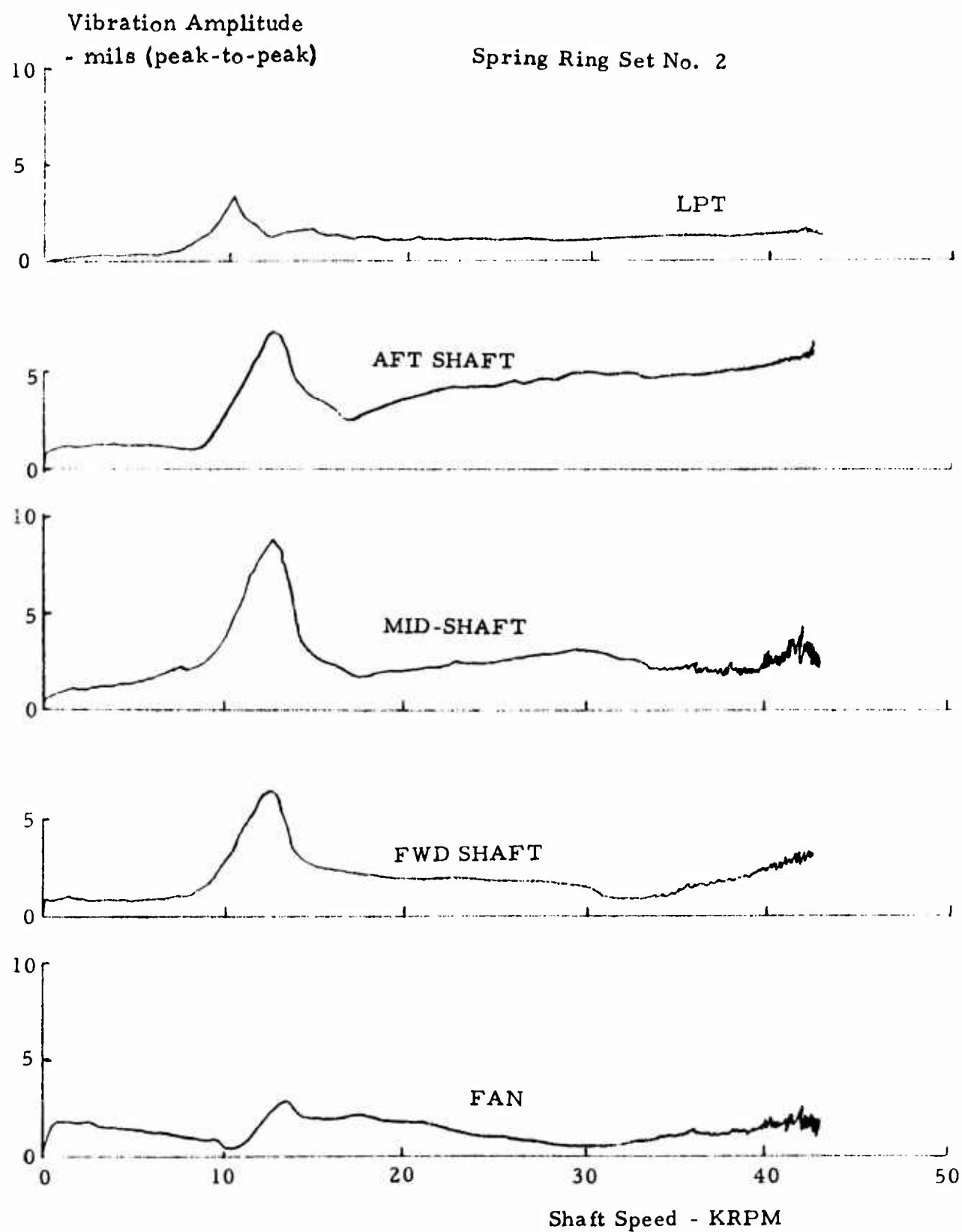


Figure 54. - Response to Unbalance - 1.0 GM-IN @ LPT
Run No. 24

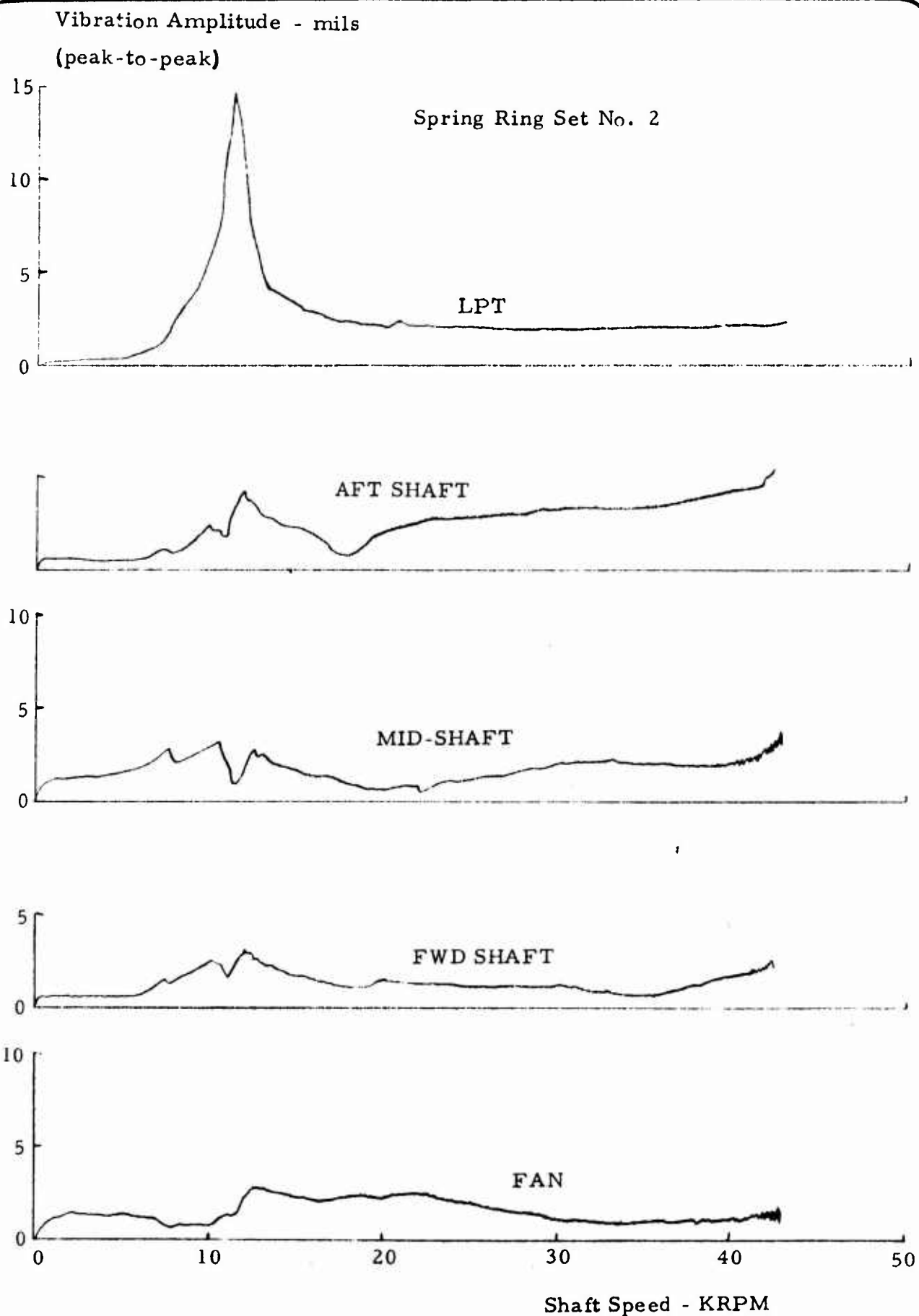


Figure 55. - Response to Unbalance - 1.0 GM-IN @ FAN
Run No. 25

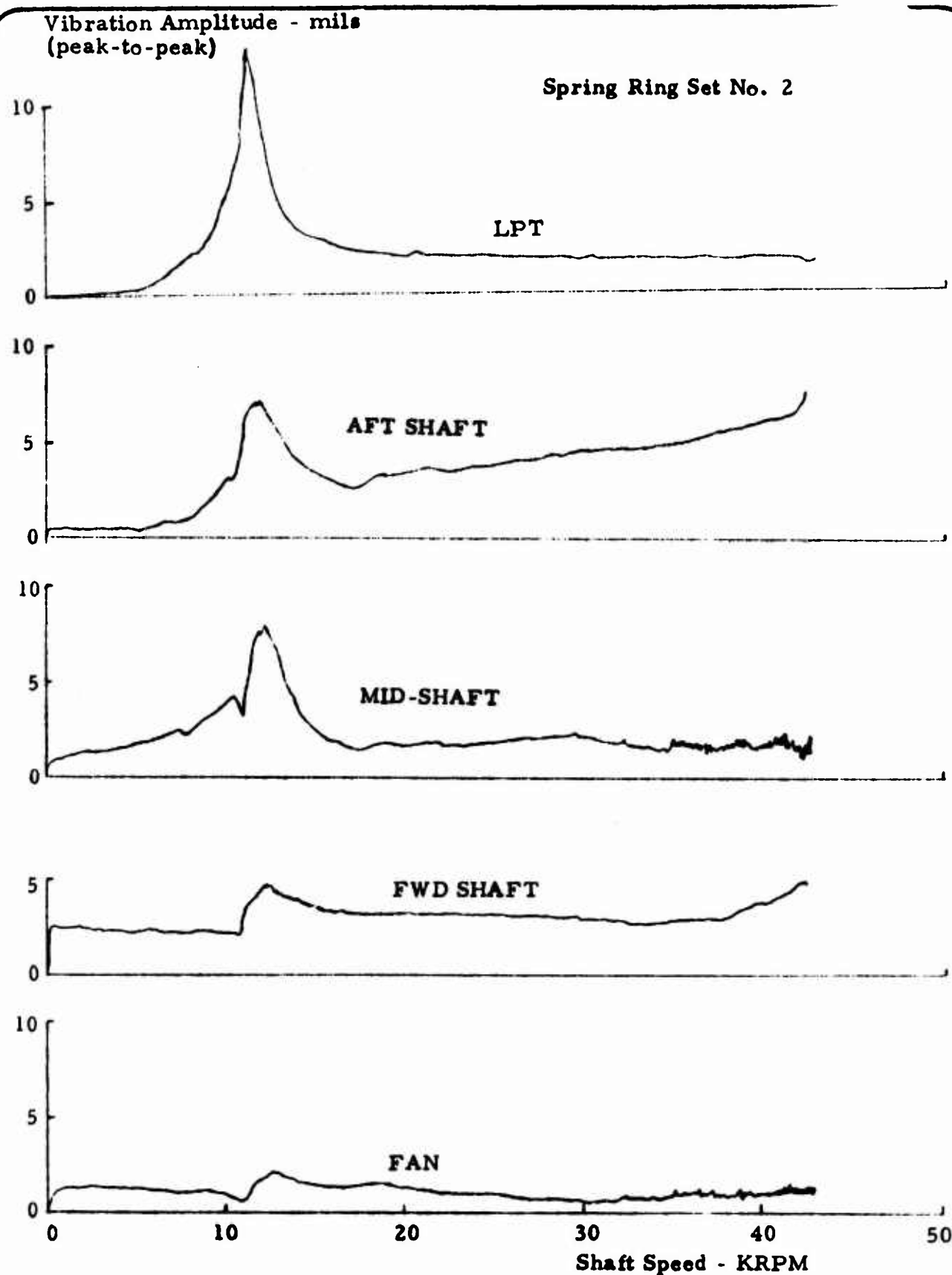


Figure 56. - Response to Unbalance - 0.75 GM-IN @ FWD. SHAFT
Run No. 26

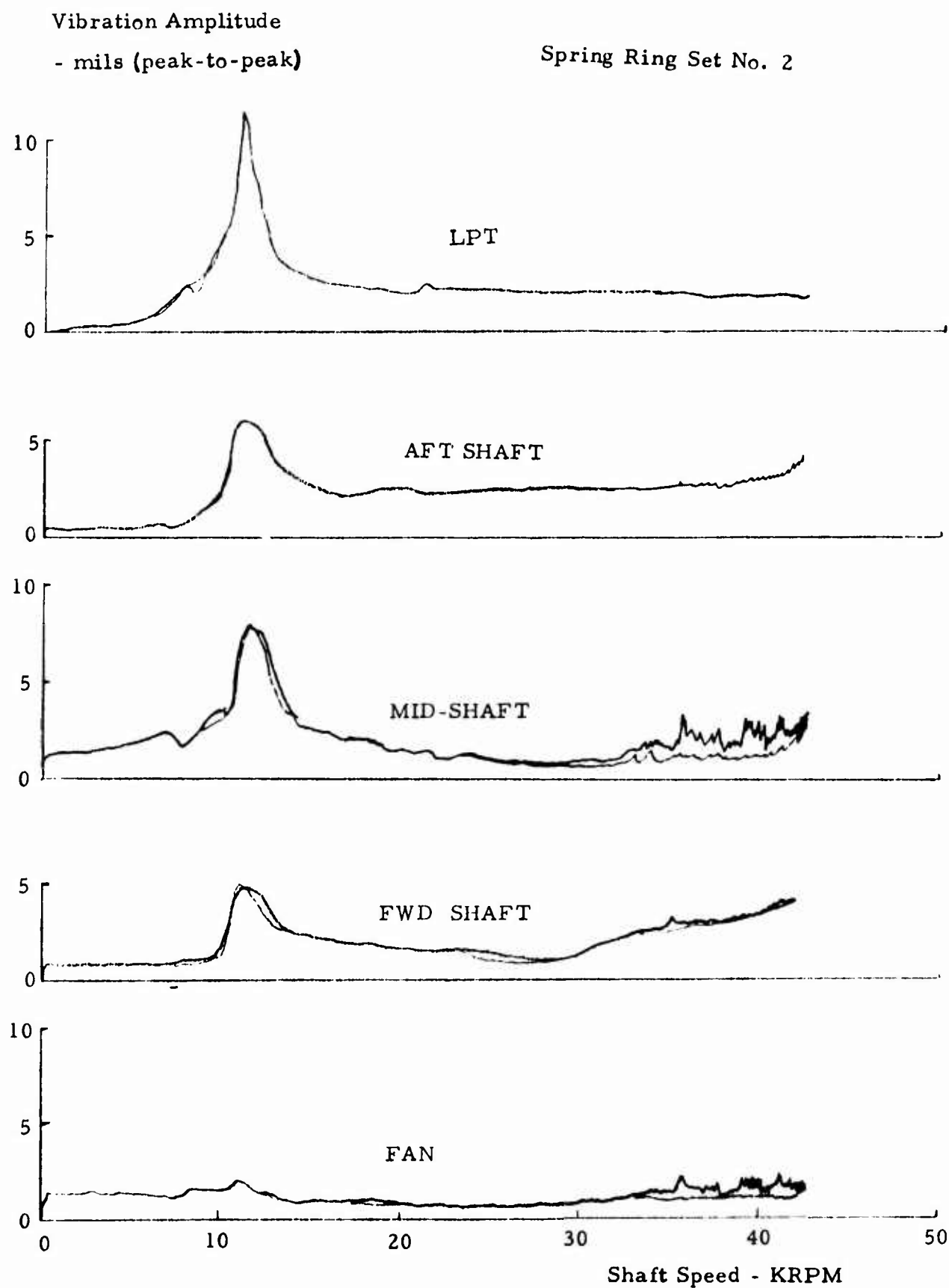


Figure 57. - Response to Unbalance - 0.75 GM-IN @ MID-SHAFT
Run No. 27

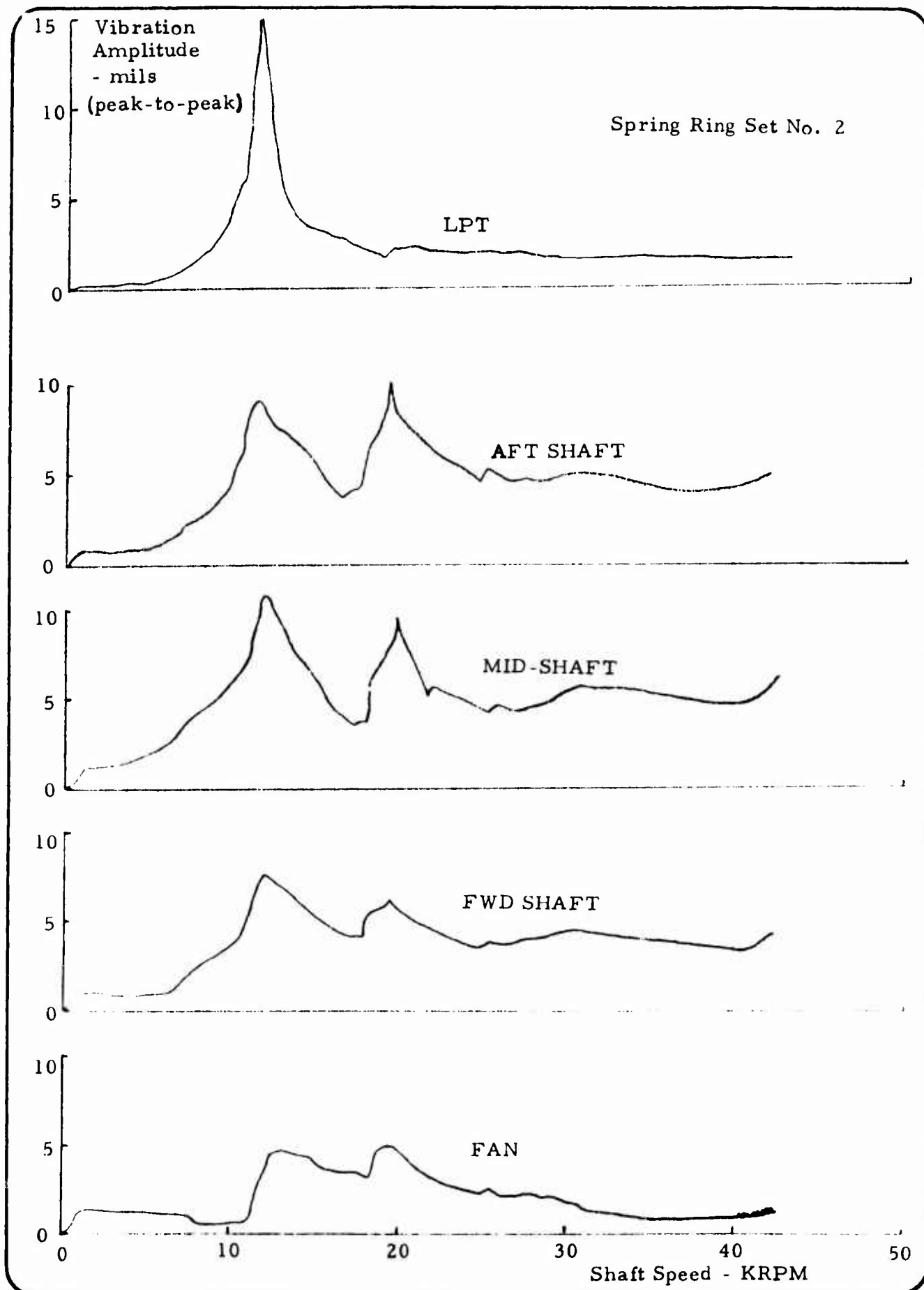


Figure 58. - Response to Unbalance - 0.75 GM-IN @ AFT SHAFT
Run No. 28

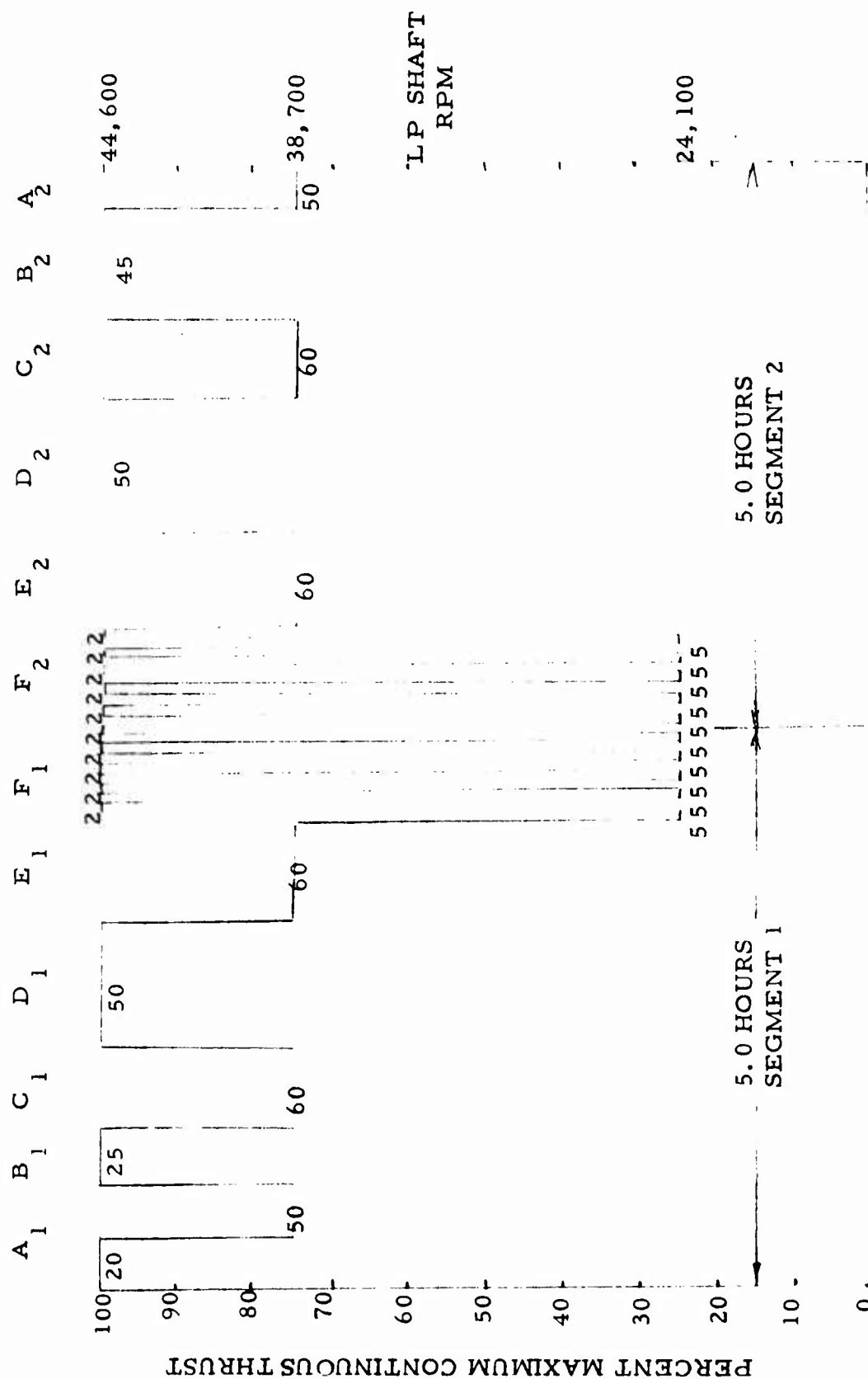


Figure 59- Mission Profile for Endurance Test.

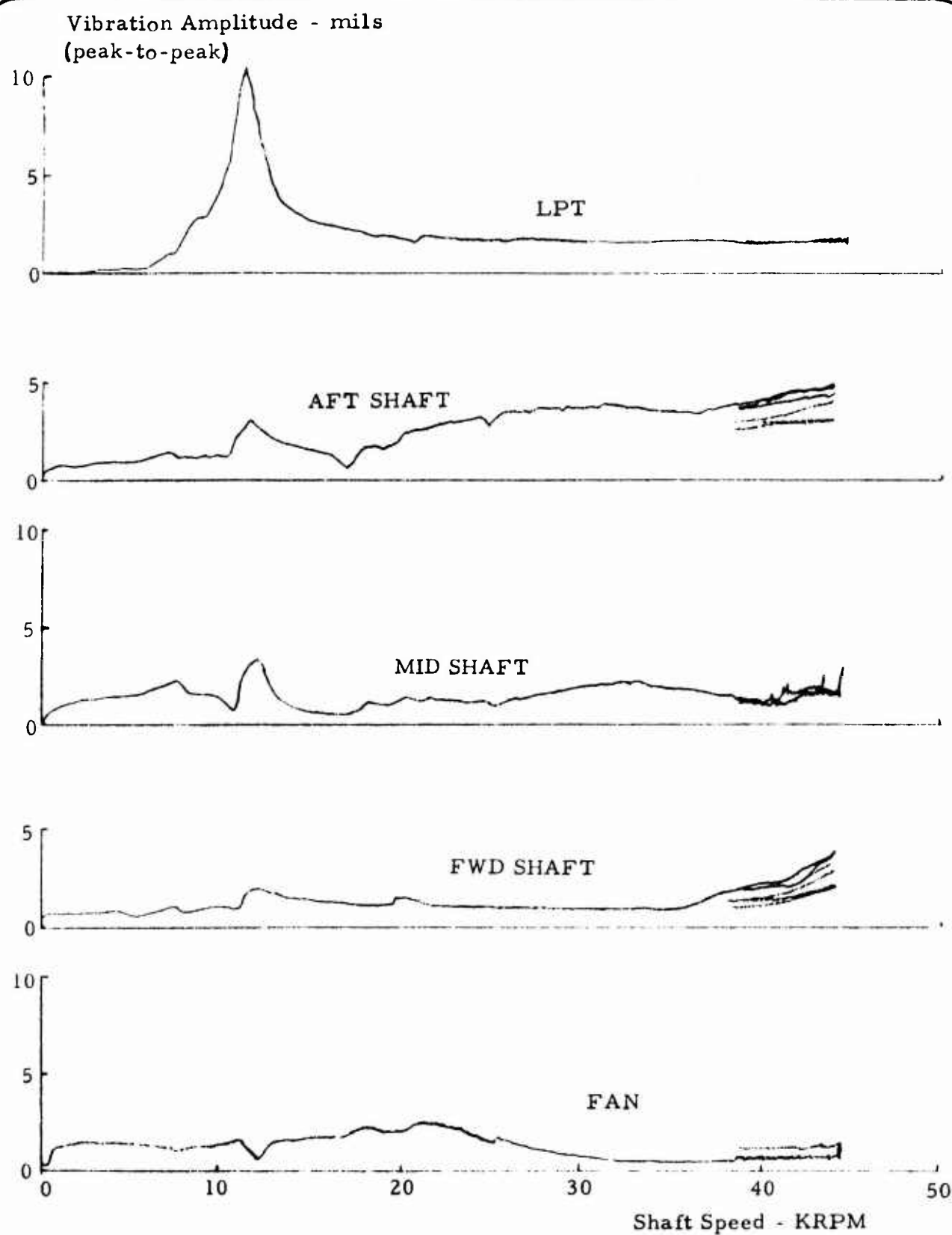


Figure 60- Endurance Test Vibration Amp. - Start-A thru E.I.

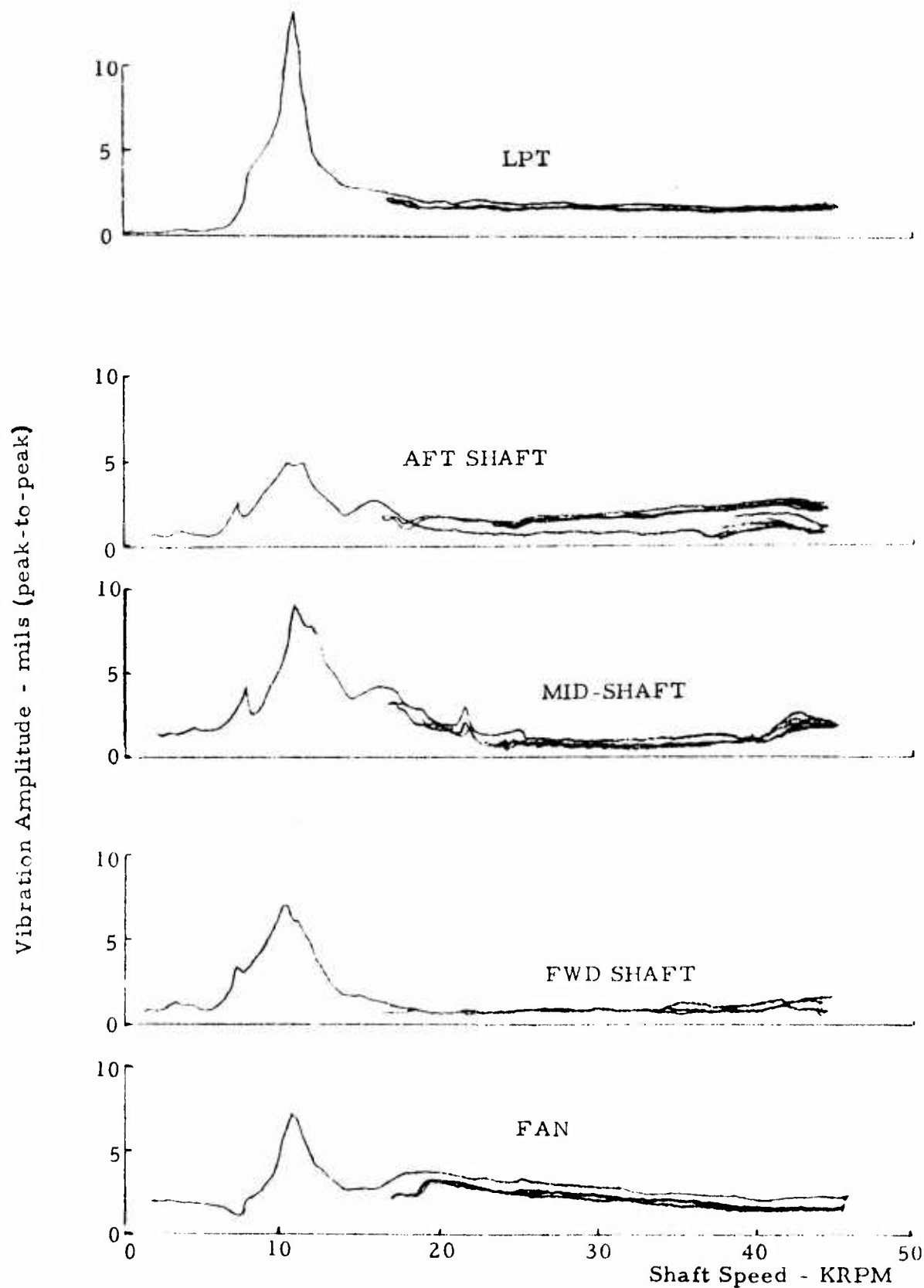


Figure 61- Endurance Test Vibration Amp. -
End-F1 thru A2.

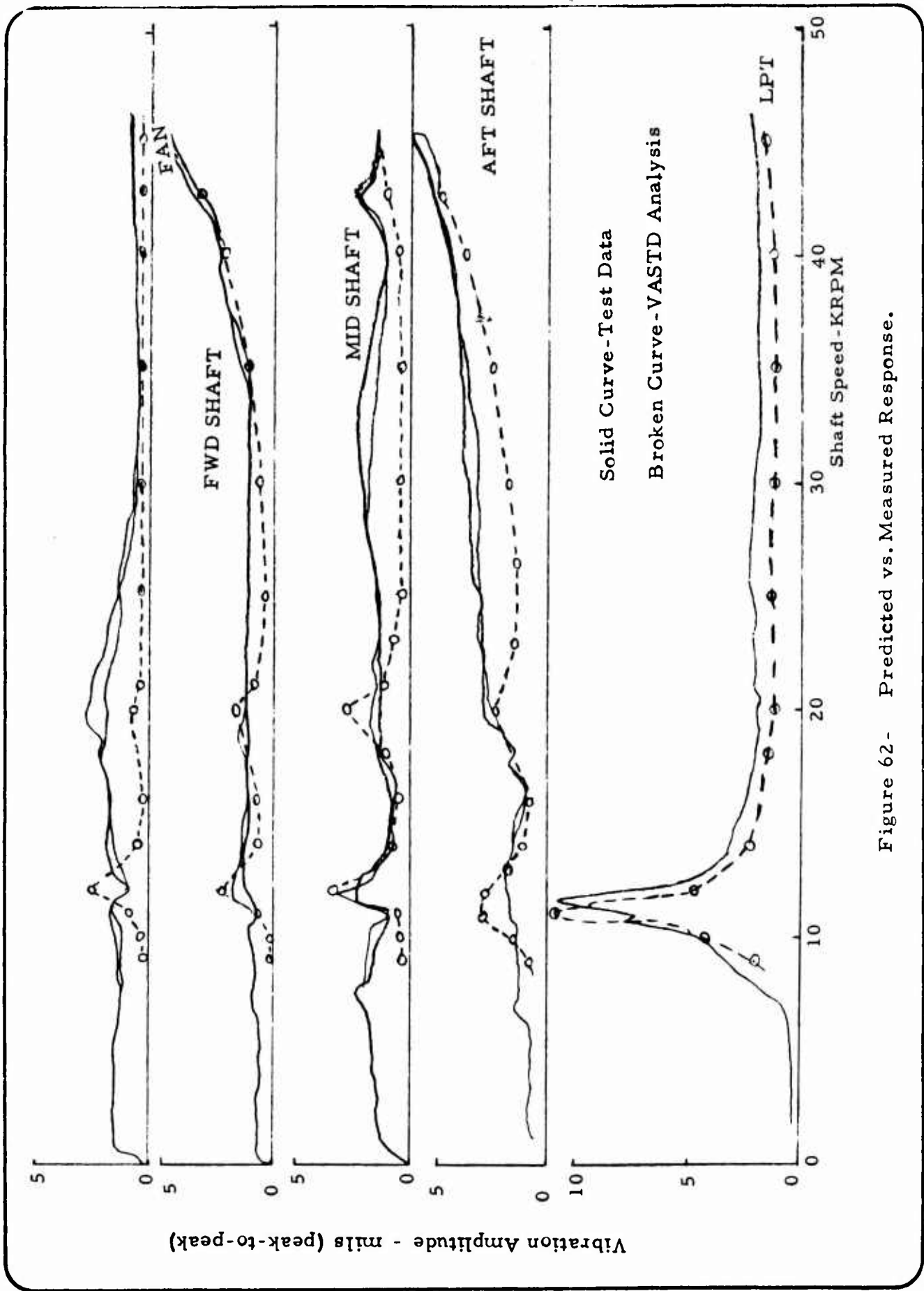


Figure 62- Predicted vs. Measured Response.